universität wien

MASTERARBEIT / MASTER'S THESIS

Titel der Masterarbeit / Title of the Master's Thesis

„Stratigraphy and Provenance of the Tauern Flysch (Wolfbachtal, Salzburg, Austria)“

verfasst von / submitted by

Christina M. Begusch BSc

angestrebter akademischer Grad / in partial fulfilment of the requirements for the degree of

Master of Science (MSc)

Wien, 2018 / Vienna 2018

Studienkennzahl lt. Studienblatt / degree programme code as it appears on the student record sheet:	A 066 815
Studienrichtung lt. Studienblatt / degree programme as it appears on the student record sheet:	Masterstudium Erdwissenschaften UG2002
Betreut von / Supervisor:	Ao. Univ.-Prof. Dr. Michael Wagreich

INDEX

ACKNOWLEDGEMENT

I am using this opportunity to express my gratitude to everyone who supported me throughout the course of my Master thesis. First of all I would like to say a huge thank you and express my sincere gratitude to my advisor **Michael Wagreich** for his aspiring guidance and constructive help with my thesis. This research was also supported by my second advisor **Kurt Decker** for his support with all structural issues concerning my thesis. Apart from my advisors I would like to thank **Susanne Gier** for her help with the XRD analysis, **Bernhard Grasemann** and **Konstantin Petrakakis** for their support concerning the microstructural analysis of the thin sections and the discrimination of the grade of metamorphosis, **Patrick Meister** for several discussions leading to a better understanding of the carbonate samples concerning this thesis, **Erik Wolfgring** for introducing me to the program PAST and for his help with the component analysis and hierarchic clustering, **Wolfgang Knierzinger** for conducting the microprobe analysis on my samples and **Shahid Iqbal** for his help with merging and interpretation of the geochemical data. I would like to especially thank my family and friends for their constant support and encouragement.

1. KURZFASSUNG

Die Herkunft und der stratigraphische Zusammenhang der metamorphen Flysch-ähnlichen Sedimente am Nordrand des Tauernfensters (Penninikum der Ostalpen, Salzburg; u.a. nach Braumüller, 1939; Prey, 1977; Ślączka, 2011) stellt ein ungelöstes Problem der Gebirgsbildung der Ostalpen dar. Unterschiedliche Modelle versuchen eine Zugehörigkeit dieser Tiefwasser-Mass-Flow-Sedimente zu finden. Diese Masterarbeit beschäftigt sich mit der Herkunft des Tauern Flyschs und damit einhergehend mit der Beantwortung der Frage nach dessen paläogeographischen und paläotektonischen Zuordnung. Hierfür wurden vor allem Schwermineralverteilungen und Bulk-Geochemie Analysen herangezogen. Eine weitere Forschungsfrage widmet sich dem Metamorphosegrad dieser Flysch Ablagerungen und dem möglichen tektonischen Einfluss der SEMP (Salzach–Ennstal–Mariazell–Puchberg; Rosenberg et al., 2008) –Störung auf diese.

Die Geländearbeit beinhaltete sedimentologische Aufnahme von zwei Hauptprofilen (das erste 780m, das zweite 400m lang) und 18 Einzelprofilen im Bereich des Wolfbachtals (südwestlich von Taxenbach, Salzburg). Die beinahe durchgehenden Aufschlüsse von metamorphen Flysch-Ablagerungen befinden sich entlang zweier Fortstraßen im Höferwald und im Bachbett des Wolfbachs. Die Ablagerungen beinhalten Meta-Tonschiefer, (teilweise) turbiditischen Meta-Sandstein, Meta-Brekzie und Marmor. Insgesamt 50 Proben wurden genommen und analysiert. Zu den Analysen zählt petrographische Mikroskopie, XRD-Analysen, Schwermineralanalyse, Mikrosonden Messungen der Schwerminerale, Bulk-Geochemie Analysen und Principal Component Analysen. Die mikrostrukturelle Analyse der Dünnschliffe ergibt höhere Metamorphose Bedingungen als erwartet (obere Grünschieferfazies, mit Temperaturen von 450°). Diese Bedingungen sind verantwortlich dafür, dass die geochemischen Analysen nicht völlig vertrauenswürdig sind und daher keine eindeutigen Ergebnisse liefern. Da es sich bei dem Hauptdeformationsmechanismus um Drucklösung handelt, können Sedimentstrukturen (beschrieben von Prey, 1977), welche die Zuteilung zum „Flysch“ bestätigen, trotz Metamorphose beobachtet werden. Die Abfolge der Hauptprofile (Modell nach Walker, 1979) lässt auf eine Bildung durch einen progradierenden, submarinen Schwemmfächer schließen. Es gibt wiederholte Hinweise auf zwei ursprünglich separate Herkunftsgebiete. Das erstellte wahrscheinlichste stratigraphische Modell zur paläogeographischen und tektonischen Zugehörigkeit dieser Metasedimente ordnet jene überwiegend der Unterkreide zu.

2. ABSTRACT

The provenance and the stratigraphic correlation of the metamorphic flysch-like sediments at the northern border of the Tauern Window (Penninic unit, Salzburg; inter alia Braumüller, 1939; Prey, 1977; Ślączka et al., 2011) represent a conundrum of the orogeny of the Eastern Alps. There are several models trying to explain Alpine palaeogeography and the derivation and stratigraphic position of these deep-water-mass-flow-sediments. Provenance of the Tauern Flysch may help to solve the question of its palaeogeographic and palaeotectonic position, mainly by making comparisons of heavy mineral associations and bulk geochemistry analysis data. Another research question is the degree of metamorphosis and how strong the possible influence of the SEMP (Salzach–Ennstal–Mariazell–Puchberg; Rosenberg et al., 2008) Fault is on these flysch deposits.

The fieldwork included the sedimentological logging of two main profiles (1st 780m, 2nd 400m in length) and 18 single profiles in the area of the Wolfbachtal (southwest of Taxenbach, Salzburg). Almost continuous outcrops of metamorphic flysch deposits along forest paths and the Wolfbach streambed can be found, including meta-black shales, turbiditic meta-sandstones, meta-breccias and marbles. Analysis-methods used on altogether 50 samples include petrographic microscope analysis, x-ray diffraction, heavy mineral associations, micro-probe analysis of heavy minerals, rock bulk geochemistry analysis and principal component analysis.

Microstructural microscope analysis (i.a. recrystallized feldspar grains and brittle deformed non-recrystallized dolomite grains in a fully recrystallized calcite matrix) indicates higher metamorphic conditions than previously reported (with upper Green-schist facies and temperatures around 450°C). Due to these conditions the results of the bulk geochemistry analysis are not fully reliable and don't give straightforward results. Nevertheless sedimentary structures (described by Prey, 1977), confirming the flysch-like nature of these meta-sediments, can be observed, due to the main deformation mechanism being pressure solution. The succession of the profile in the Wolfbachtal was formed by a prograding, small submarine fan (fitting the model of Walker, 1979). There is an enhanced possibility of two (originally) separate sources. The most likely stratigraphic model for the paleogeography and tectonic attribution of these meta-sediments indicates that the deposition started during the end of the Late Jurassic and continued mainly throughout the Early Cretaceous.

3. INTRODUCTION

The Alps represent one of the best studied orogens of the world and serve as a natural laboratory of fossil continental margin evolution, subduction, continent-continent collision, accretionary wedge and fold-and-thrust belt evolution. Early geological studies to unravel the structure of the Eastern Alps culminated around 1900, when overthrusts and nappe structures, and the existence of tectonic windows, such as the Tauern Window (TW), were recognized (e.g. Termier, 1904). Since that time numerous studies have been undertaken in the TW and it's adjacent units, which led to still debated contrasting models for the palaeogeographic and palaeotectonic evolution of this geological Alpine key area, and the whole Alpine orogeny (e.g. Frisch, 1979; Kurz et al., 1998; Faupl & Wagreich, 2000; Schuster et al, 2004; Schmid et al., 2004, 2013; Handy et al., 2015).

Flysch-like sediments at the northern border of the TW are referred to as "Tauern Flysch". They form part of the Upper Penninic nappes (after Schmid et al., 2004) and were first discovered and analysed by Braumüller in 1939. He called these deposits between the Fuscher- and the Rauristal "Sandstein-Breccien-Decke des Tauernnordrandes". He found sedimentary structures, like grading similar to known flysch sediments and described the composition of occurring components, such as quartz, mica, feldspar, and many more (see Braumüller, 1939). In 1975, based on Braumüller's work, Prey (1975) started to analyse the area, mainly focusing on finding fossil evidence of a possible sedimentation age ranging from Upper Cretaceous to Paleogene. Under consideration of the metamorphism influencing the area, Prey was able to compare the heavy mineral composition of the "Tauern Flysch" with the "Praettigau- and Oberhalbsteiner-Flysch deposits". However his attempt to find fossils useful for sedimentation age analysis was unsuccessful. Further evidence of the deposit's flysch-like nature was found in 1977 in the course of further fieldwork and analysis inter alia in the area western of the Rauristal, and the Wolfbachtal by Prey and Braumüller. They observed several graded sandstone beds and a few characteristics of the Bouma Sequence (Bouma, 1962), characteristic for turbidites.

The stratigraphy, age and position of these units remain unclear until today. The relations and correlations to other, non-metamorphosed deep-water clastic flysch units of the Alps are quite dubious, especially the Rhenodanubian Flysch Zone at the northern margin of the Eastern Alps, with largely unknown basement and questionable tectonic attribution, and its continuations into the Central Alps and the Western Carpathians provide still a puzzling problem in Alpine paleogeography and orogeny. There are several models trying to explain the derivation of these deep water-mass flow-sediments. According to older models (i.a. Faupl & Wagreich, 2000) the Tauern Flysch may represent a northern Penninic deep-sea-trough, classifying these deposits equated to the non-metamorphic Rhenodanubian Flysch. More recent models consider the original position of the Tauern Flysch to be south of the Subpenninic unit, and therefore a southern Penninic or even Austroalpine position (i.a. Schmid et al.,2013; Handy et al.,2015).

Because in this work the main focus lies on the sedimentary description and provenance of the Tauern Flysch, in the following I will use the sedimentologic terminology for these metasediments.

4. Location – Geological Position

The research area is located at Thannberg, in the Höferwald (forest) of the Wolfbachtal (Salzburg, Austria), southwest of Taxenbach and south of Hasenbach. This northern border of the TW is part of the Penninic unit of the Eastern Alps, Salzburg; (i.a. Braumüller, 1939; Prey, 1977; Pestal et al., 2009; Ślączka et al., 2011).

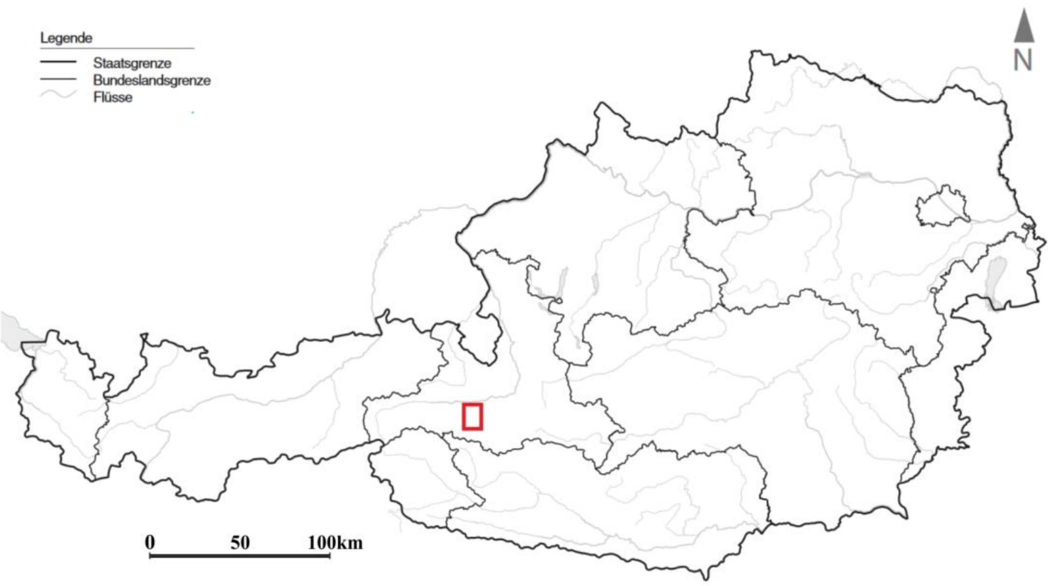

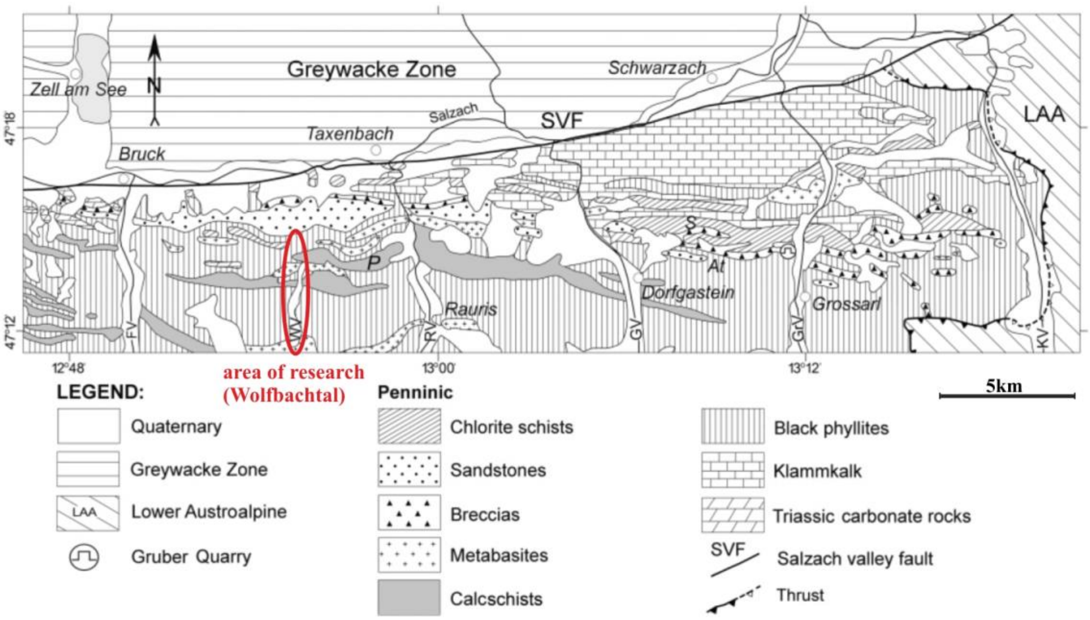

Figure 1: Overview map of Austria (source: www.schulatlas.com); Geological sketch map of the NE Tauern Window (from Slaczka et al., 2011) showing the area of research; the red fields show the area of research.

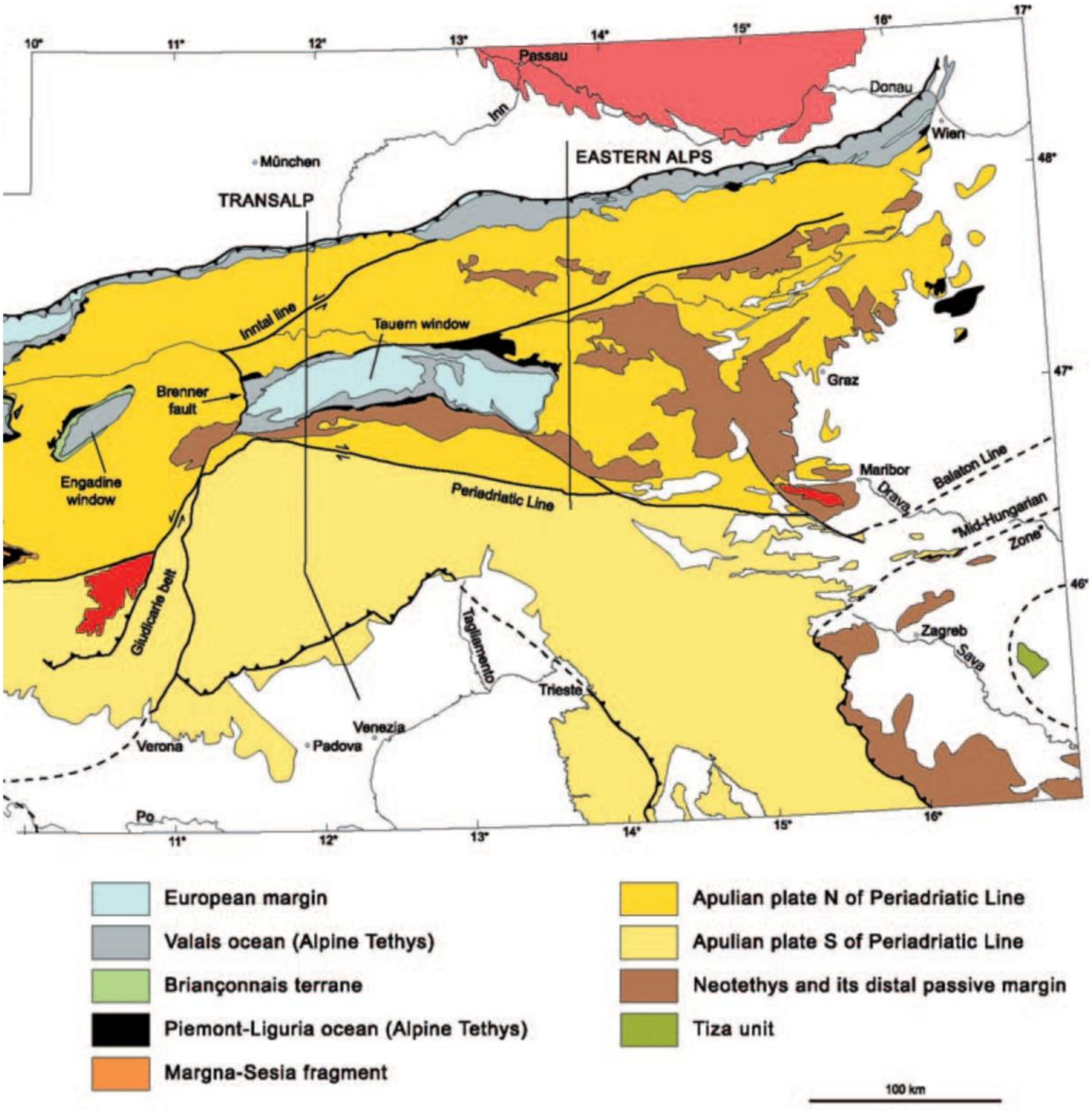

Figure 2: Part of a map of the major paleogeographic units in the Alps from Schmid, 2004.

The Tauern Flysch is positioned at the northern margin of the TW. It is part of the southern Penninic (Piemont-Liguria) unit, which is visualized in black colour in Figure 2 (after Schmid, 2004). The belt of the Rhenodanubian Flysch in the north belongs to the northern Penninic (Valais) unit. In this geological map the Glockner nappe is allocated to this unit as well (after Schmid, 2004), however other authors classify this nappe as part of the southern Penninic (Piemont-Liguria) unit (i.a. Faupl, 2003).

6. PALEOGEOGRAPHIC BACKGROUND

The Penninic nappes can be divided into three paleogeographic-tectonic domains (see Figure 3), the northern Penninic (Valais), the middle Penninic (Brianconnais) and the southern Penninic (Piemont-Liguia) unit, which developed due to plate tectonic movement between the European plate and Apulia (after Faupl & Wagreich, 2000).

The southern Penninic unit derived from the Piemont-Liguria Ocean, which opened in the Jurassic, north of the Lower Austroalpine unit (after Schmid, 2004). It can be seen as an extension of the Jurrasic Atlantic Ocean (after Faupl, 2003).

The existence and extension of the middle Penninic unit in the Eastern Alps is still controversial. It may represent a continuation of the continental fragment and terrestrial Brianconnais terrain from Switzerland to Austria (according to Faupl, 2003). In Jurassic times it is positioned south of the Helvetic unit and adjacent to the Piemont-Liguian Ocean (after Schmid, 2004). Rocks derived from this microcontinent are common in the Western and Central Alps and can be found in the Tasna nappe and the lower part of the Penninic Engadine Window (Schuster et al, 2004).

The deposition of material belonging to the northern Penninic unit started in the Cretaceous, as the Valais Ocean opened between the middle Penninic terrain in the south and the Helvetic unit in the north (see Faupl, 2003). The northern Penninic unit contains calcareous flyschoid sediments, which for instance form large parts of the Central Alps, part of the Engadine Window and the lower nappes of the Rhenodanubian Flysch Zone (after Schuster et al, 2004).

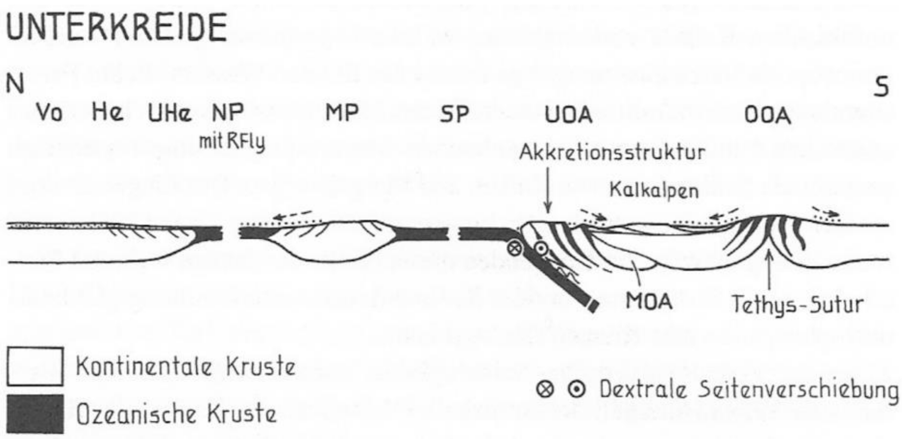

Figure 3: Paleogeographic model of Eastern Alps showing the western Tethyan Ocean and the opening of the Penninic Ocean in Lower Cretaceous (from Faupl, 2003). [NP] for the northern Penninic, [MP] for the middle Penninic and [SP] for the southern Penninic unit, [RFly] for Rhenodanubian Flysch units.

7. Outcrops

Several outcrops of Tauern Flysch on the eastern slope of the Wolfbachtal, alongside of two forest roads can be found. Some outcrops are well-preserved including exposed intervals of almost every lithofacies (see Figure 4). One of the best preserved outcrops analysed is a small former quarry (47°16'08.7"N, 12°55'59.0"E) at the top of the main profile of the upper road in the Höferwald (see Figure 4 [A]). These, not strongly weathered rocks mainly include two lithofacies, marble and breccia. The river bed of the Wolfbach provides good outcrops as well. However due to the high water flow discharge and velocity during the field season it was not possible to log more than the first few metres from the bridge (47°16'03.0"N, 12°55'38.9"E) alongside the river downstream.

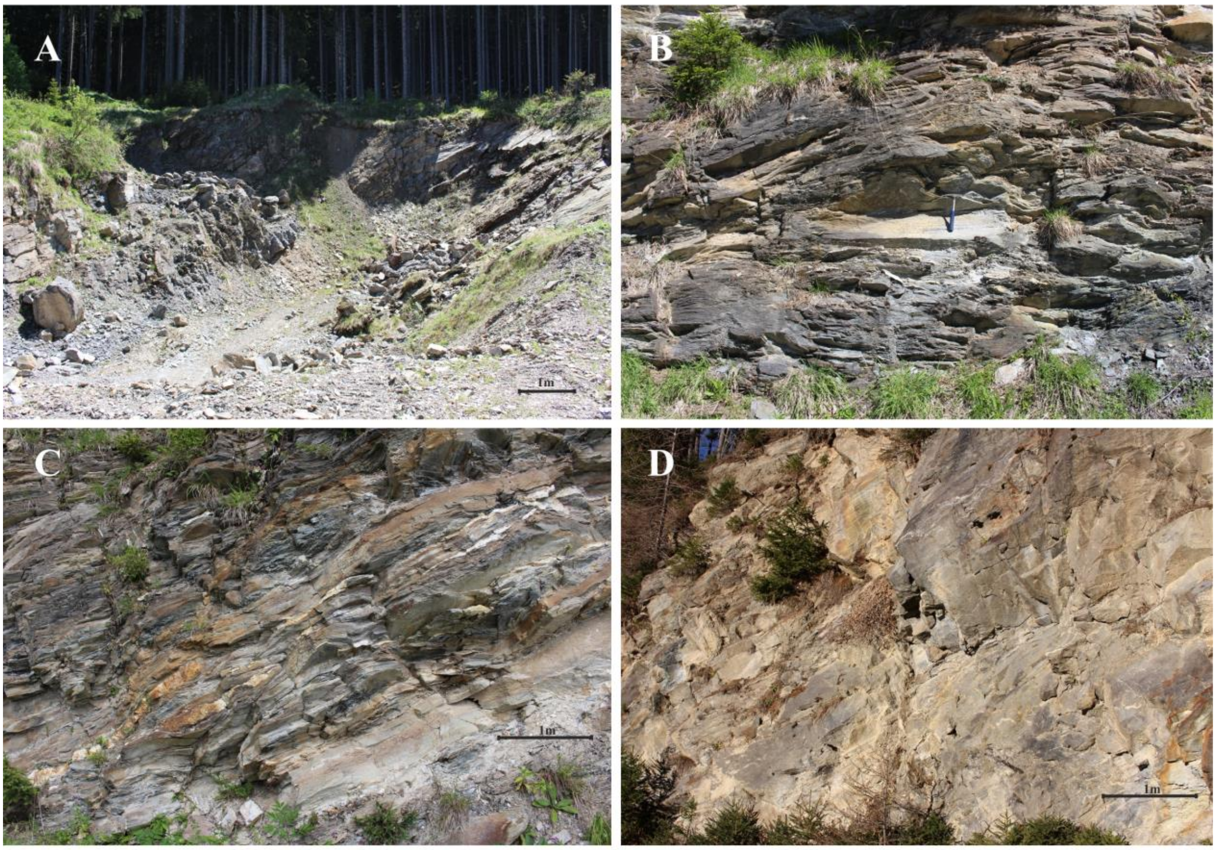

Figure 4: A variety of well-preserved outcrops in the Höferwald, Wolfbachtal.

***A** shows the small, former quarry (lithofacies9 and lithofacies 10); **B** shows a typical section of lithofacies 6; **C** shows the position of the single profile A9 of lithofacies 8; **D** shows the position of the single profile A15 of lithofacies 5; **E** shows the position of the single Profile A7 of lithofacies 2.*

However, not all outcrops are preserved this well. Often strongly weathered outcrops with i.a. red-brown coloured FeOH-coating and strongly altered components (e.g. feldspar grains of lithofacies 10) are common (see Figure 5). In many cases outcrops are strongly overgrown by vegetation. Highly weathered, crumbly rocks are more common, which makes the search for fresh, useful samples for further analysis in the lab sometimes hard. Partly outcrops are visible from the distance, but physically not reachable because of for instance steep slopes and slippery slope debris. Areas, which show no rocks on the surface at all, were logged as sequence gaps.

Figure 5: A variety of strongly weathered outcrops in the Höferwald, Wolfbachtal.

A, ***B*** *and* ***E*** *show black shales of lithofacies 1.* ***C*** *shows sequence of lithofacies 6 in the higher area of the main profile A.* ***D*** *shows a section of lithofacies 10.*

8. METHODS AND PROFILES

8.1. GENERAL DESCRIPTION

Two main composite profiles (profile A = 780m, profile B = 390m in thickness) were logged in the Höferwald in the Wolfbachtal, southwest of Taxenbach (Salzburg). Profile A was logged along a forest road in the higher area of Thannberg (47°16’09.5”N 12°55’57.8”E) and profile B parallel to it along a second forest road in the lower area of Thannberg (47°16’08.2”N 12°55’46.5”E). Furthermore, the reachable area of the streambed of the Wolfbach (47°16’02.7”N, 12°55’39.4”E) shows the characteristics of lithofacies 1 and can therefore be correlated to the bottom of the two main higher lying profiles. From distance it is also observable that banked sandstone beds and shale layers occur further along the streambed, similar to those described as lithofacies 2 and lithofacies 3. This gives indication of a further continuation of these flysch deposits towards the east. For better classification 18 single profiles (A1-A18), representing specific sections of all flysch-related lithofacies were logged (of which more in chapter 6).

8.2. METHODS

Before starting the logging of the profiles, the lithofacies were classified based on obvious differences in composition and appearance (inter alia bedding, colour, grain size and sandstone to shale – ratio). In general the well reachable outcrops of the profile were logged using a measuring rod and a small measuring tape, both of 2m length. The measuring device was placed perpendicular to the bedding and logged bit by bit. The profile was first drawn on graph paper and later digitized using Corel Draw X5. The categorisation of grainsize (after Wentworth, 1922) includes [shale] for everything that is smaller than 63 µm, [f] for fine-grained, [m] for middle-grained and [c] for coarse-grained sandstones and breccia. Fine-grained sandstones include grain sizes of 63µm to 250µm, middle-grained sandstones include grain sizes of 250µm to 500 µm and coarse sandstones include grain sizes of 0.5mm to 2mm. Fine-grained breccia includes grain sizes of roughly 2mm to 4mm, middle-grained breccia includes grain sizes of roughly 4mm to 25mm and coarse-grained breccia includes everything coarser than 25mm.

Areas that were either not exposed or outcrops that were not accessible for safety reasons but could be allocated to specific lithofacies from distance were measured in a different way. For this purpose a 20m measuring tape was used to measure the length of the path in front of the outcrops. Later in conjunction with the measurements of the layers orientation, the real profile thickness was recalculated using the formula: $t = \pm\, d \cdot \sin\alpha \cdot \sin\beta \pm\, h \cdot \cos\alpha$ (oral information Wagreich, M.). Included in the formula are the values: *[d]* is the horizontal distance - it is positive if the traverse dips in the same direction as the dipping of the layers, *[α]* is the dip angle of the layer, *[*β*]* is the angle between the traverse and the strike direction (±90°), *[*h*]* is the altitude difference - it is positive if the traverse increases.

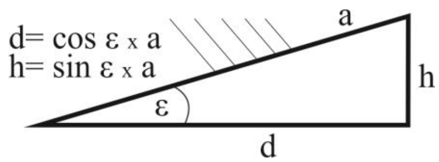

8.3. VISUALIZATION

Each lithofacies is visualized in a different colour (see legends of Figure 6 and Figure 7) and show graphical patterns depending on their rock type. In that sense sandstone-dominated-lithofacies are visualized using a dotted pattern, shale layers using horizontal lines, breccia layers using different-sized triangles and limestone layers using a tiles-structure. Sequence gaps are visualized with uncoloured fields and a X through them, to clarify that these areas are not exposed to the surface. Their thickness was measured the same way as not exposed areas (described in chapter 3.2.). Lighter coloured areas of sequence gaps, which are additionally marked with a question mark (?), represent areas which are not open to the surface, but can be interpreted as a specific lithofacies. Their colour matches the lithofacies they can be associated with. Uncoloured areas, which are solely marked with a X, represent sequence gaps without any interpretation regarding their facies. Additionally the carbonate content (light blue) and the shale content (dark grey) is shown next to the main profiles. The carbonate content is classified as a factor between a low carbonate proportion and a high carbonate proportion including cement phases. The shale content is determined as a percentage between 0 and 100 percent. These two properties were determined through the combination of (1) the observations during the microscopic analysis of the thin sections and (2) field observations and documentation - in particular shale-to-sandstone- ratios. Therefore, these values are estimates and not absolute values and simply provide a rough overview of the total change in carbonate and shale content within both main profiles. Furthermore, the main composite profiles contain information about the positions of single profiles (red arrows) and areas containing fossil remnants of echinoderms, marked with circles, or Fe-hydroxides, marked with orange coloured stars. Red continuous lines represent tectonic faults

8.4. PROFILE A, UPPER ROAD SECTION

The main focus lies on profile A along the upper road (see Figure 6) mainly because these outcrops are better preserved. The base of the profile is at 0 metres and the top at 780 metres. It is not precluded that folding influenced the section, which could interfere with and double parts of the stratigraphical sequence of lithofacies, especially as folding on smaller scale (cm – m scale) was observed several times. However, no clear sign of recurring lithofacies or overturning of the beds was observed. In order to log a composite stratigraphic profile it is therefore assumed that the profile is more or less continuous without recurring sections. Altogether 13 lithofacies were classified.

The base of profile A consists of greenschists, i.e. ophiolite-related rocks. They are associated with the Glockner nappe and considered to represent the base of the deposits of the Tauern Flysch. These metamorphic magmatites were classified as the greenschist lithofacies, lithofacies 15 (dark green colour in the profile. Above the greenschists, the next outcrop comprises lithofacies 11, the chert lithofacies (dark red colour in Figure 6). This lithofacies is strongly recrystallized and consists almost solely of quartzites, showing strongly folded quartzite veins in a very fine-grained quartz matrix. Again this lithofacies is not part of the flysch sedimentation and clearly separated from lithofacies 1, the black shale lithofacies (black colours in Figure 6), through a normal fault. Lithofacies 1 represents the beginning of clastic sedimentation, containing fine black shale layers, and rarely including small intercalating sandstone layers (fine yellow lines in Figure 6). As described in this main profile, the sandstone/shale ratio and the overall grainsize of lithofacies 1 increases towards the top as more and more thin (<2.5 cm) sandstone layers occur. The outcrops of lithofacies 1 were partly overgrown and unstable due to the high shale content, which is the highest out of all lithofacies.

Overlying lithofacies 1 follows lithofacies 2 (turquoise colour in Figure 6). It is the first lithofacies, which was formed mainly by mass-flow sedimentation. It contains calcareous sandstone layers interbedded with black shale layers. Lithofacies 2 contains the by far highest amount of fossil remnants of echinoderms observed. Lithofacies 5, follows (orange colour in Figure 6). Both, its carbonate content and shale content are significantly lower than those of lithofacies 2. After a 23 metres gap in the profile due to a vegetation-covered interval, the two lithofacies 3 and 4 are logged. Lithofacies 3 (light green colour in Figure 6) only occurs for a few metres in this main profile A along the upper road, however in the main profile B at the lower road it occurs in more significant thickness.

Profile A

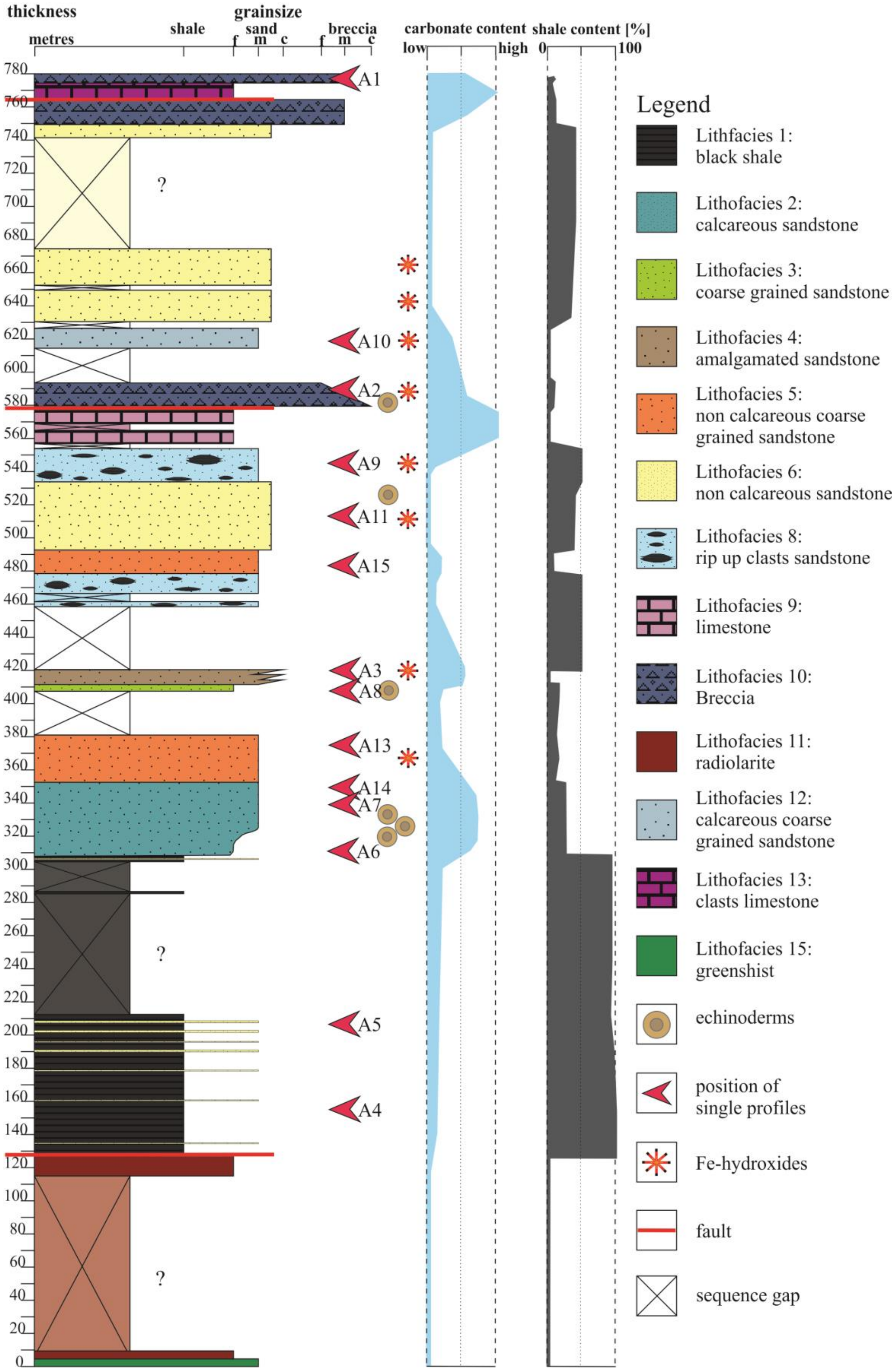
thickness
metres
grainsize
shale
sand
f m c
breccia
f m c
carbonate content
low
high
shale content [%]
0
100
780
760
740
720
700
680
660
640
620
600
580
560
540
520
500
480
460
440
420
400
380
360
340
320
300
280
260
240
220
200
180
160
140
120
100
80
60
40
20
0
?
?
?
A1
A10
A2
A9
A11
A15
A3
A8
A13
A14
A7
A6
A5
A4
Legend
Lithfacies 1:
black shale
Lithofacies 2:
calcareous sandstone
Lithofacies 3:
coarse grained sandstone
Lithofacies 4:
amalgamated sandstone
Lithofacies 5:
non calcareous coarse grained sandstone
Lithofacies 6:
non calcareous sandstone
Lithofacies 8:
rip up clasts sandstone
Lithofacies 9:
limestone
Lithofacies 10:
Breccia
Lithofacies 11:
radiolarite
Lithofacies 12:
calcareous coarse grained sandstone
Lithofacies 13:
clasts limestone
Lithofacies 15:
greenshist
echinoderms
position of single profiles
Fe-hydroxides
fault
sequence gap

Figure 6: The main profile A along the upper road was logged in the higher area of Thannberg. Included are carbonate content and shale content, the position of the logging of various single profiles, the occurrence of echinodermata remains and the occurrence of Fe-hydroxides.

Lithofacies 4 is characterized by amalgamated sandstones (sand-grey colour in Figure 6). This lithofacies shows thick graded sandstone banks and does not include any intercalating shale layers. After a gap of 38 metres lithofacies 8 (light blue colour in Figure 6) occurs. This lithofacies resembles lithofacies 5, however, the sandstone layers contain large black shale rip-up clasts, which clearly distinguish lithofacies 8 from any other lithofacies. Overlying lithofacies 8 for a few metres is again lithofacies 5. It could represent a transition zone between lithofacies 6, which shows a lack of carbonate and other carbonate lithofacies. After this second occurrence of lithofacies 5, lithofacies 6 is logged. Because of its nearly horizontal bedding, the field lithofacies 6 is exposed along a significant part of the road track. After a few metres of lithofacies 8 overlying lithofacies 6, lithofacies 9 occurs. This is the limestone lithofacies (pink colour in Figure 6). It is clearly separated from overlying lithofacies 10, the breccia-lithofacies (dark blue colour in Figure 6), by a fault. This lithofacies shows fining-upwards within its 10-15 meter of thickness. Between the two occurrences in profile A there are a few metres of lithofacies 12 (grey colour in Figure 6) and again lithofacies 6. The top of the profile is represented again by lithofacies 10 being intercalated by lithofacies 13. This lithofacies is reminiscent of the limestone lithofacies 9, only it also includes diverse clasts, consisting of e.g. dolomite and quartzite.

14 single profiles were logged in detail within this main profile A1-A11, A13 and A14 (see chapter 4). The carbonate content within the sandstone layers decreases towards the top (compare lit.2. vs. lit 6.). The shale content is especially low twice within the profile, mainly in the areas of lit.3, lit.5, lit10 and the limestone lithofacies lit.9 and lit.13.

8.5. Profile B, Lower Road Section

Profile B of the lower road only shows a total thickness of 390 metres. The general stratigraphic succession of lithofacies occurring within this profile roughly matches the order of lithofacies of profile A (visualized in identical colours in Figure 7). In contrast to profile A this profile does not include lithofacies 4, because no amalgamated, thick sandstone layers could be found. However, a 2.5 metres thick lithology, a feldspar-rich breccia, occurs at 358 m, which has not been observed in profile A, but is herein included into lithofacies 10 breccias.

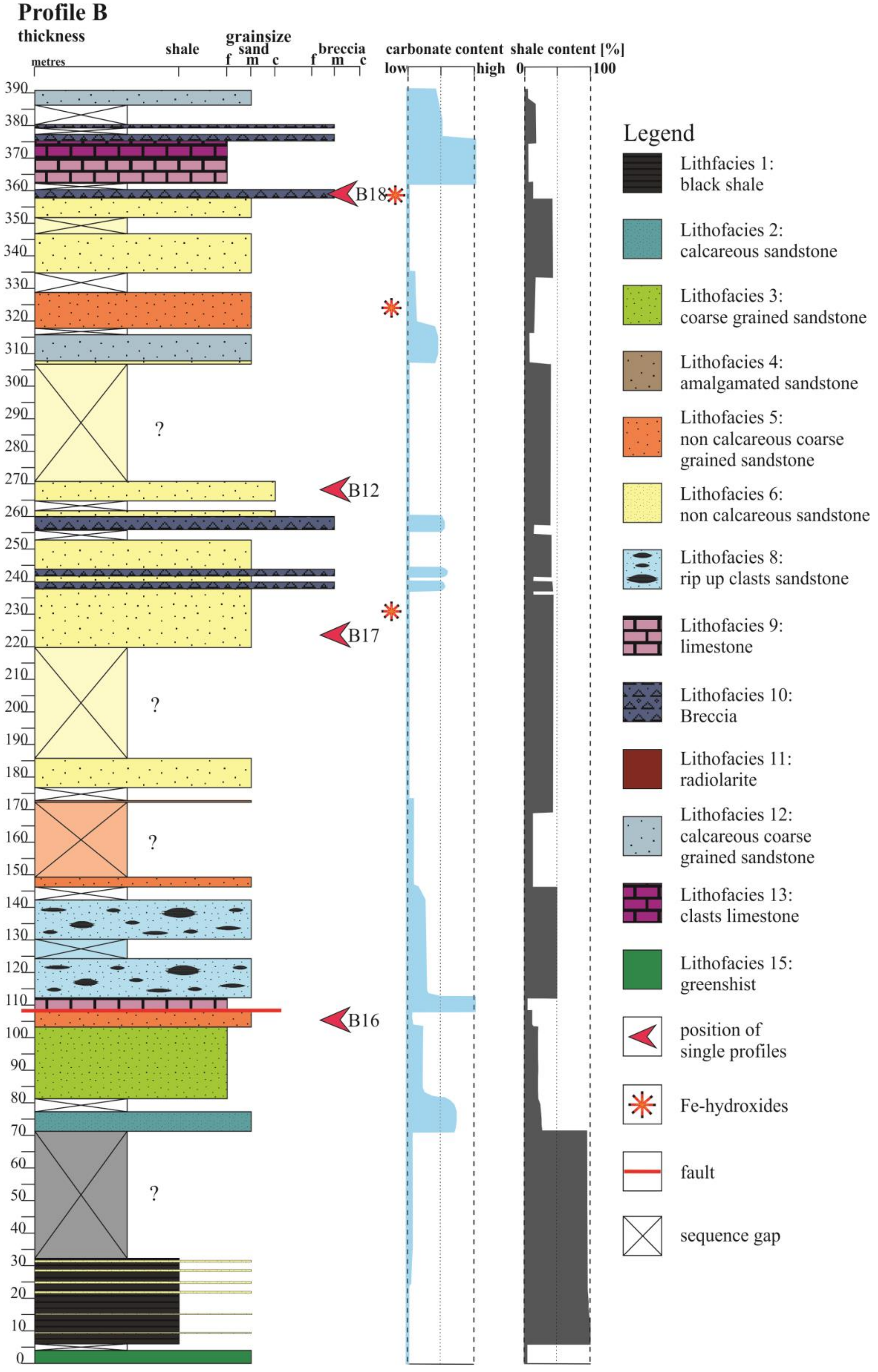

Figure 7: Profile B along the lower road was logged in the lower area of Thannberg. Included are the carbonate content and shale content, the position of the logging of various single profiles and the occurrence of Fe-hydroxides.

9. LITHOFACIES

9.1. GENERAL DESCRIPTION

To document and describe the distinguished lithofacies associations as accurate as possible, all together 13 lithofacies were distinguished. However, these 13 lithofacies combine all lithofacies shown in the main profiles, not just those related to the flysch sedimentation. Only the 11 “flysch-type” lithofacies are further evaluated in detail and documented with single profiles. These representative single profiles were taken and sampled to give a better impression of each defined lithofacies. The comparison of the single profiles within different lithofacies helps to bring out the subtle distinctions between them more clearly.

9.2. LITHOFACIES 1: BLACK SHALE

The predominant black shale lithofacies marks the beginning of the clastic Tauern Flysch sedimentation in the area and the bottom of main profile A. In the profile it is marked as lithofacies 1. It is separated from the chert lithofacies by a normal fault, which overlies the greenschist lithofacies at the very bottom of the profile.

The sandstone layers to shale layers relation in most areas of this lithofacies is 2 percent of sandstone layers to 98 percent of black shale layers. Only a few sections show up to 5 percent of sandstone layers (sandstone/shale ratios ca. 1:50 to 1:20). Shale intervals in general can show high amounts of silt layers interbedded with shale layers. These silt layers display brighter colours, like beige or light grey. They can easily be identified in the field and differentiated from the fine-grained, darker shale layers, by help of a magnifying glass or through further sample preparation and analysis in the laboratory. The most common type of shale, observed in the field, is black-coloured. It is fine-grained, shows layers and strong schistosity. It breaks brittle and flaky in layers of only a few millimetres thickness. Rarely silver-coloured shale can be found. Occasionally traces of graphite within the shale were observed. Interbedded, thin sandstone layers were found within the black shale of lithofacies 1 and sampled. This sandstone layers reach a maximum bed size of 2.5 cm. Their average bed size is about 0.5 cm. They show slightly calcareous behaviour in the field and comprise very little amounts of white mica. On the whole lithofacies 1 shows slight coarsening upwards trend, as more and more interbedded sandstone layers occur.

The two single profiles A4 and A5 (Figure 8) of lithofacies 1 are characterized by extremely fine-grained thin-bedded black shales, easily distinguished from other lithofacies within the profile, with interbedded fine-grained sandstone layers. No silver-grey coloured shale layers, compared to higher parts of the main profile were observed.

Several black shale samples have been taken in the field for palynology analysis. Out of those samples, the optically least deformed six samples were sent to Polina Pavlishina, Sofia University in Bulgaria for pollen analysis. Unfortunately, the attempt to find pollen in the samples was unsuccessful. Every trace of fossil evidence for sedimentation age was probably erased by the metamorphism.

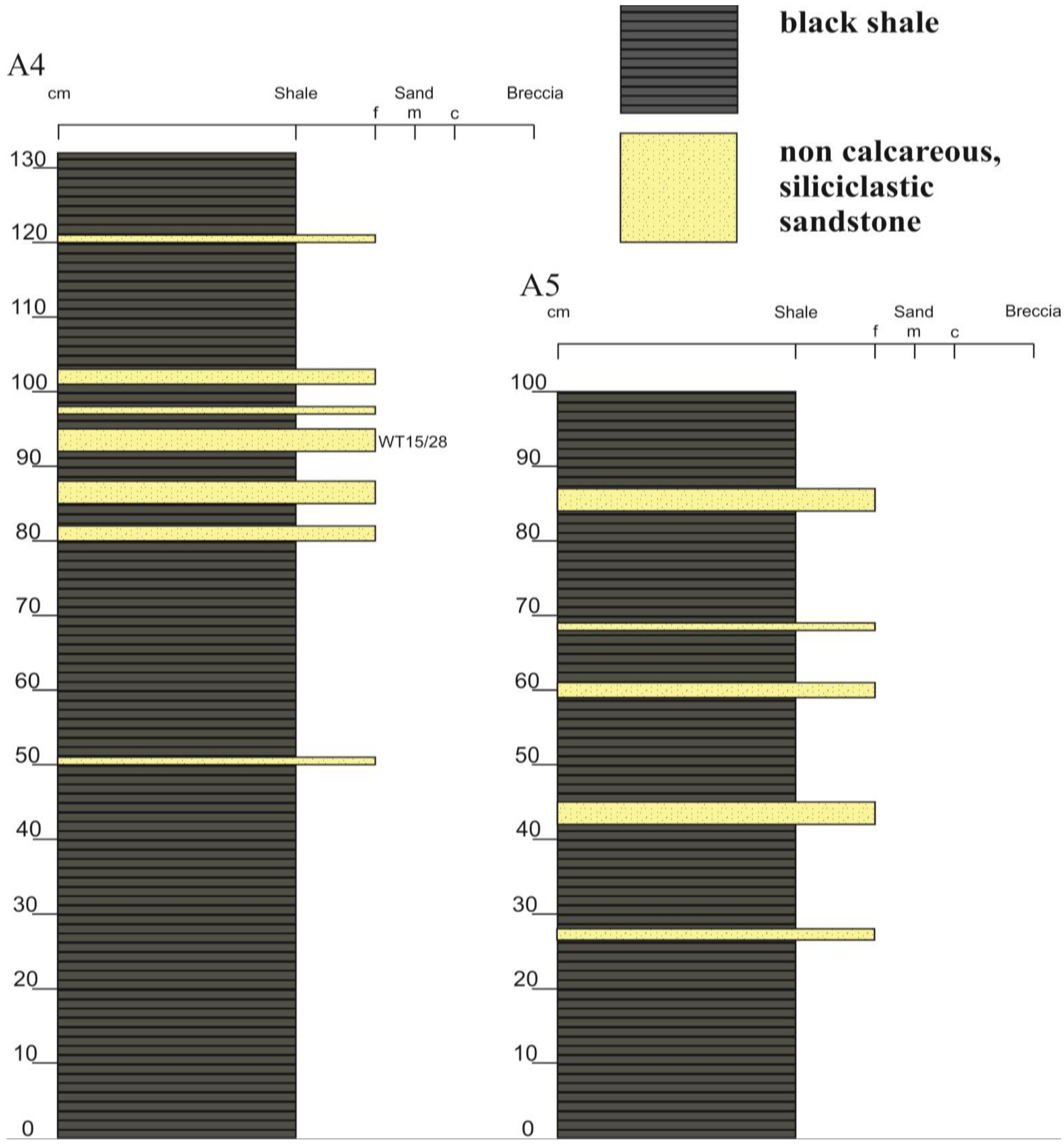

Figure 8: The two single profiles A4 and A5 show the characteristic alternation of black-shale layers and sand layers of lithofacies 1. The exact position of sampling WT15/28 is marked in the single profile A4.

9.3. Lithofacies 2: Calcareous Sandstone

The calcareous sandstone lithofacies 2 overlies the black shale lithofacies. It shows a thickening- and coarsening-upwards trend of both the bedding and the grain size within its total occurrence in the profile.

The lithofacies consists of an alternation of sandstone and shale layers. The sandstone layers to shale layers relation in most areas of this lithofacies is 80 percent of sandstone layers to 20 percent of shale layers (sandstone/shale ratio 4:1). The sandstone layers are middle- to coarse-grained and show thin-bedding with bed thicknesses up to 15 cm. They comprise a lot of carbonates (marked by a bluish colour in Figure 9) and more white mica than any other lithofacies. Two types of shale were recognized in the field, silver-grey-coloured shale (grey in Figure 9) and black-coloured shale (black in Figure 9). However, the differentiation of these two types is solely based on their optical appearance in the field and not on their general composition.

Three single profiles (see Figure 9) have been logged A6, A7 and A14. The outcrops of lithofacies 2 are well reachable. The two single profiles, A6 and A7, were taken in a lower area of lithofacies 2 (A6 at 310 meters and A7 at 322 meters of profile A) and show the typical alteration of sandstone and shale layers. The profile A14 was taken in the upper part of the calcareous sandstone lithofacies that was extremely rich in carbonates. In this area pure limestone beds are present (pink colour in Figure 9). This single profile was turned upside down, because of the graded (coarse to middle) bed at 92 -104 metres which shows inverse grading in the field, suggesting tilting or (local) folding.

A closer look at the thin sections of lithofacies 2 (see Figure 10) shows a strong dominance of carbonate minerals, especially calcite cement. In general the material is strongly recrystallized. However, remnants of echinoderms as cloudy single overgrown calcite crystals were observed. Other occurring minerals are quartz, feldspar (most commonly in WT15/39) and more seldom mica components. Mica bands are absent. The averages of the maximum grainsizes of the measured samples show a maximum of 1.8 mm.

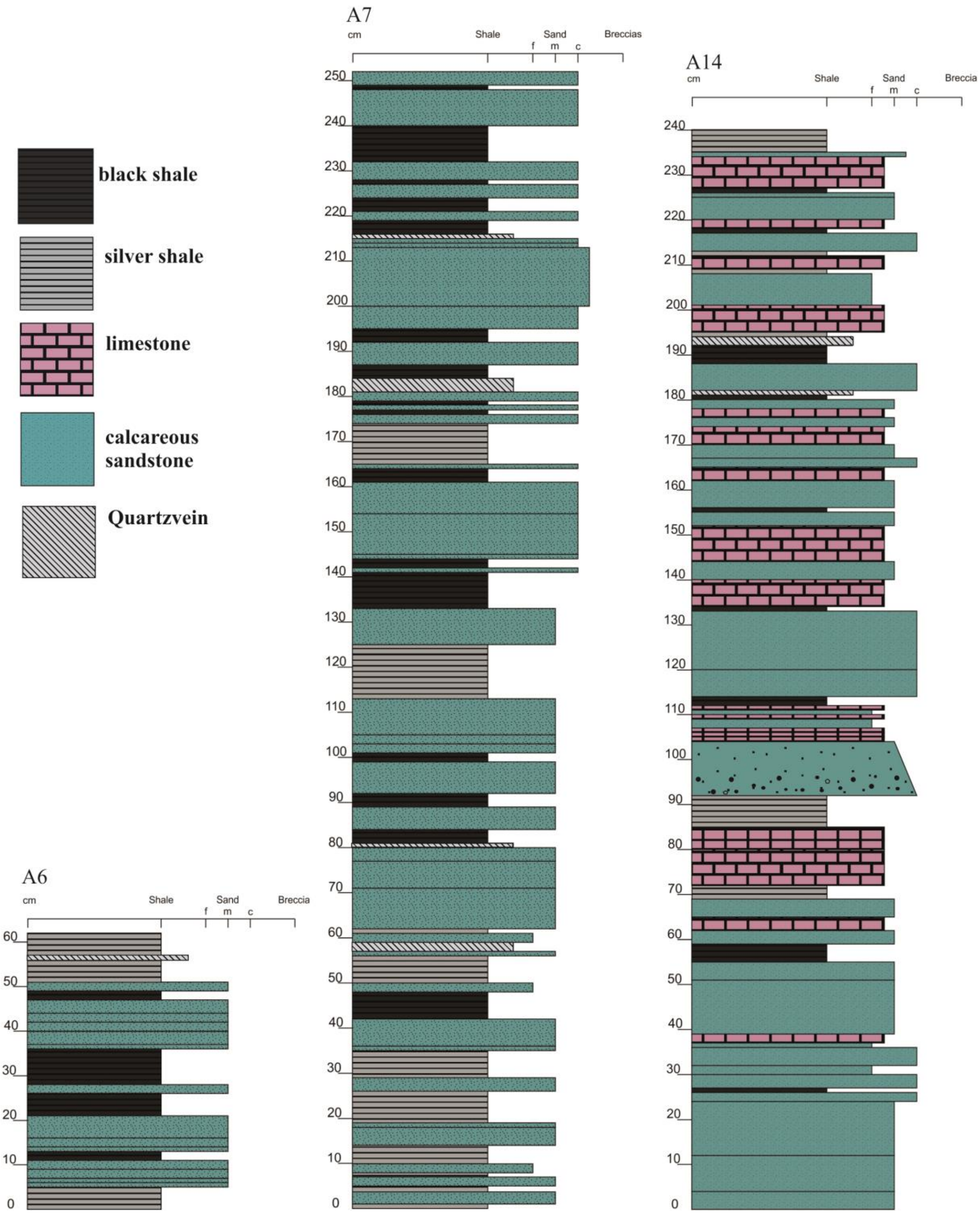

Figure 9: The three single profiles A6, A7 and A14 show the characteristic alternation of calcareous sandstone layers and black and silver coloured shale layers of lithofacies 2. The silver coloured shale layers are partly predominant. A14 also shows limestone layers inter bedding.

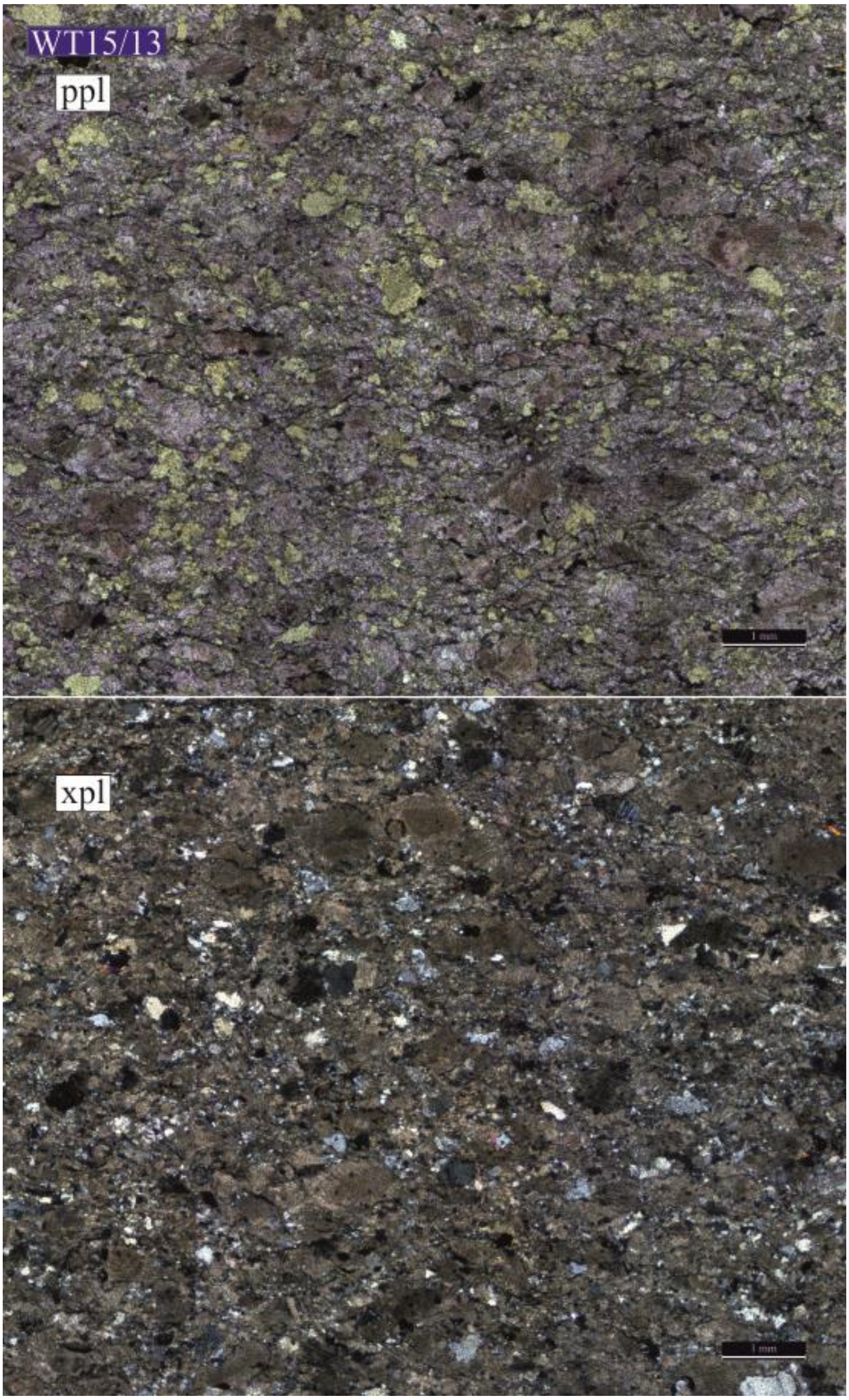

Figure 10: Overview of the thin section of sample WT15/13 of lithofacies 2 shown with parallel polarizers (ppl) at the top and crossed polarizers (xpl) at the bottom.

9.4. LITHOFACIES 3: COARSE-GRAINED SANDSTONE

The coarse-grained sandstone lithofacies 3 overlies lithofacies 5 (non-calcareous coarse-grained sandstones) and is overlain by lithofacies 4 (amalgamated sandstones). Thickness is only four meters in profile A, but a total thickness of 22 metres is present in profile B. The alternation of sandstone layers and shale layers displays a sandstone to shale ratio of 85 percent of sandstone layers and 15 percent of shale layers (sandstone/shale ratio ca.6:1).

The detailed profile A8 (see Figure 11) of section B displays the typical succession of sandstones interbedded by solely silver-grey coloured shale. This is the only lithofacies showing a complete lack of black shales. Other than the overlying amalgamated sandstone lithofacies lithofacies 3 does not include any visible graded sandstone beds - the majority of sandstone beds of lithofacies 3 are around 20 to 25 cm thick, middle to thick bedded and coarse-grained throughout. They show hardly any calcareous content and are barren of detrital white mica. These coarse-grained, thick-bedded non-calcareous massive sandstone (yellow colour in Figure 11) differ clearly from few thinner, calcareous, fine-grained sandstone layers

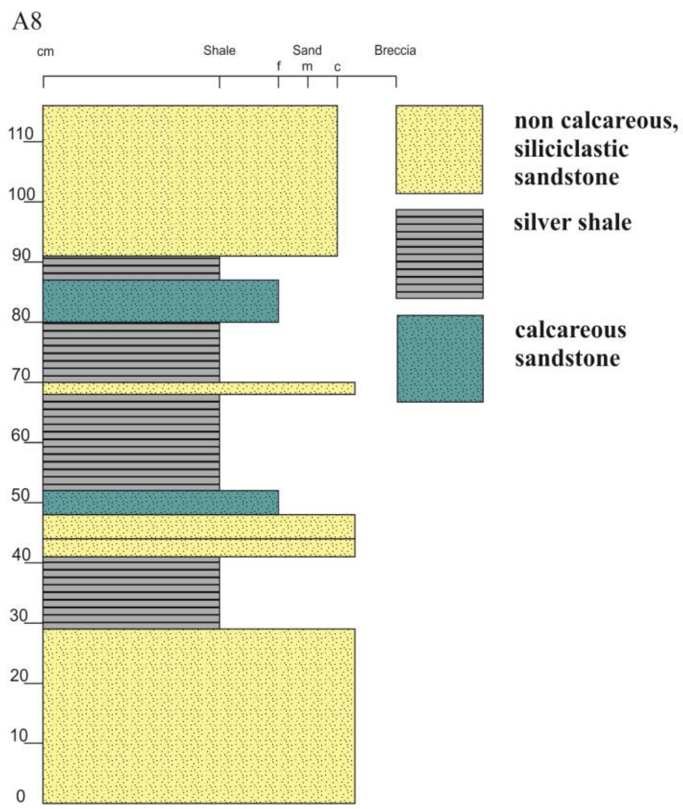

Figure 11: Single profile A8 shows the characteristic alternation of almost carbonate-free sandstone layers, a few carbonatic sandstone layers, and silver coloured shale layers.

(bluish in Figure 11). These smaller, thin-bedded, intercalated fine-grained sandstone layers show a significant amount of calcite of 77% (compare WT15/16;Figure 12). There is a clear difference in grainsize between calcite clasts, which partly contain remnants of echinoderms, and fine-grained calcite cement (see Figure 12). Other components observed within WT15/16 are quartz, feldspar and rare single mica flakes. Commonly thin layers of mica together with Fe-hydroxides (probably former Fe-rich clay layers) occur, showing pressure solution in the form of micro-stylolites.

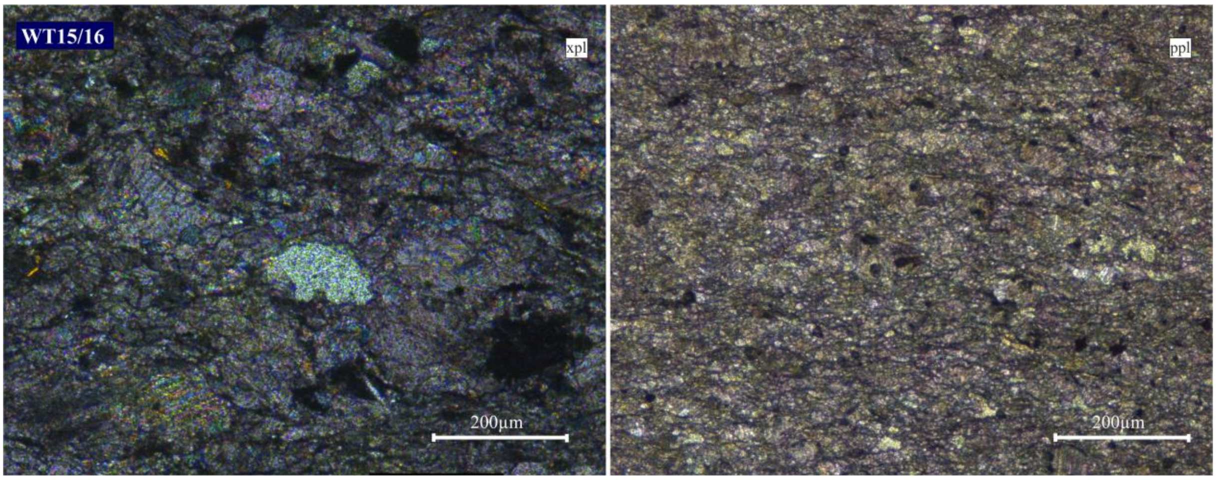

Figure 12: Overview of the thin section of sample WT15/16 of lithofacies 3 shown with parallel polarizers (ppl) on the right side and crossed polarizers (xpl) on the left side. Note the difference in magnification and therefore in scale of 1mm for the section using ppl on top and 200µm for the close up calcite cement section using xpl at the bottom.

9.5. LITHOFACIES 4: AMALGAMATED SANDSTONE

The amalgamated sandstone lithofacies 4 overlies the lithofacies 3. It shows a total thickness of 10 meters in profile A, but was not found within profile B. The main characteristic of this lithofacies is that it consists of very thick, graded sandstone beds of a bed thickness of up to 1m. It also differs from the other lithofacies, by the complete absence of any shale layers.

The sandstone layers show grading starting off with a middle to coarse sand grainsize at the bottom of every layer and ending up with an extremely fine sand grain size at the top of every layer. The fine-grained top parts of the layers and also partly areas within the layers show parallel lamination (profile A3, Figure 13). Comprising hardly any calcareous components, the sandstone beds are also depleted of white mica.

The single profile A3 shows the characteristic thick beds of lithofacies 4. It has a total thickness of 3.3 m and includes 4 thick sandstone beds. They all show grading and faint lamination parallel to the bedding mostly at the top parts of every bed. Additionally, the bed at 0.65 to 1.56 m shows lamination parallel to the bedding also at a finer grained interval within the bed as well as at the top. The two beds that represent the top of A3 are slightly coarser grained than the two beds at the bottom.

All of the samples taken from this lithofacies have a high content of feldspar and quartz (see chapter thin sections). However, one of the samples (WT15/18) shows also a significant amount of carbonates. This sample was taken from the middle part of a graded bed at the base of the lithofacies in profile A. The averages of the maximum grainsizes of the measured samples is 1.80 mm in the coarsest interval at the bottom of the bed, 1.19 mm in the middle and 0.67mm at the top of the bed.

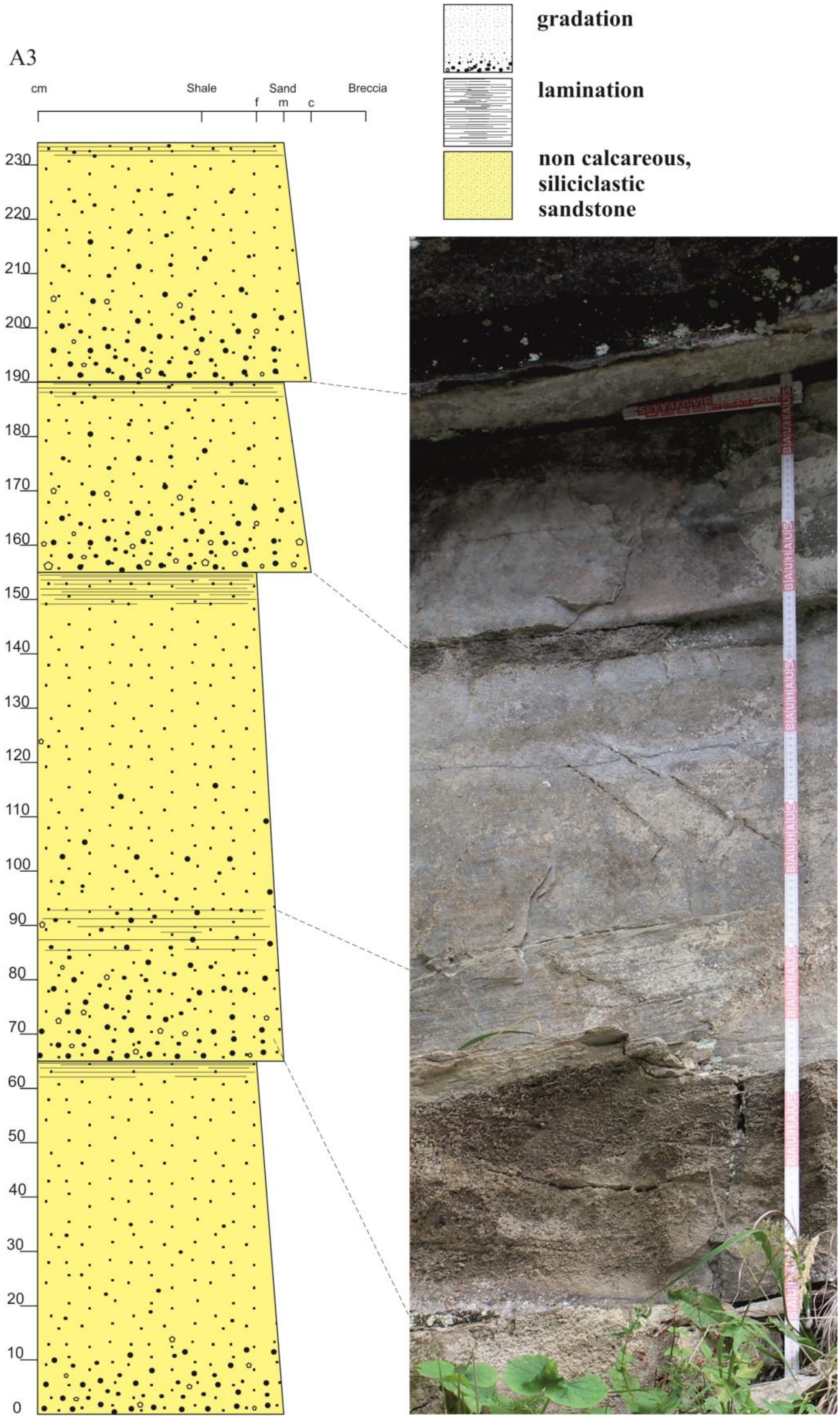

Figure 13: The single profile A3 shows the characteristic thick beds of lithofacies 4. The photograph on the right shows what the beds look like in the field. Dashed lines connect areas in the profile with their real position in the photograph. The scale on the photograph shows red and white areas where every coloured part stands for 10 centimetres.

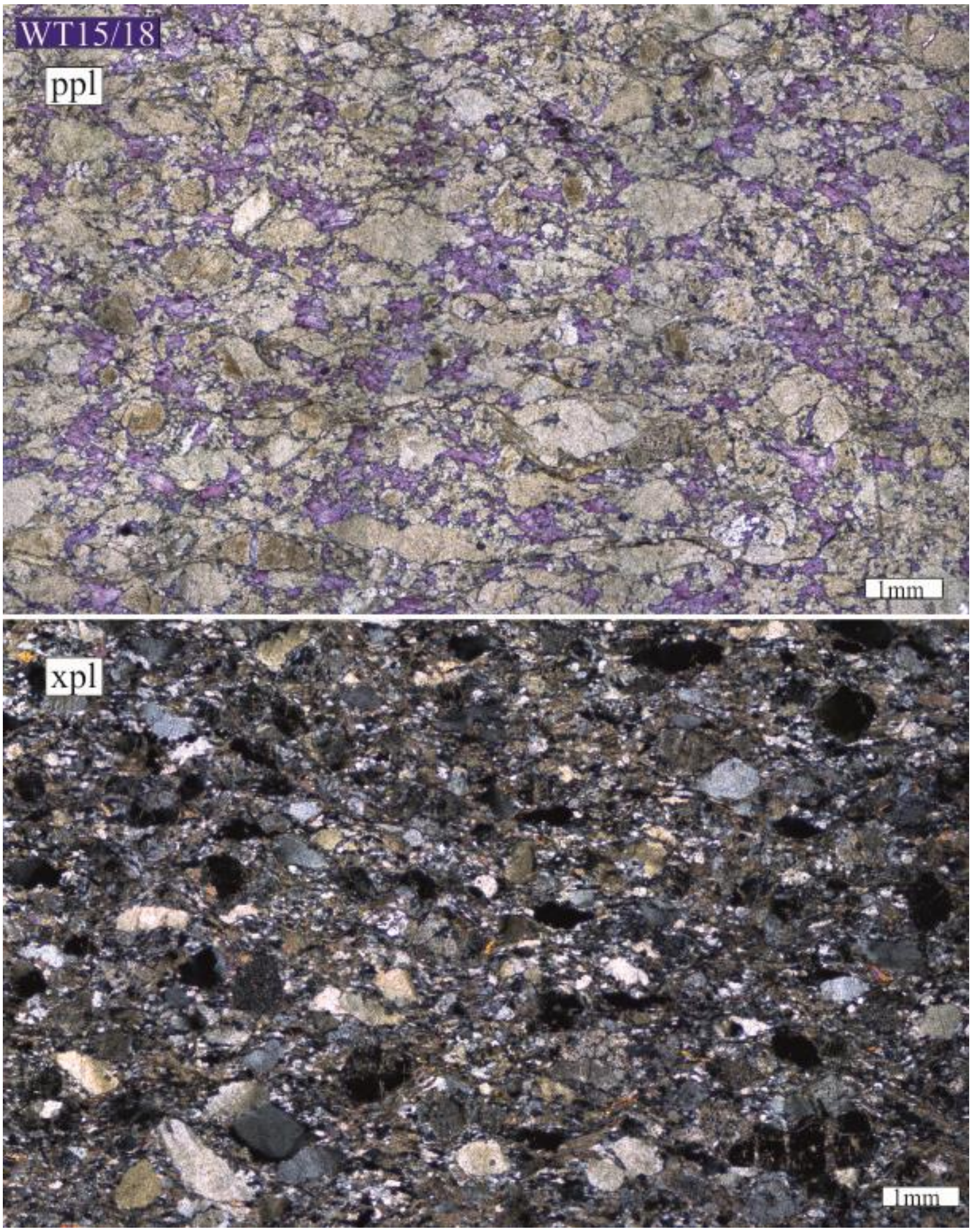

Figure 14: Overview of the thin section of the sample WT15/18 of lithofacies 4 taken in the middle-coarse grained area of these graded beds shown with parallel polarizers (ppl) at the top and crossed polarizers (xpl) at the bottom. The pink areas in the ppl figure is coloured calcite.

9.6. LITHOFACIES 5: NON-CALCAREOUS COARSE-GRAINED SANDSTONE

Characteristic for the non-calcareous coarse-grained sandstone lithofacies is the thick bedding of the sandstone layers and the coarse grain size, a conspicuous feature of this lithofacies. The sandstone layers to shale layers relation is 92 percent of sandstone layers to 8 percent of shale layers (sandstone/shale ratio ca. 12:1). This lithofacies occurs in both profiles A and B several times. It could alternatively also be seen as a transitional lithofacies between lithofacies 6 and lithofacies 8, and it usually occurs in contact with at least one of them in both profiles.

In general the sandstone layers are non-calcareous, although calcareous clasts were found rarely in the sandstone. Also other clasts were identified such as small rip-up clasts consisting of shale which are remindful of the “rip-up clasts lithofacies” in higher areas of the two main profiles.

Figure 15: The bedding of the sandstone layer of lithofacies 5 is marked in green colours. Boudinage of a quartz vein is marked in blue.

Other components that are comprised within the sandstone layers are small components that appeared black in the field, turning out to be small pyrite crystals, recognized under the microscope. The sandstone layers comprise hardly any white mica.

The averages of the maximum grainsizes of the measured samples are 2.39 mm in the coarser interval and 2.19 mm in the less coarse parts.

Also fine quartz veins can occur parallel to the bedding, partly showing boudinage (see Figure 15), i.e. deformed during metamorphism caused by stretching.

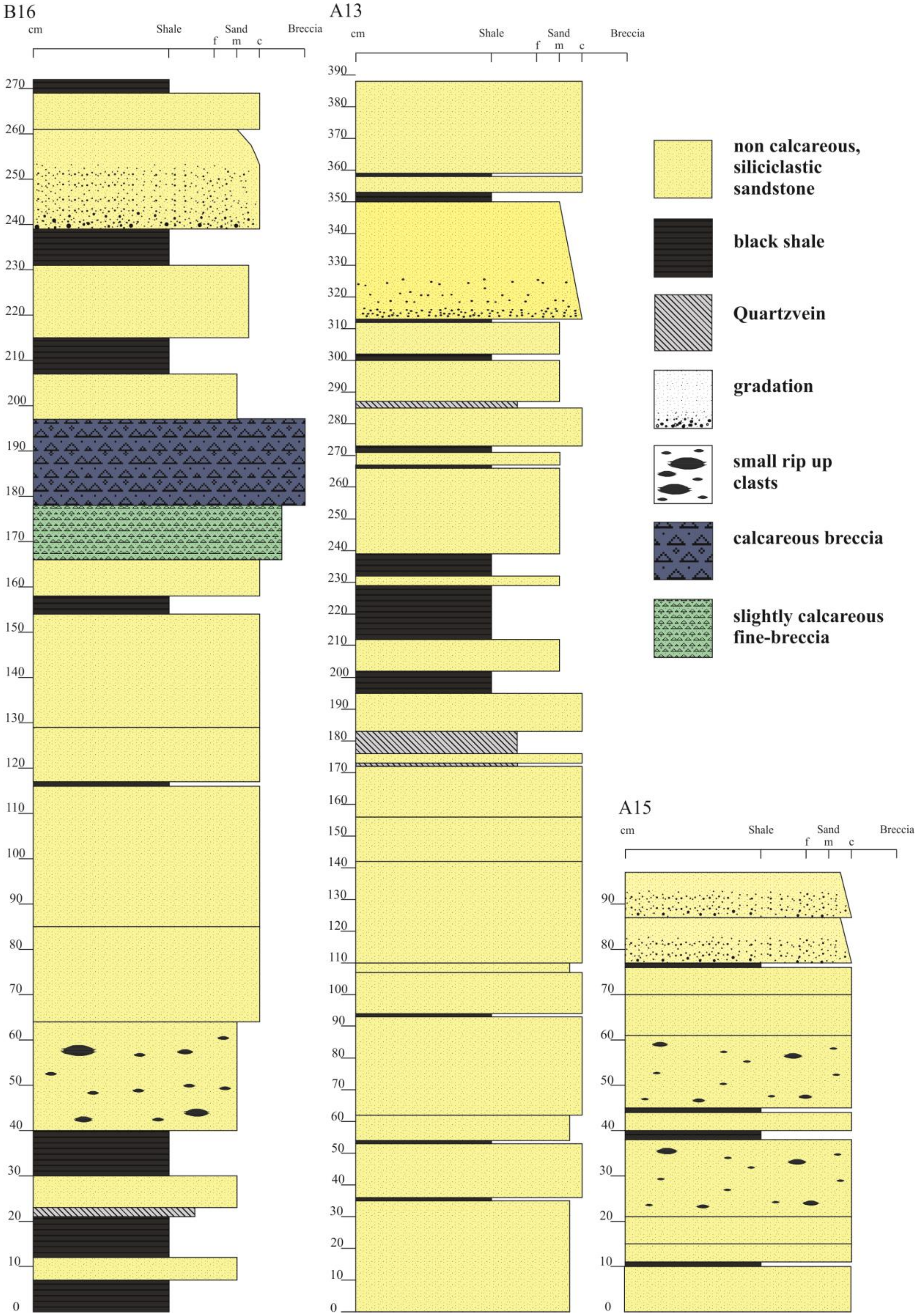

Figure 16: The single profiles A13 and A15 show the characteristics of lithofacies 5; thick non-calcareous sandstone layers and small thin black shale layers interbedding. A15 also contains small rip-up clasts. Graded beds occur in both single profiles.

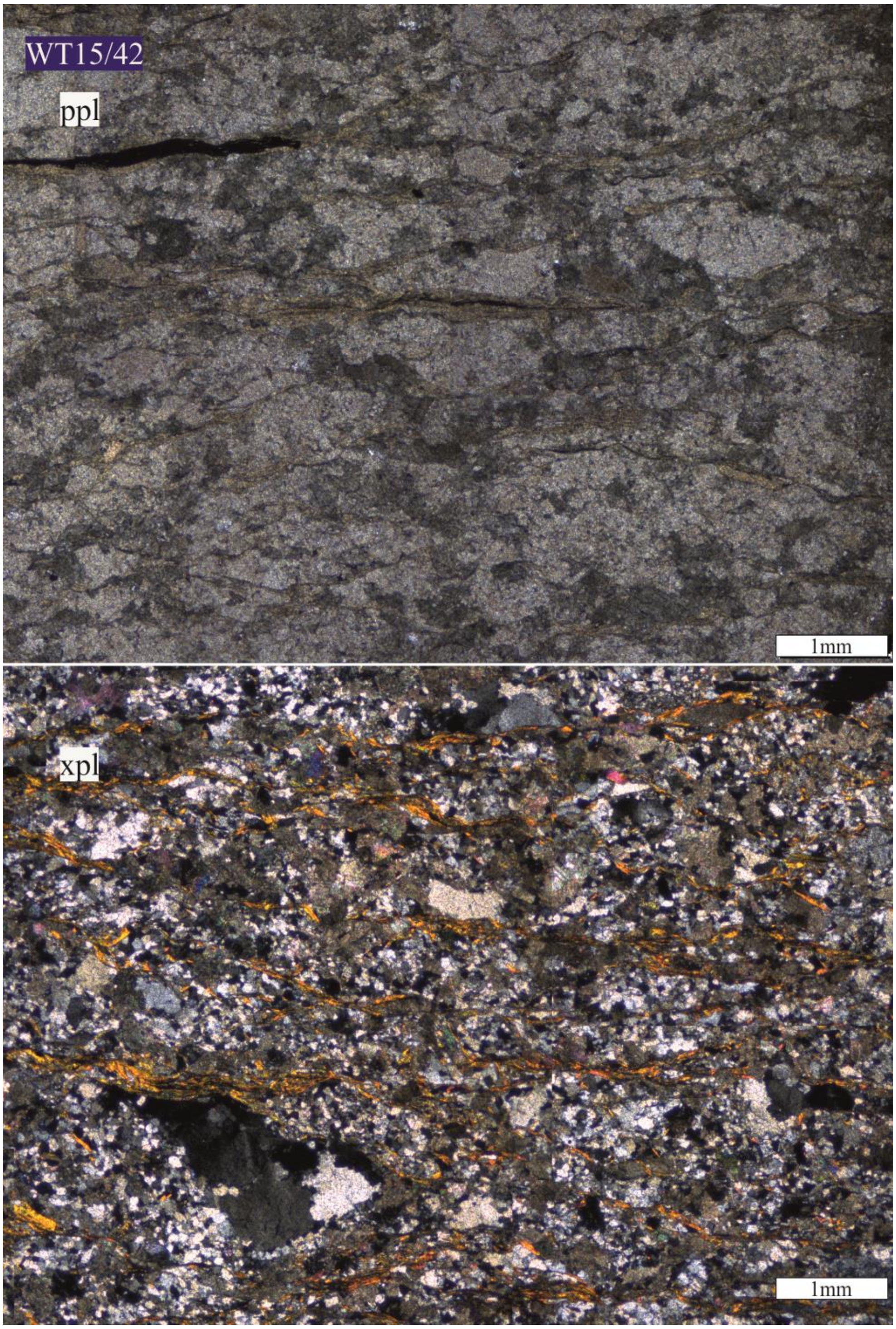

Figure 17: Overview of the thin section of sample WT15/42 of lithofacies 5 shown with parallel polarizers (ppl) at the top and crossed polarizers (xpl) at the bottom.

9.7. Lithofacies 6: Non-calcareous sandstone

In contact with the “non-calcareous coarse-grained sandstone lithofacies” in almost all areas of its occurrence in the main profiles is the non-calcareous sandstone lithofacies 6. Compared to lithofacies 5 it shows thinner bedding and a clear difference in sandstone layer to shale layer relation of 60 to 40 % (sandstone/shale ratio 1.5/1).

Lithofacies 6 represents the most frequent lithofacies in both main profiles. It shows a typical alternation of middle-coarse-grained sandstone layers, black shale layers and rarely layers of fine-breccia interbedded as shown in the single profiles B12 and B17 (Figure 19). A third single profile (A11) was taken in the transition area between lithofacies 5 (bottom of the single profile A11) and lithofacies 6 (top of the single profile A11) (see Figure 19). Here, grainsize and bedding thickness decreases and the shale content increases towards the top. The averages of the maximum grainsizes of the measured samples are 1.52 mm in the coarser intervals and around 0.61mm in finer intervals. Both the layers of sandstone and the layers of breccia comprise almost no white mica. No silver-grey-coloured shale layers were observed. Worth mentioning, is a big cubic pyrite-crystal with the size of 2.5 x 3.0 mm found in the sample WT15/45.

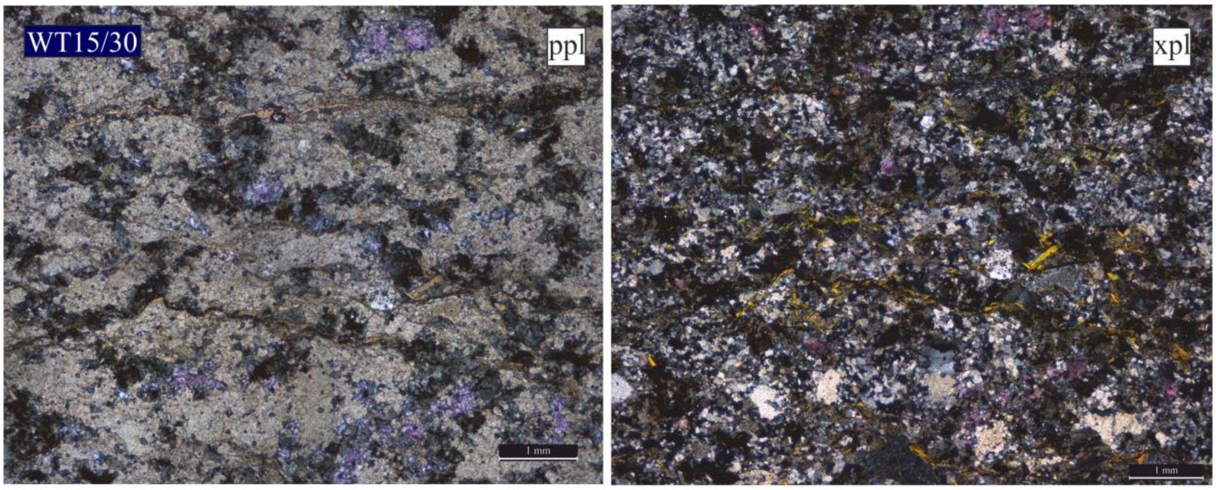

Figure 18: Overview of the thin section of sample WT15/30 of lithofacies 6 shown with parallel polarizers (ppl) at the top and crossed polarizers (xpl) at the bottom.

Figure 19: the single profiles B12 and B17 show the typical alternation of sandstone layers, shale layers, and two different types of breccia layers. The single profile A11 represents the transition zone between lithofacies 5 and lithofacies 6 and therefore shows fewer amount of shale layers than B12 and B17. Intercalated quartz veins and graded sandstone beds also occur.

9.8. LITHOFACIES 8: SANDSTONE WITH RIP-UP CLASTS

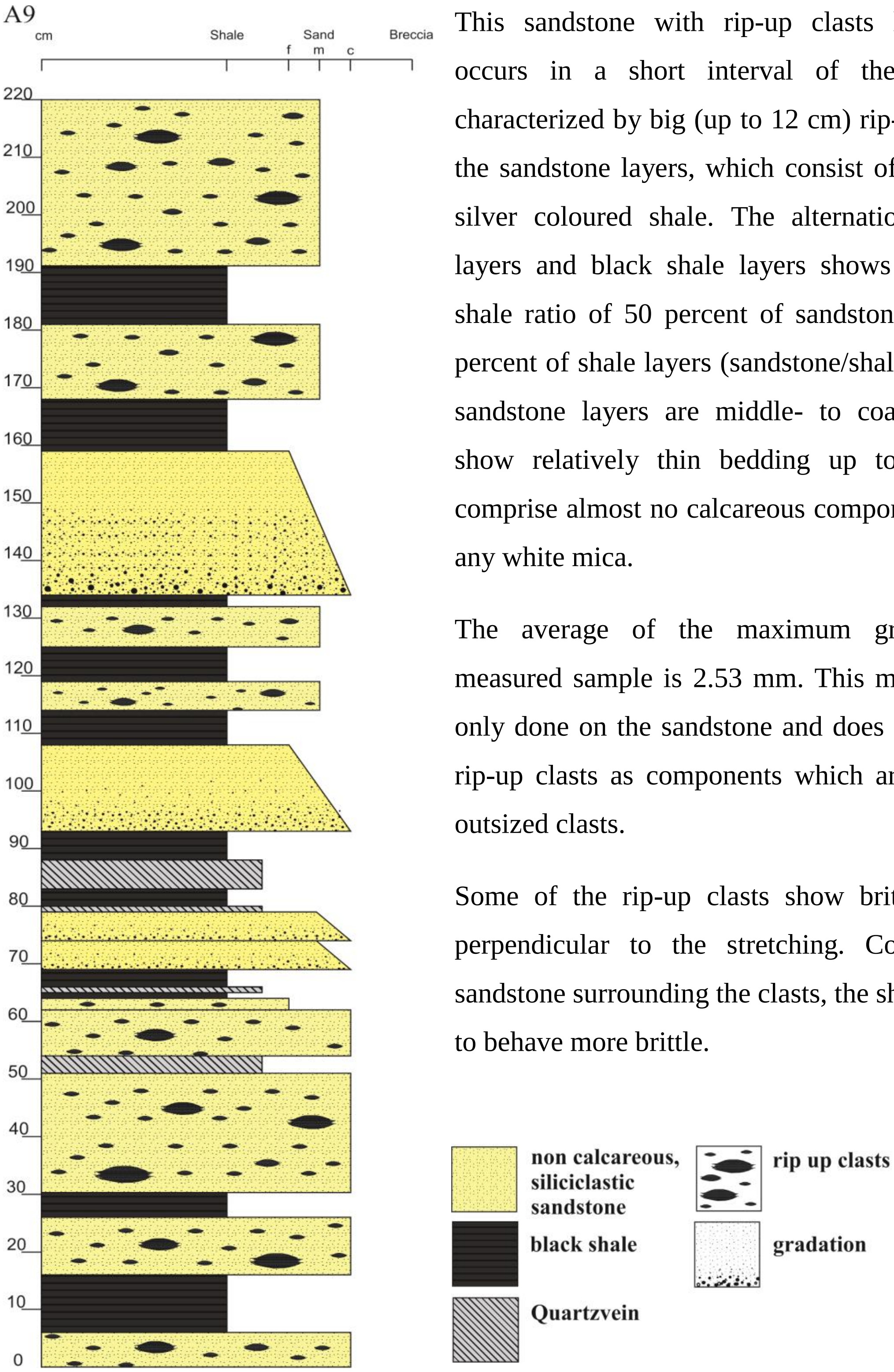

This sandstone with rip-up clasts lithofacies only occurs in a short interval of the profile. It is characterized by big (up to 12 cm) rip-up clasts within the sandstone layers, which consist of both black and silver coloured shale. The alternation of sandstone layers and black shale layers shows a sandstone to shale ratio of 50 percent of sandstone layers and 50 percent of shale layers (sandstone/shale ratio 1:1). The sandstone layers are middle- to coarse-grained and show relatively thin bedding up to 25 cm. They comprise almost no calcareous components and hardly any white mica.

The average of the maximum grainsize of the measured sample is 2.53 mm. This measurement was only done on the sandstone and does not consider the rip-up clasts as components which are interpreted as outsized clasts.

Some of the rip-up clasts show brittle deformation perpendicular to the stretching. Compared to the sandstone surrounding the clasts, the shale blocks seem to behave more brittle.

Figure 20: The single profile A9 shows the characteristic alternation of lithofacies 8. Middle to thick bedded, rip up clasts containing middle to coarse-grained sandstone beds are visualized in yellow colour with black dots as explained in the lithofacies on the right side. Graded sandstone layers and black shale layers are intercalating these sandstone beds.

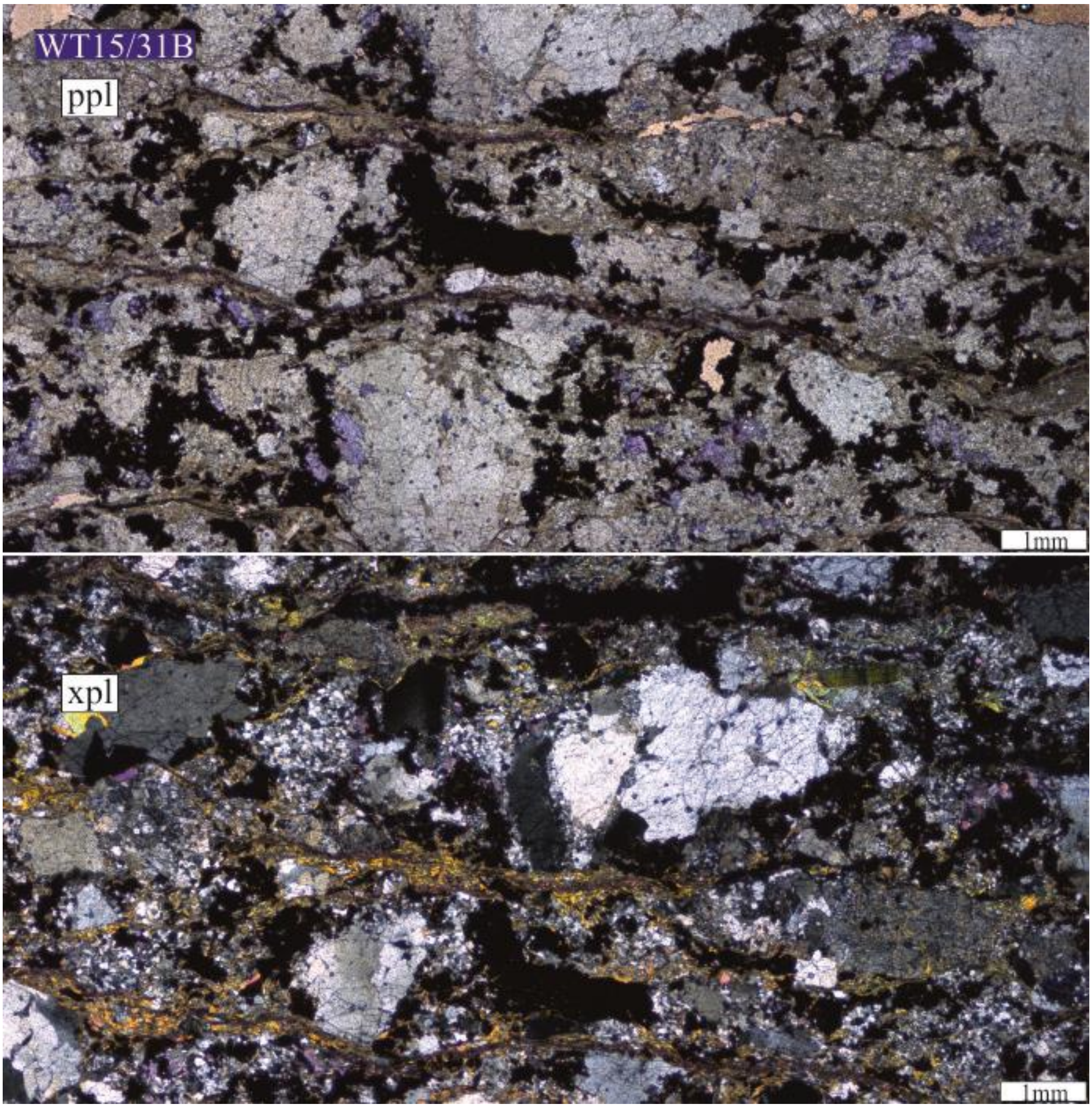

Figure 21: Overview of the thin section of sample WT15/31B of lithofacies 8 shown with parallel polarizers (ppl) at the top and crossed polarizers (xpl) at the bottom.

9.9. Lithofacies 9: Limestone

All together limestone occurs in two different lithofacies, which can be distinguished by whether they contain clasts of other materials or not. Thus, limestones without clasts are grouped into lithofacies 9 (“limestone lithofacies”), the others into lithofacies 13 (“clasts-containing limestone”).

The limestone lithofacies 9 has a recrystallized crystalline appearance in most intervals. It occurs overlying lithofacies 8, the sandstone with rip-up clasts, and terminates at the sharp contact to the breccia lithofacies 10 at 580 metres in profile A. However, in profile B lithofacies 9 occurs twice. Its first occurrence in profile B is at 108 m overlying lithofacies 5 with a thickness of only 4 m and its second occurrence is at the top of this profile with a thickness of 6 m, being overlain by the second limestone lithofacies 13. The different stratal context of the two occurrences argues against doubling by folding or faulting.

The lithofacies is mostly massive, though within some intervals, fine lamination has been recognized as in sample WT15/21.

Figure 22: The photograph shows the contact between lithofacies 9 at the bottom and lithofacies 10 at the top. This faulted contact (red line) is positioned at 580 metres in profile A.

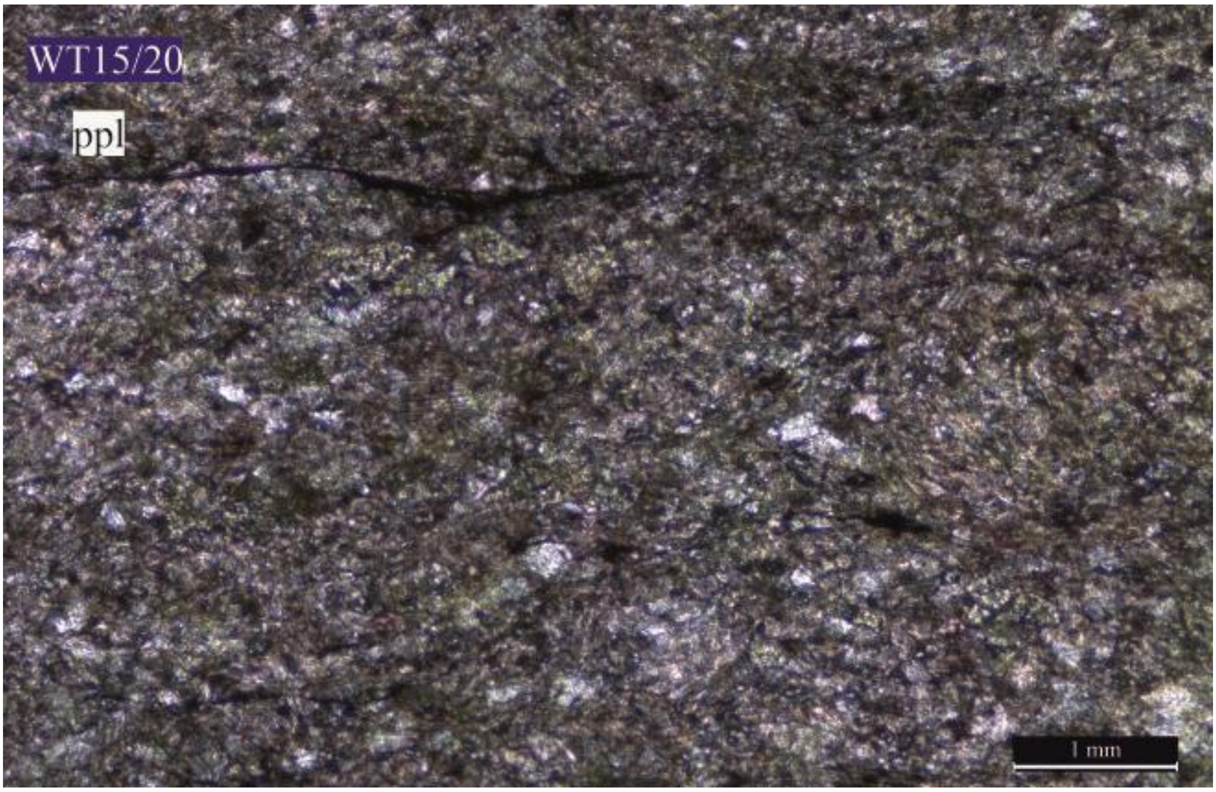

Figure 23: Overview of the thin section of sample WT15/20 of lithofacies 9 shown with parallel polarizers (ppl).

9.10. Lithofacies.10: Breccia

The breccia lithofacies only occurs in the higher parts of the profiles and marks the profile's top of profile A, in which has its first occurrence at 580 m overlying lithofacies 9. The two lithofacies are separated by a (brittle) fault (Figure 22). Lithofacies 10 predominantly consists of layers of calcareous fine-grained breccias. These layers are only a few centimetres thick and do not show any grading. The components reach grain sizes of up to 15 mm, not including outsized rip-up clasts. The bigger clasts within the breccia mainly consist of dolomite and limestone rock fragments. The dolomite clasts are easily recognized in the field because of their characteristic yellow-light brown-grey colour, caused by weathering. However, less commonly also bigger quartzite clasts can appear within the breccia (Figure 24). Only one breccia layer of 2.5m contained high amounts of feldspar and minor carbonate clasts (profile B). Intercalated with the breccia layers are middle- to coarse-grained sandstone layers and black and less commonly silver-grey-coloured shales. The sandstone layers do not show any calcareous content in the field and have a maximum bed size of 6 cm. However, the average bed size of these thin sandstone layers is only 1.5 to 2 cm and they mostly occur in contact with black shale layers.

Various rip-up clasts were observed as clasts within the coarser grained areas of the breccia beds (see Figure 24). Both, smaller black-coloured rip-up clasts and bigger, over 10 cm long silver-grey-coloured rip-up clasts were observed.

The sandstone/breccia layers to shale layers ratio is 90/10 (sandstone/shale ratio 9/1). Two single profiles (see Figure 25), A1 and A2, show the characteristics of this lithofacies more clearly, with A2 at the first occurrence of this facies in profile A, and A1 at the top of this profile. A2 shows a higher black shale content than A1. The coarse-grained sandstone layers show thin bedding of a maximum bed size of 2 cm and an average bed size of 1 cm. The single profile A1 shows the contact between lithofacies 13, limestone layers containing clasts (pink in Figure 25), at the bottom overlain by the breccia at its top. The fault separating the two lithofacies is marked with a red line. Other than A2, A1 shows less shale content and thicker beds of both the breccia layers and the middle- grained sandstone layers. All together lithofacies 10 shows faint thickening-upwards as more and more of the thicker breccia layers occur.

Figure 24: The photograph shows part of lithofacies 10; the different coloured arrows show special components that occur: silver-grey-coloured and black coloured rip-up clasts and bigger components within the breccia such as dolomite (orange) and quartz (purple).

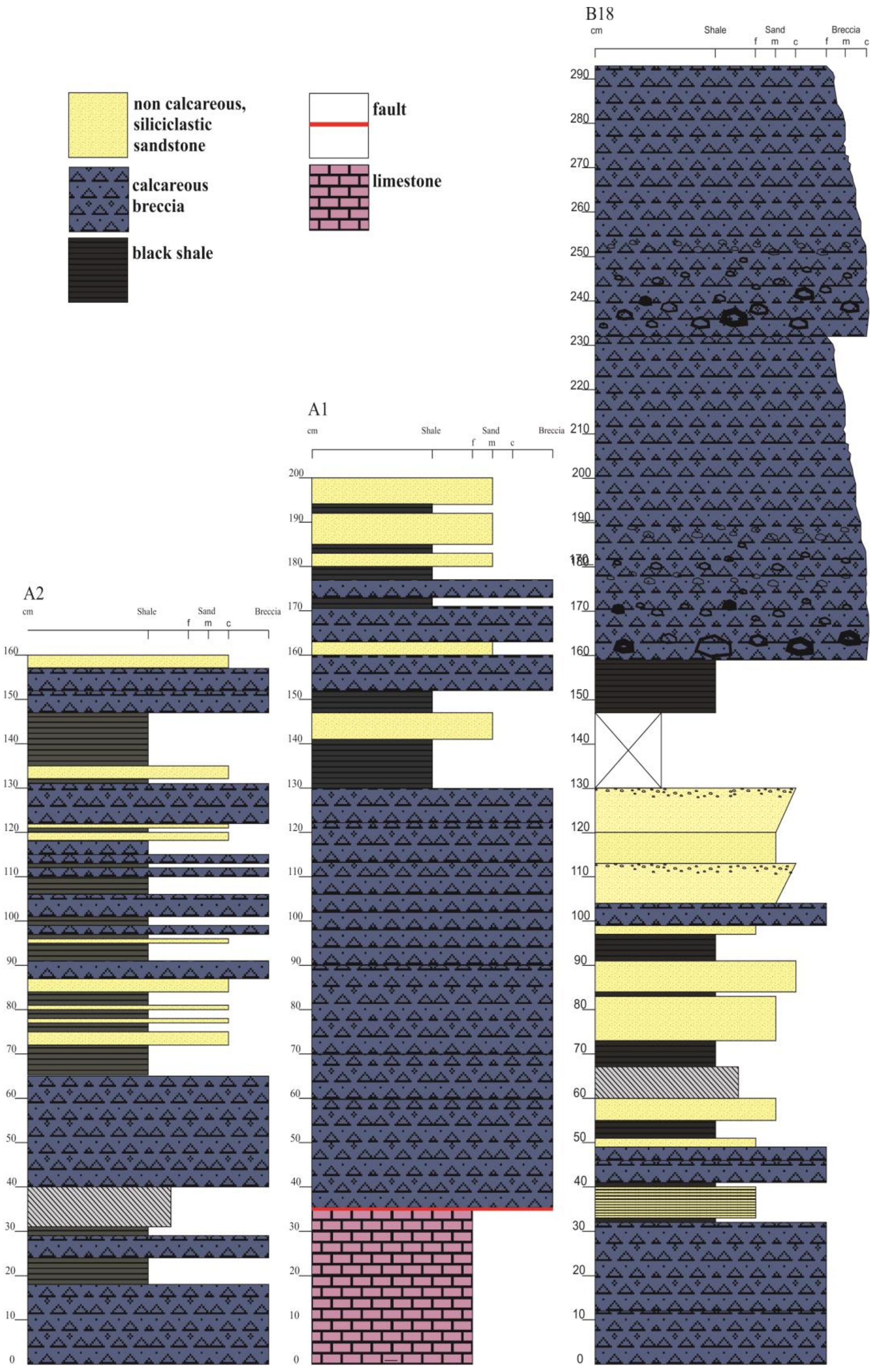

Figure 25: The single profiles A1, A2 and B18 show the characteristic alternation of lithofacies 10. A1 was taken in the highest area that lithofacies 10 occurs in and shows limestone layers of lithofacies 9 at its bottom. The dark blue coloured layers are calcareous breccia. Intercalating coarse-grained non-calcareous sandstone layers and black shale layers occur repeatedly.

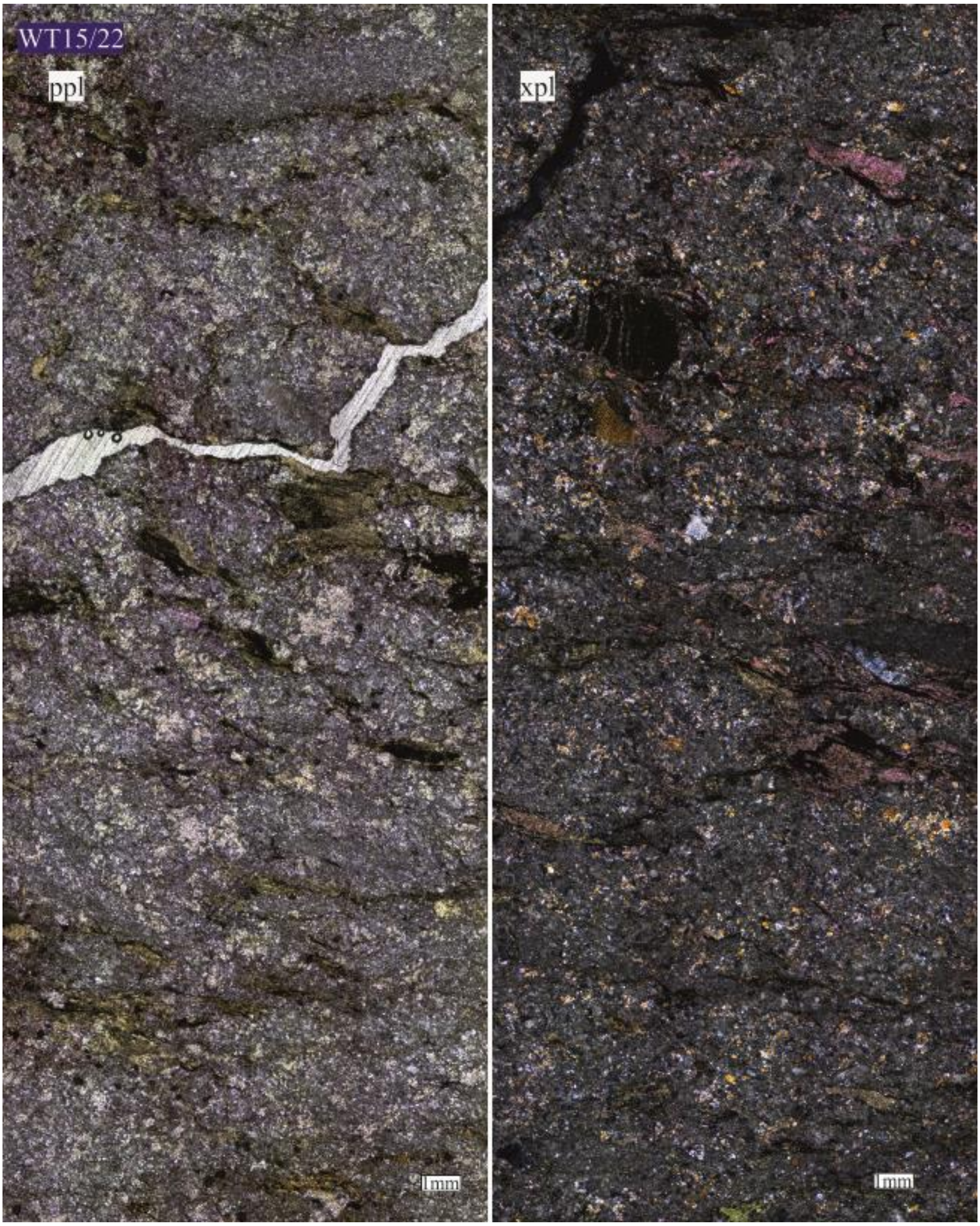

Figure 26: Overview of the thin section of sample WT15/22 of fine-grained sandstone part of lithofacies 10 shown with parallel polarizers (ppl) on the left and crossed polarizers (xpl) on the right side..

9.11. LITHOFACIES.12: CALCAREOUS COARSE-GRAINED SANDSTONE

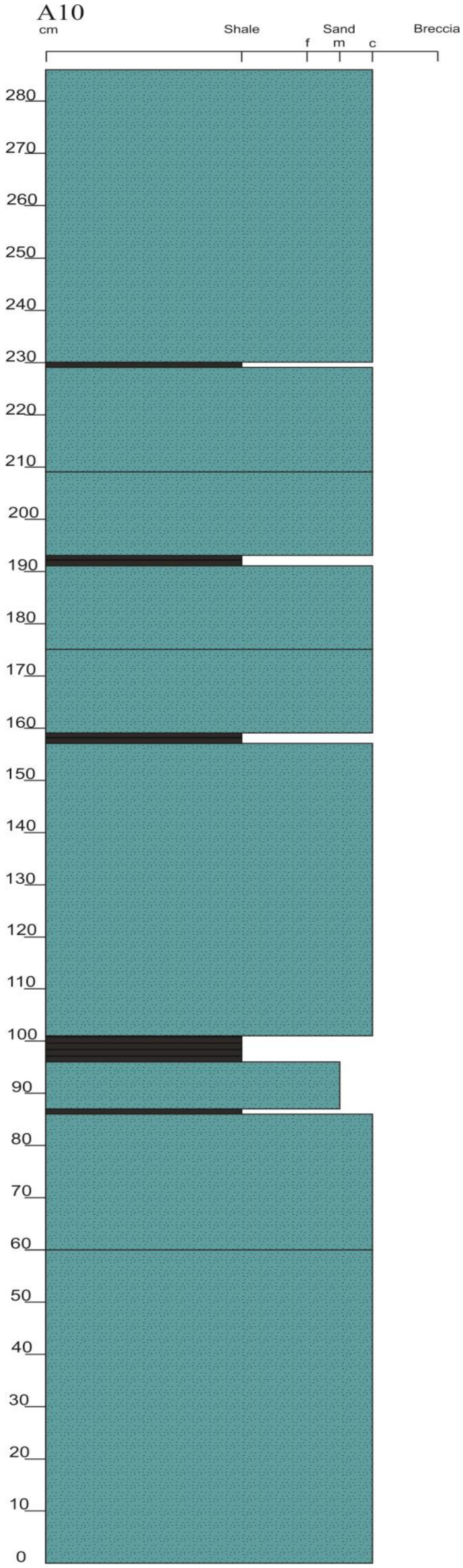

Lithofacies 12 appears in both main profiles in combination with lithofacies 5 and lithofacies 6. Instead of giving it a lithofacies of its own this facies may have also been logged as a slightly different variation of either one of these two lithofacies.

However, compared to both of those lithofacies, lithofacies 12 is distinguished by its extremely high sandstone to shale ratio of 98% to 2% (sandstone/shale ratio 50:1), its coarse grain size and the middle- to thick-layered bedding. Also, its carbonate content serves as a distinctive feature already in the field.

The typical log of lithofacies 12 (single profile A10, Figure 27) shows a total thickness of over 2.8m characterized by almost a total lack of intervening shale layers interbedding. The shale layers are solely consisting of black shale.

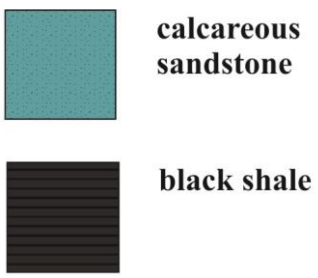

Figure 27: The single profile A10 shows the typical alternation of lithofacies 12. The middle to coarse grained calcareous sandstone layers are shown in blue colours.

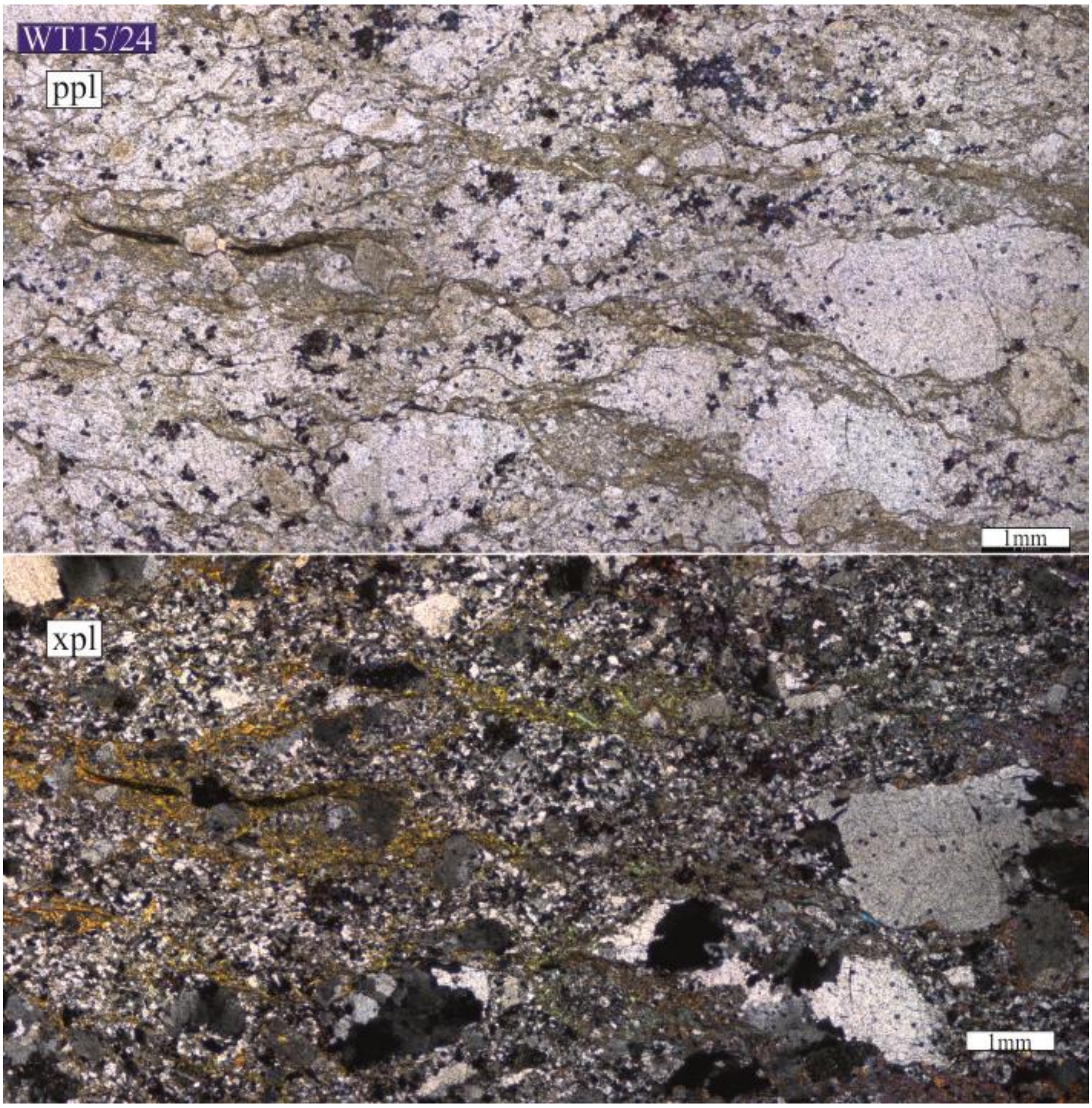

Figure 28: Overview of the thin section of sample WT15/24 of lithofacies 12 shown with parallel polarizers (ppl) at the top and crossed polarizers (xpl) at the bottom. The coarser-grained, recrystallized clasts are quartz grains. The matrix contains high amounts of quartz, feldspar and white mica. Areas containing high amounts of calcite cement show strong FeOH coating.

9.12. LITHOFACIES.13: CLASTS-CONTAINING LIMESTONE

The clasts-containing limestone lithofacies 13 can be found at the top of both main profiles interbedded with the breccias. It shows a thickness of 10 m and mostly occurs as massive crystalline limestones, only partly showing bedding between 15-20 cm.

Even though similar characteristics to the basic description of lithofacies 9 can be observed, the clasts-containing limestone lithofacies differs clearly through its characteristic clasts sizes and distribution, which in average reach a maximum grain size of up to 7 mm, but in certain intervals rarely range up to 9 cm. The clasts consist mainly of dolomite, but also black shale clasts were observed. Clasts often appear surrounded by calcite matrix giving a more matrix-supported appearance than the mostly clast-supported breccias of lithofacies 10.

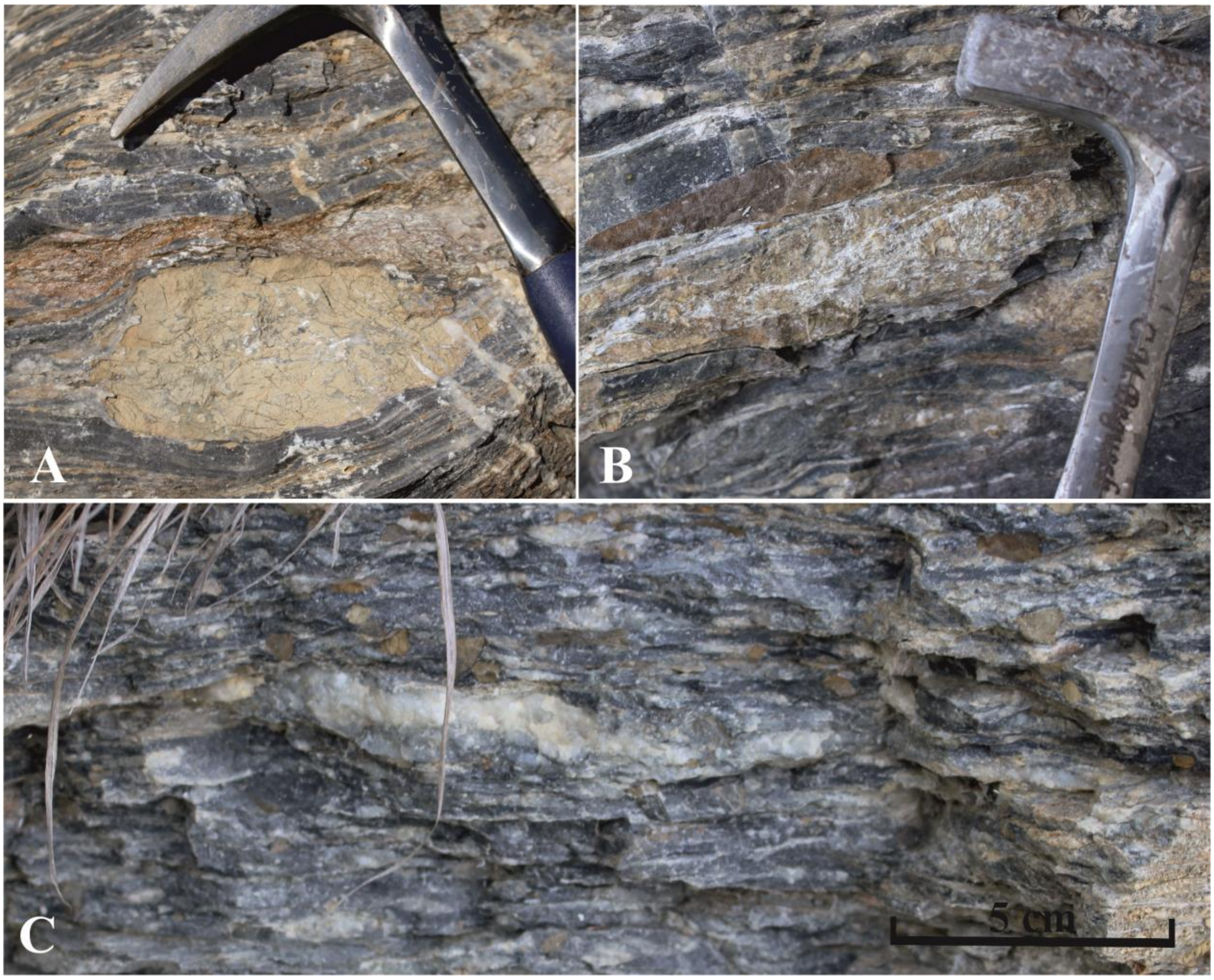

Figure 29: The photographs show lithofacies 13. Photograph A and B show the coarser area of the lithofacies. The dolomite clast in Photograph A was the biggest measured clast of lithofacies 13. The rocks in this area seemed stronger affected by deformation than other areas of the lithofacies like photograph C visualizes. C shows the characteristic occurrence of lithofacies 13. The clasts show a maximum grain size of o.7 centimetres and consist mainly of dolomite. Also clear white calcite veins are occurring repeatedly.

The contact between lithofacies 10 and lithofacies 13 is shown in the single profile A1 (Figure 25). Lithofacies 13 only occurs in direct contact with lithofacies 10, basically solely surrounded by breccia, which contains the same clast lithofacies 13. Thus, lithofacies 13 and 10 are very similar and only differ in the amount of carbonates and the proportion of clasts versus matrix.

The sandstone/breccia to shale ratio is hard to reconstruct considering the recrystallization; however, shales are very minor, and sandstone/shale ratios may be relatively high (above 10:1).

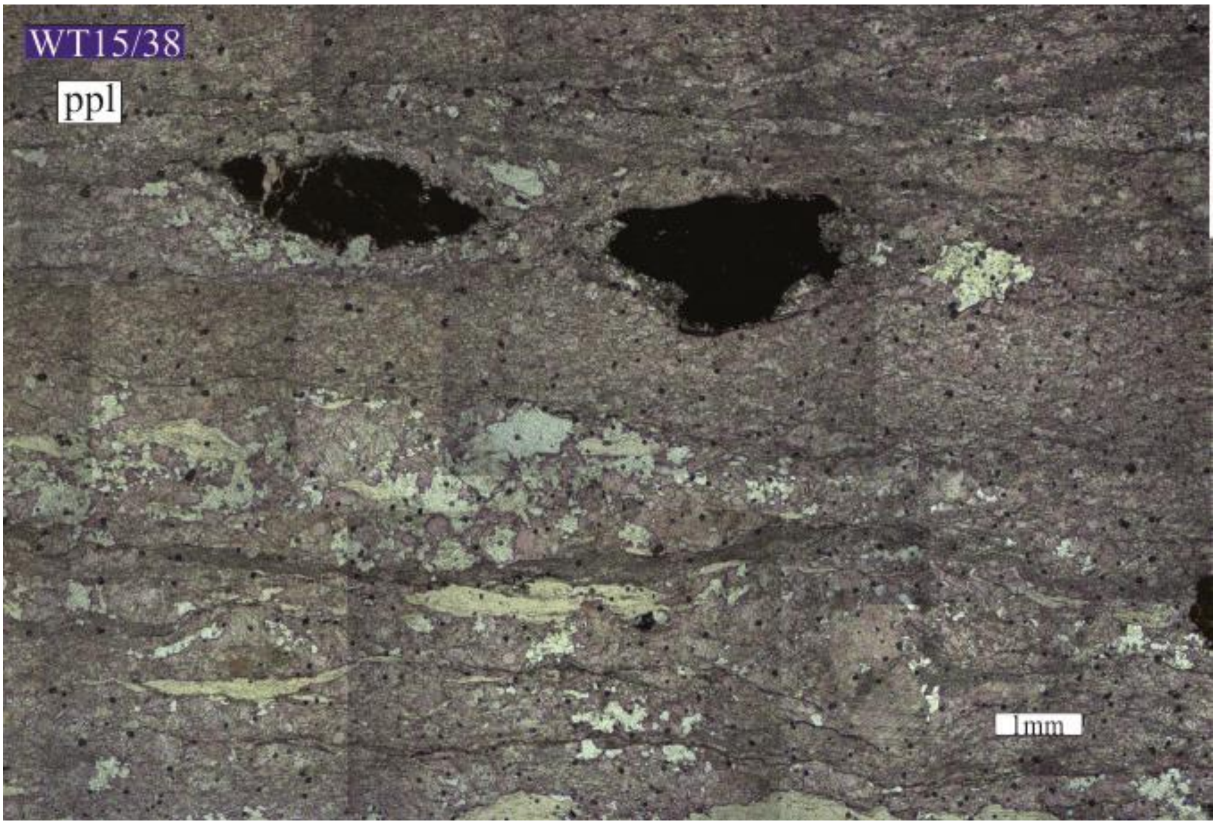

Figure 30: Overview of the thin section of sample WT15/38 of lithofacies 13 shown with parallel polarizers (ppl). Noteworthy are the micritic dolomite clasts further explained in chapter "thin sections".

9.13. LITHOFACIES 11: CHERT

Lithofacies 11 overlies lithofacies 15 and underlies, separated with a normal fault the base of shales and sandstones of lithofacies 1. In the field it appears grey-green, hard and extremely fine-grained. Due to characteristics found in the thin sections (e.g. texture and mineralogy) using optical microscopy, all samples of lithofacies 11 resemble somehow a fine-grained, mylonitic version of lithofacies 15 (greenschists). WT15/9 resembles the greenschist sample WT15/5b in its mineralogy and the mylonitic features. Additionally to quartz, epidote and a lot of chlorite sample WT15/9 contains fine-grained sericite, and recrystallized, ductile folded quartz veins.

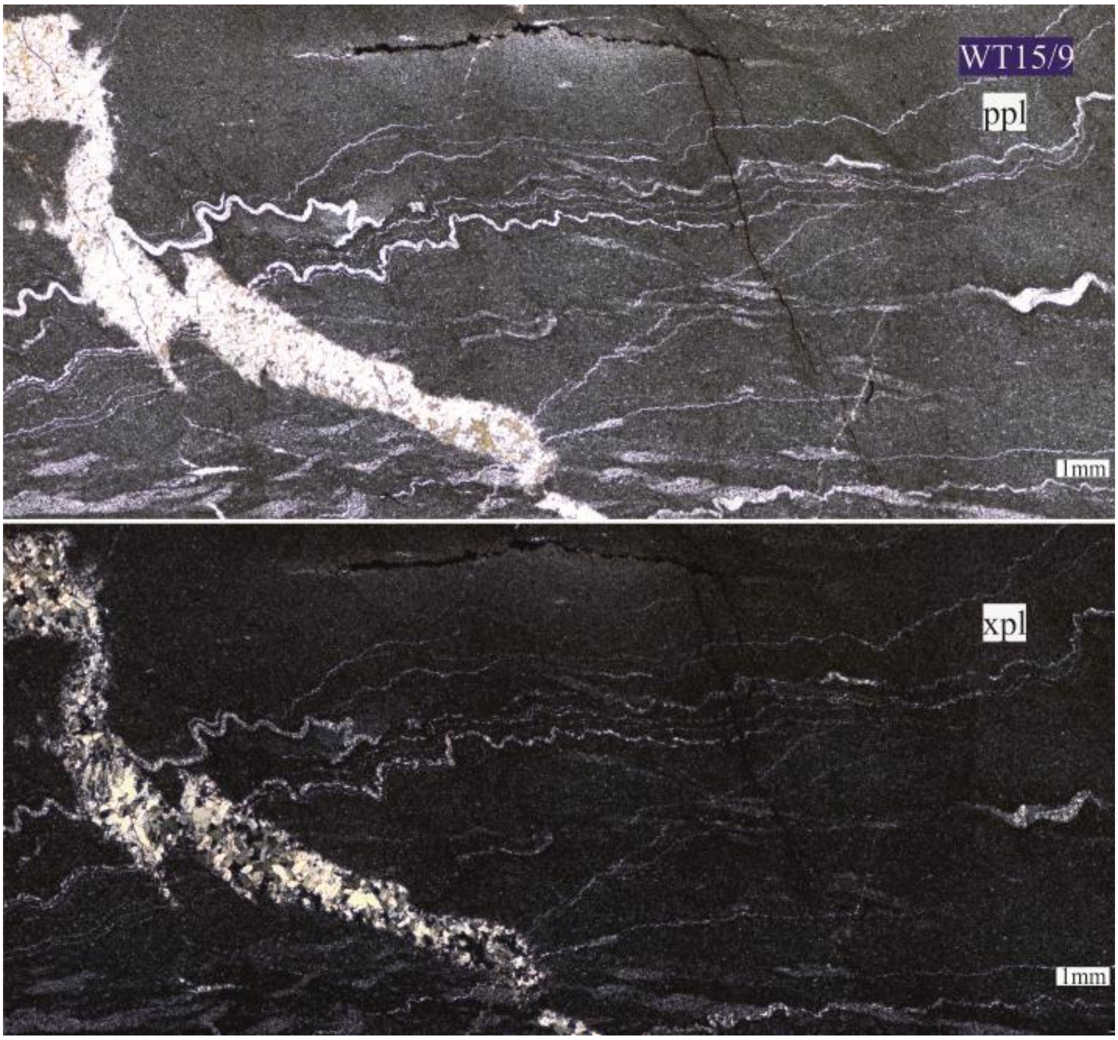

Figure 31: Thin section of sample WT15/9 of lithofacies 11 using ppl (at the top) and xpl (at the bottom).

9.14. LITHOFACIES 15: GREENSCHIST

Lithofacies 15 represents rock units at the base of both main profiles (compare Figure 6, Figure 7). As shown in both main profiles this lithofacies is only excavated for a few metres.

The two samples from lithofacies 15 are WT15/5a and WT15/5b. WT15/5b resembles lithofacies 11, which overlies lithofacies 15. This sample shows meaningful characteristics concerning the P/T-conditions of the metamorphosis. It is a carbonate free, extremely fine-grained, and completely recrystallized ultra-mylonite. Foliation can be observed, forming a banding of mainly chlorite. Other minerals observed are quartz, feldspar, epidote and green-blue chlorites. The veins are refilled with quartz, which later fully recrystallized. Sample WT15/5a is more characteristic for lithofacies 15. It contains feldspar, quartz, white mica, epidote, colourless amphiboles, pyroxene and a lot of secondary formed chlorite. Its matrix consists of feldspar, mainly plagioclase, quartz and white mica. The amphiboles are translucent. Because of their lack of colour they cannot be part of the hornblende-group and most likely are tremolites. The samples paragenesis resembles those of the typical greenschist facies, including colourless amphiboles.

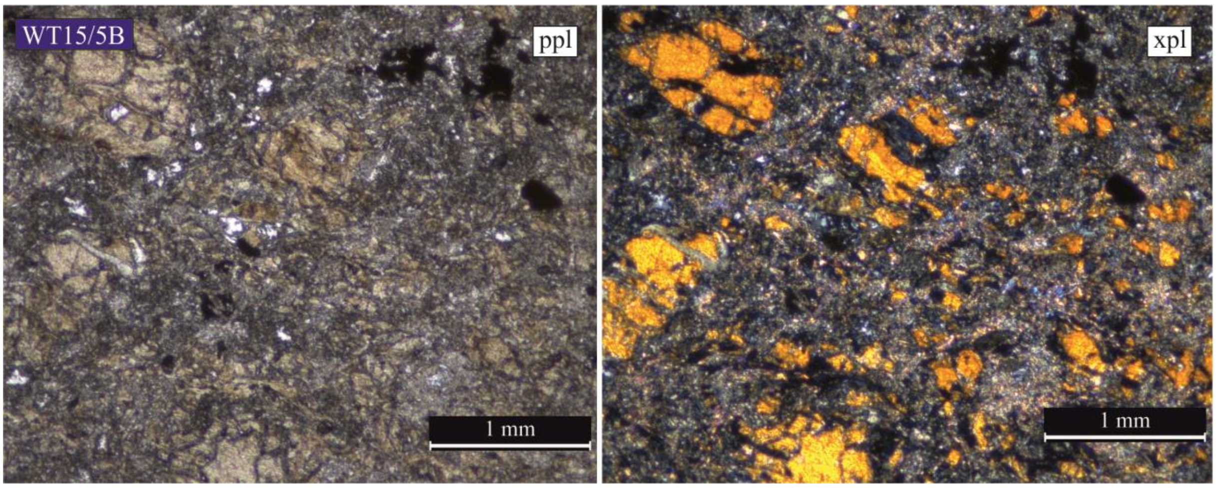

Figure 32: Sample WT15/5b (lithofacies 15, greenschist) showing colourless amphiboles (tremolites?) using ppl (left side) and xpl (right side).

10. THIN SECTIONS

10.1. METHODS & GENERAL DESCRIPTION

To prepare the samples for the production of the thin sections a masonry saw was used. Every sample was cut into a small rectangular block aligning the cut perpendicular to the foliation and insofar it was possible to parallel to the lineation. The cut perpendicular to the foliation was chosen to get out most of the information of sedimentological interest. The cut parallel to the lineation allows a better interpretation of microstructures within the thin sections. Altogether 41 thin sections were produced, whereby 5 thin sections have 5x5cm dimensions and the remaining 36 thin sections have 2.5x5cm dimensions. To distinguish between different types of carbonates, the thin sections underwent straining. For differentiation between calcite and dolomite components within a thin section a mixture of 2.2 ml of HCl, 492ml of deionized H2O, 1g of Alizarin S and 4g of K-hexacyanoferrate was prepared. After immersing each thin section into the liquid for no longer than one minute, the dyed thin sections were carefully washed off with deionized water. While Alizerin S dyes calcite red, it does not affect dolomites, which stay uncoloured. K-hexacyanoferrate reacts to the iron concentration within both carbonates. The higher the iron concentration of the calcite, the more their colour changes into purple. The colour of the dolomite is uncoloured when they have low iron concentrations and dark blue when they have high iron concentrations.

Combining the results of all sandstone thin sections together, the occurring mineralogical composition consists of the original detrital phases quartz, feldspar, white mica and carbonates, including both calcite and dolomite grains. Also autigenic minerals were found in form of calcite cement secondarily formed after deposition (Tucker,1988). Other accessory components found are biotite, chlorite, an opaque phase that is reminiscent of plant remnants (graphite), clay rests, heavy minerals (mostly zircon), ores such as hematite and pyrite (recognized by their cubic crystal form) and ferrous oxide, that occurred only in a few thin sections and mostly in combination with carbonate cement.

10.2. COMPONENTS

10.2.1. QUARTZ

Quartz occurs in different variations. Monocrystalline quartz grains were only found in low number. As a result of the metamorphism the rocks went through most quartz grains are strongly recrystallized. A large number of grains show “foam structure”, characterized by triple grain contacts of 60° and 120°. Furthermore bulging, sub-grain rotation and undulose extinction with xpl of this tempered quartz texture was observed (see Figure 33). The undulose extinction of grains which also show foam structure allows a reconstruction of the rocks metamorphic history. First, higher metamorphic conditions caused the quartz grains to recrystallize and form a foam structure. In a second step, these already recrystallized quartz grains got retrograde overprinted, causing their undulose extinction.

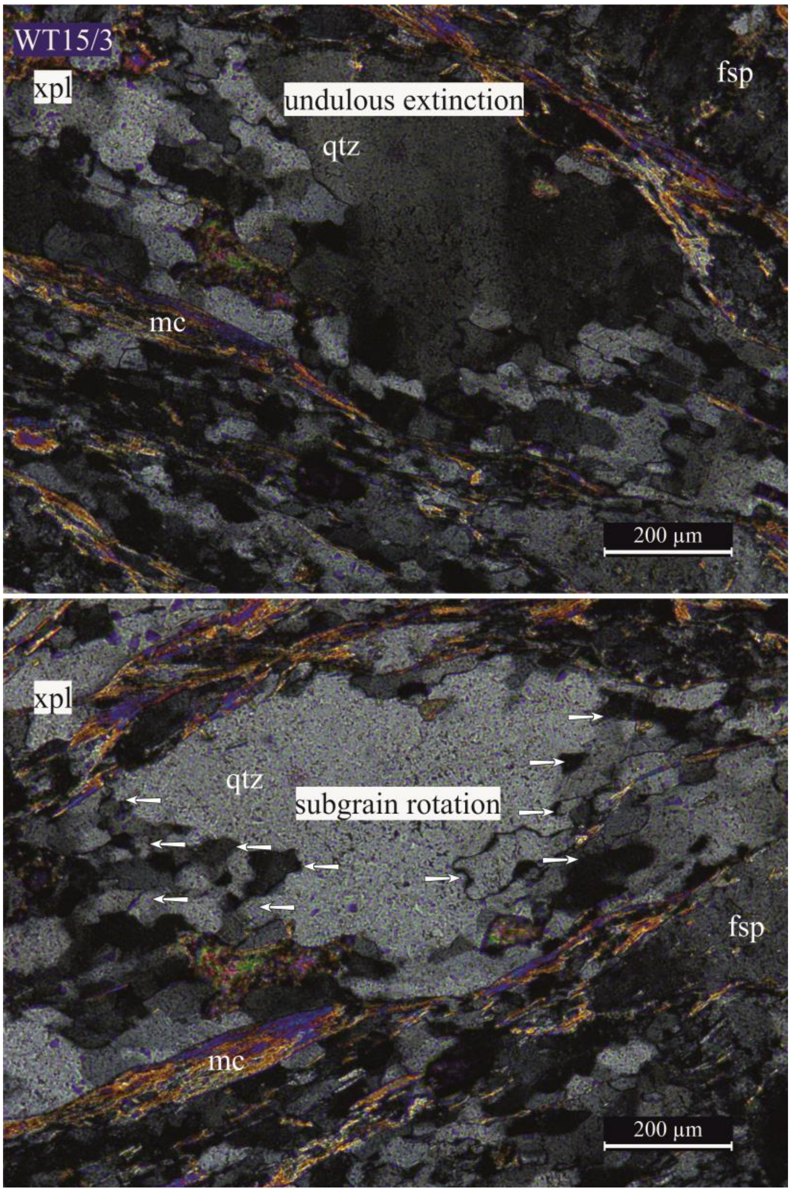

Figure 33: two photographs of the thin section of sample WT15/3. The quartz grain shows both sub-grain rotation and undulose extinction with crossed polarizers (xpl).

10.2.2. Feldspar

Two types of feldspar were found within the thin sections. Plagioclase as well as potassium feldspar (K-feldspar; see Figure 34) occur, whereby potassium-feldspar forms the majority of counted feldspar grains. The grains comprise various inclusions of opaque phase, heavy minerals, micas and carbonate crystals, mostly idiomorphic dolomite rhombs. In some thin sections recrystallized feldspar crystals have been observed. Rarely commencing bulging was observed. More frequently broken feldspar grains occur. The recrystallization indicated that the PT-conditions of the metamorphism were high enough to influence not just the occurring carbonate and quartz grains but also feldspar components.

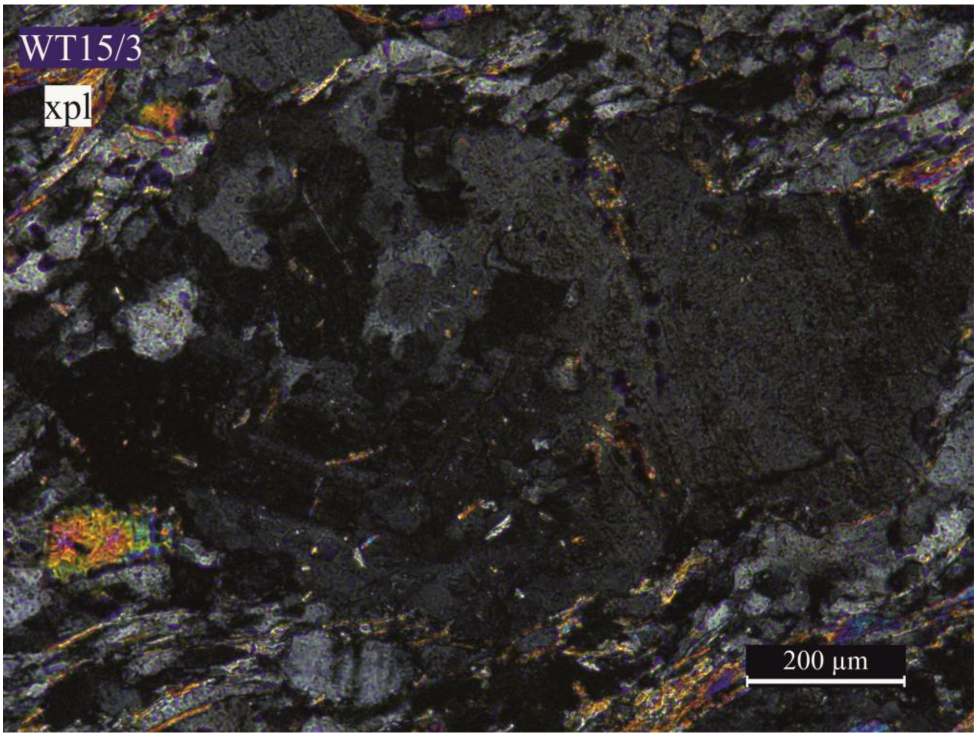

Figure 34: Recrystallized feldspar grain within the thin section of sample WT15/3; several inclusions of mica and quartz grains.

10.2.3. Mica and matrix

The majority of occurring mica components is white mica. However rarely bland coloured biotite and chlorite components occur. There are at least two generations of micas distinguishable (see Figure 35). The 1st generation consists of detrital, big white mica flakes, which do not show any characteristic orientation. The 2nd generation of micas occurs way more often in all thin sections than the 1st generation. This 2nd generation probably formed secondary during the metamorphism from former black clay-rich layers within the sandstones. Their extremely fine crystals are oriented perpendicular to the main pressure direction. This forms a foliation parallel to the initial sedimentological layering. Together with partly intercalated non-converted clay or black shale layers they form bands through the entire thin section. Another form of appearance of this 2nd generation micas is between bigger mineral grains, like feldspar and quartz. They for instance function as a trigger for pressure solution causing saturated grain boundaries. Mica pressure caps and pressure shadows have also been observed several times. The smallest mica grains observed can hardly be differed from each other. During the counting for the Dickinson method, they were added towards matrix.

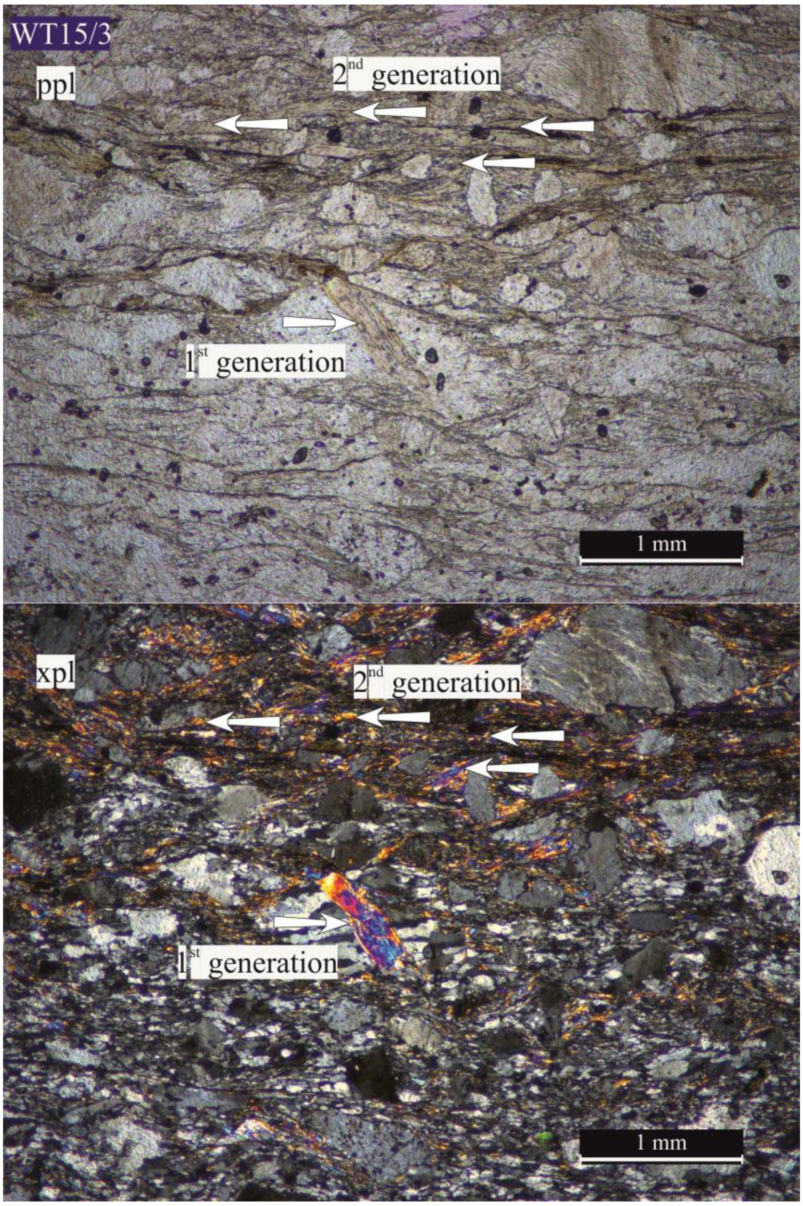

Figure 35: Generations of mica grains within thin section of sample WT15/3.

However as an exception to other thin sections based on mica crystal orientation, the thin section WT15/44 is noteworthy. This thin section is the only one of its kind showing relatively coarse-grained idiomorphic white micas, which show a crystal growth orientation perpendicular to the other orientated fine-grained mica shear bands and therefore perpendicular to the deformation direction.

10.2.4. CARBONATES

Basically three types of carbonates, namely calcite clasts, dolomite clasts and carbonate cement, have been differentiated. The calcite grains are mostly coarse-grained compared to the dolomite grains. They show both, growth twins and deformation twins (see Figure 36), due to metamorphism. They occur in several thin sections of various lithofacies.

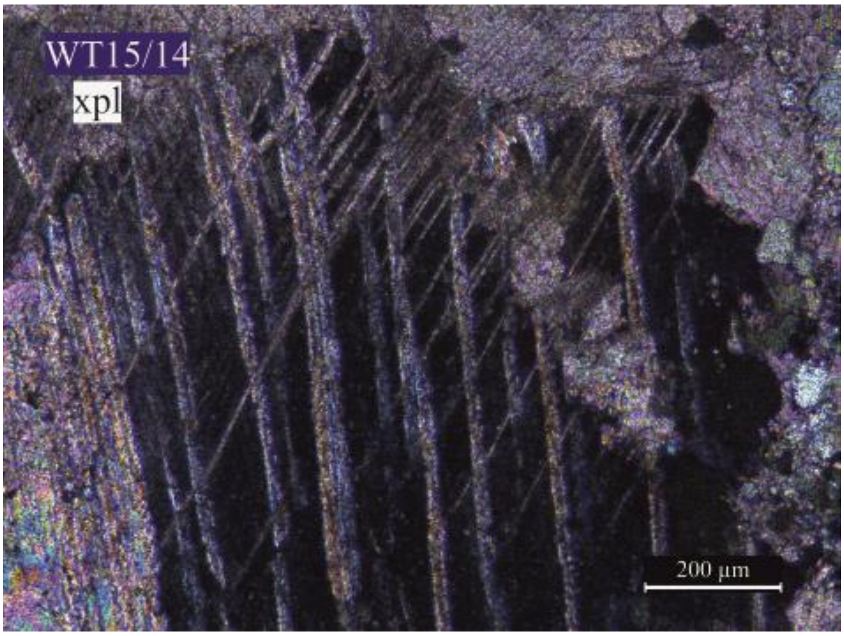

Figure 36: Several generations of deformation twins of a calcite grain (thin section of sample WT15/14).

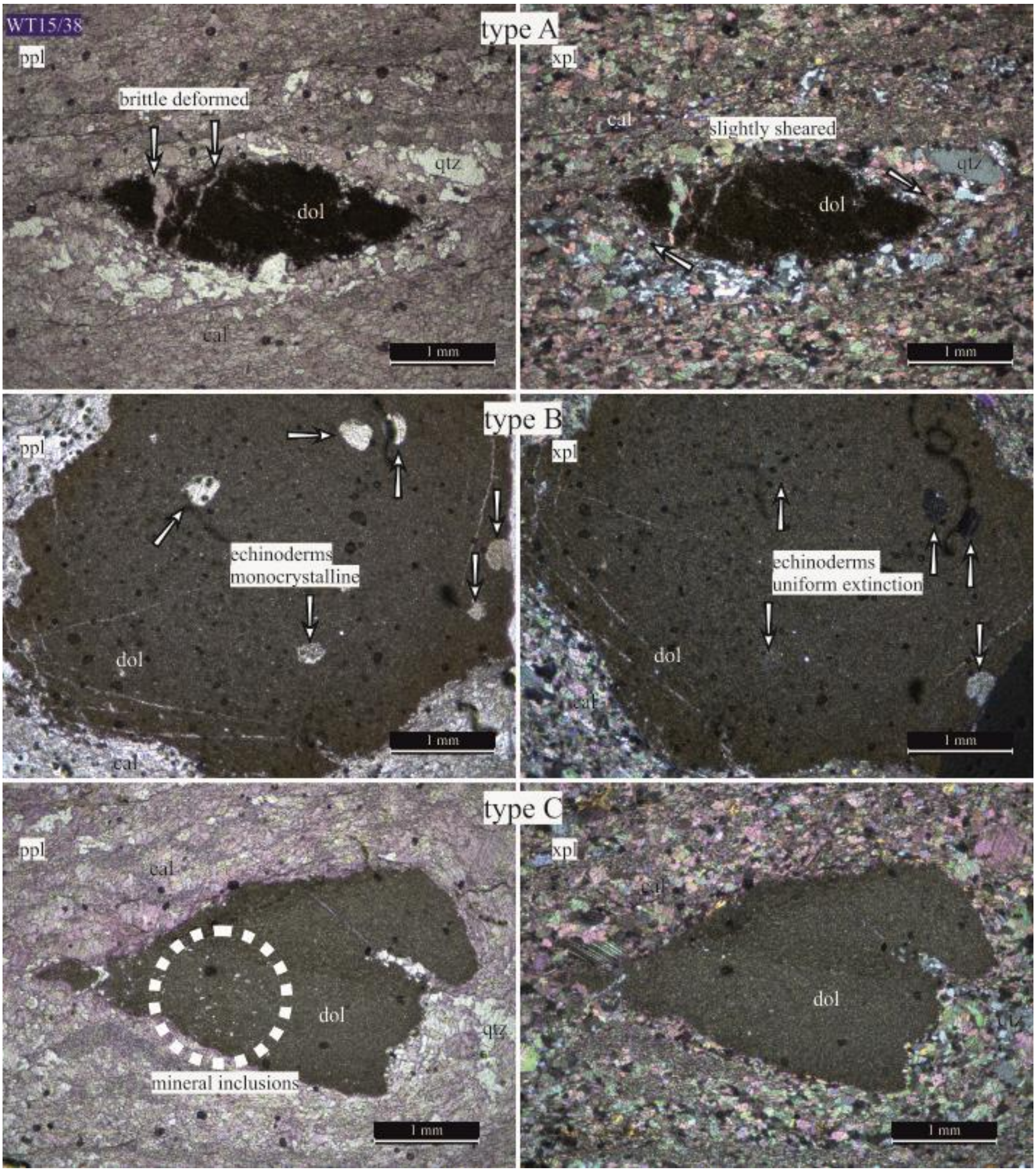

Figure 37: Various types of micritic dolomite clasts in a calcitic matrix of sample WT15/38 shown with parallel polarizers (ppl) on the left side and with crossed polarizers (xpl) on the right side.

Dolomite grains can be found as micritic clasts (see Figure 37) within several thin sections of lithofacies 13. Fully recrystallized calcite and rarer quartz grains surround the dolomite clasts. It is likely that the recrystallized calcite "matrix" surrounding the dolomite originally also consisted of detrital calcite grains and micritic calcite. Metamorphism caused a full recrystallization of the calcite. The micritic dolomite clasts however remained unaltered. Only a brittle pull apart of the dolomite layers, separating the detrital clasts, can be observed. This difference in recrystallization behaviour indicates metamorphosis conditions with temperatures high enough to cause full recrystallization of the calcite, but too low to affect the dolomite.

The interpretation that dolomite layers have been initially formed by accumulated detrital micritic dolomite grains, and not been dolomitized in situ, is supported by the unlikelihood of the formation of primary micritic dolomite layers between calcite layers and especially by the occurrence of various types of dolomite clasts. WT15/38 represents the sample that contains most of the observed dolomite clasts. Within only this sample, three different types of micritic dolomite clasts have been observed. The first type (type A) shows traces of slight shearing and brittle deformation forming veins through the clasts, which later were refilled with calcite cement. The micritic dolomite remains non-recrystallized. Around these type A dolomite clasts a reaction rim of small, newly formed, radial minerals (maybe talc?) can be observed. The second type of dolomite clasts (type B) does not show any evidence of shearing. It contains several remnants of echinoderms/crinoids. However, the uniform extinction of these monocrystalline fossil remnants limits the fossil species down to echinoderms. The third type of dolomite clasts (type C) contains small terrigenous mineral inclusions.

Several thin sections contain fossil remnants (see Figure 38) identified as echinoderms. They can be found in both calcite (e.g. WT15/13) and dolomite (e.g.WT15/38; see Figure 37 type B) grains. The echinoderms found in dolomite grains are detritally transported within the grains from the source rock. The echinoderms within the limestone beds are probably younger and may be deposited contemporaneously to the flysch sedimentation. In contrast to those within the dolomite grains they show recrystallization due to metamorphosis. Even though i.a. Prey, 1975 described these echinoderms as crinoids, a clear echinoderm group cannot be defined. Due to metamorphism these echinoderms don’t show any structures characteristic for crinoid stems. The main evidence, to determine these monocrystalline grains as echinoderms, is their characteristic uniform extinction using crossed polarizers (xpl). Their original round form is still visible as dark round centres of big calcite crystals. The margin of these darker areas shows the former grain boundary of the fossil remnants, which got overgrown in the course of diagenesis and metamorphism. Their original growth twins were “taken over” by the cement rim that formed around them, expanding the grain. This overgrowing of older generations of carbonates, in our case of echinoderms, by younger generations of carbonates can already be achieved during diagenesis and does not necessarily need metamorphic conditions.

The carbonate cement within most thin sections shows a uniform appearance. It shows strong recrystallization and consists of calcite. However, previous colouring of the thin sections shows a chemical zonation within the calcite cement. The dolomite cement crystals are idiomorphic and relatively small, show a high iron content and can be found as both, as single crystals or as inclusions in bigger potassium-feldspar grains.

:

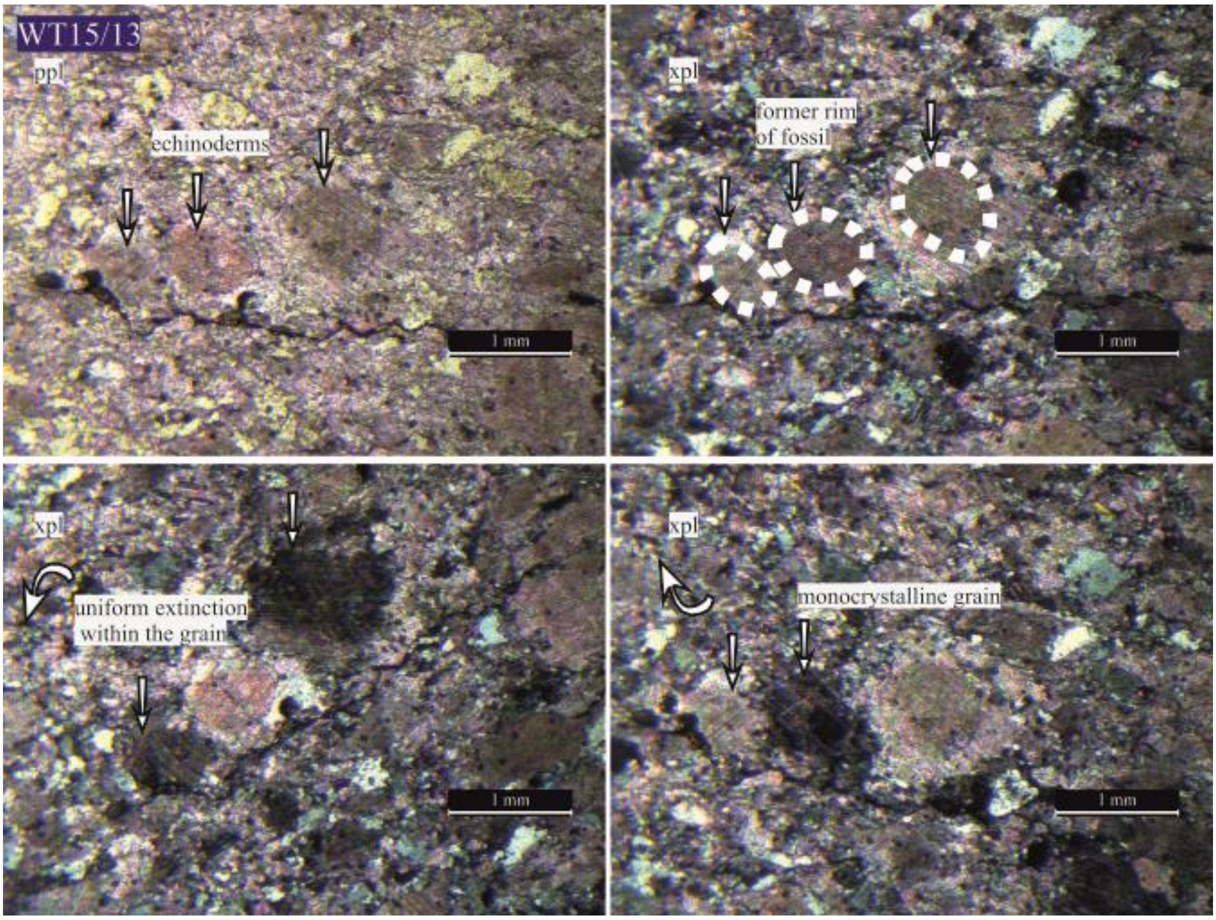

Figure 38: echinoderms of sample WT15/13. Calcite cement shows rose colouring, the uncoloured grains are quartz.

The dominant deformation mechanism is pressure solution. There is hardly any indication for shearing, excluding the micritic dolomite of type A. Clear indication is given by i.a. strongly saturated grain boundaries (see Figure 39). This can be observed in all types of mineral grains, but mainly in quartz and feldspar grains. As trigger-minerals mica grains occur in these saturated grain boundaries between the grains. Another indication for pressure solution can be found in WT15/13 (see Figure 38). These traces are micro-stylolites - forming dark brown – black jagged lines through the thin section. The dark colour is probably caused by clay minerals, which are exceptionally good trigger-minerals for the formation of such micro-stylolites.

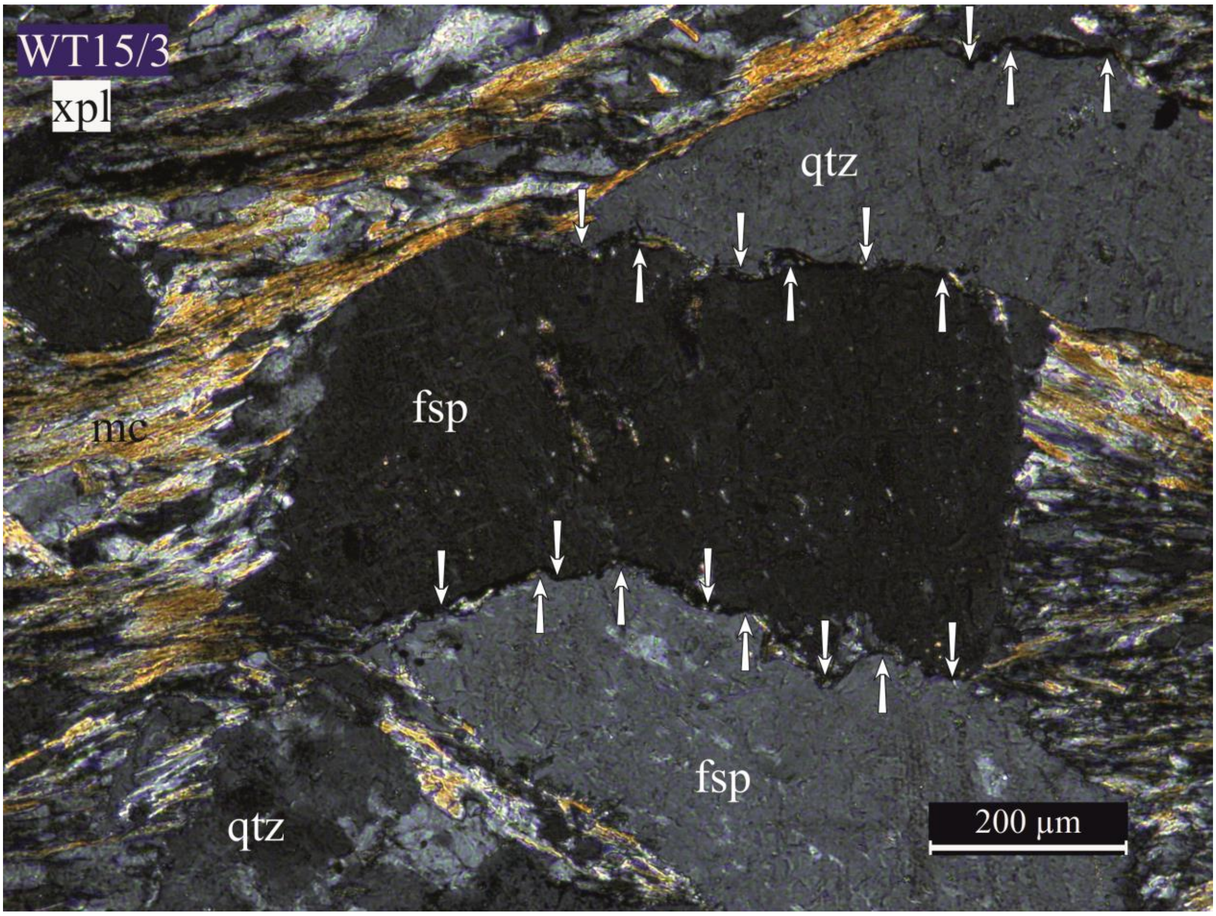

Figure 39: saturated grain boundaries of feldspar and quartz grains of the thin section of sample WT15/3. The arrows show the former direction of pressure. Small mica flakes are function as trigger minerals between the harder, bigger grains (like feldspar and quartz).

10.3. MICROSTRUCTURES AND GRADE OF METAMORPHOSIS

Combining the variety of microstructures, the metamorphic history can be reconstructed. The minimum temperature conditions during metamorphism can be set by the type of deformation twins within the calcite grains. The deformation twins observed within calcite are identified as Type 2 and Type 3 deformation twins, both indicative for metamorphic temperatures of around 200°C. However the calcite cement is strongly recrystallized. The recrystallization of the calcite happened first. The deformation twins probably formed retrograde. Another indicator for metamorphic conditions is quartz. The undulose extinction of the quartz grains showing foam structure also indicates a first higher tempered metamorphic event, during which the formation of the foam structure happened and a second, lower tempered, retrograde metamorphism causing the undulose extinction.

The two minerals most indicative for the maximum temperature conditions during metamorphosis are feldspar and dolomite. Therefore the two thin sections WT15/3 (lithofacies 6) and WT15/38 (lithofacies 13) are most representative. The first temperature indication is the recrystallization of the K-feldspar grains and their commencing bulging. Compared to quartz grains, which already start to show bulging at temperatures around 300-400°, feldspar grains need higher temperatures to start recrystallization. The second temperature indication is the behaviour of dolomite clasts within a calcite matrix. The matrix probably consisted of separate calcite grains and calcite micrite at time of deposition. Metamorphism caused a complete recrystallization of all calcite components However the dolomite clasts were only broken apart and boudinaged, but not recrystallized. The metamorphic conditions were not high enough to have an impact on the dolomite.

Summarizing all indication- microstructures the maximum temperatures had to be high enough to recrystallize the feldspar, but not so high to affect the dolomite grains. This limits the maximum temperature conditions of metamorphism to around 450°C. This represents the first, high tempered prograde metamorphic event. The retrograde metamorphic conditions causing the calcite deformation twins and undulose extinction of quartz grains was probably around 100-200 degrees.

10.4. Gazzi-Dickenson- method

10.4.1. General description

Additional to the conventional analysis of thin sections below the polarizing microscope, detailed analysis regarding to sandstone provenance relations have been made on the 36 smaller thin sections using the “Gazzi-Dickenson- method” (Dickinson, 1985). The approach was to find out the provenance of the samples by using their mineralogical compositions and then plot the data in a ternary diagram.

10.4.2. Method

300 grains within each thin section have been counted (for detailed listing of all samples compare Table 2). For the procedure of counting an electric counting-sleigh has been used. The counting-sleigh can be programmed to move a certain distance within the thin section, depending on the grainsize of the sample. The results were grouped in two different ways and separately plotted in ternary diagrams, first in a QtFL-diagram (see Figure 40 A) and second in a QmFLt-diagram (see Figure 40 B; after Dickinson, 1985).

10.4.3. Symbols of grain types after Dickinson

1. Quartz fraction:

Qt	total quartzose grains
Qm	monocrystalline quartz grains
Qp	polycrystalline quartz grains

2. Feldspar fraction:

F	total feldspar grains (both plagioclase and K-feldspar)

3. Lithic fragments fraction:

L	total lithic fragments
Lt	total lithic fragments and Qp

The shortcut Qt stands for quartz grains in total, Qm stands for monocrystalline quartz grains, F stands for the feldspar grains in total, L stands for the lithic fragments and the Lt stands for the lithic fragments and Qp in total (Dickinson, 1985).

10.4.4. CATEGORIES

Additionally, before producing the ternary diagrams a classification of different categories of thin sections, based on their main components, was done (see Table 1). These categories were visualized by using different colours within the plots, each colour standing for a category of thin sections. As the main discriminating basis the two main components of every thin section were used (see Table 1). Category 1 (dark pink colour), two main components are carbonates and quartz. In Category 4 (light pink colour) two main components are also quartz and carbonate, but the quartz content is significantly higher than category 1. Category 2 (purple colour), mainly consists of carbonate and feldspar. The two main components of Category 3 (dark blue colour) are quartz and feldspar. Category 5 (black colour) has quartz and mica as its two main components. Category 6 (green colour) consists of the two main components mica and quartz, with mica slightly higher than quartz.

Table 1: Categories of thin sections based on their two main components

Category	2 main components	Samples
1	1.Carbonates 2.Quartz	WT15/1, WT15/7, WT15/38, WT15/14, WT15/12, WT15/13, WT15/37, WT15/26, WT15/39, WT15/40
2	1.Carbonates 2.Feldspar	WT15/35, WT15/36, WT15/18
3	1.Quartz 2.Feldspar	WT15/3, WT15/17, WT15/24, WT15/8, WT15/41
4	1.Quartz 2.Carbonates	WT15/ 23
5	1. Quartz 2. Mica	WT15/ 25, WT15/29, WT15/32, WT15/30, WT15/31B, WT15/42
6	1.Mica 2. Quartz	WT15/ 31A, WT15/15, WT15/44, WT15/45
7	1.Carbonates 2.Mica	WT15/ 16 , WT15/ 43A

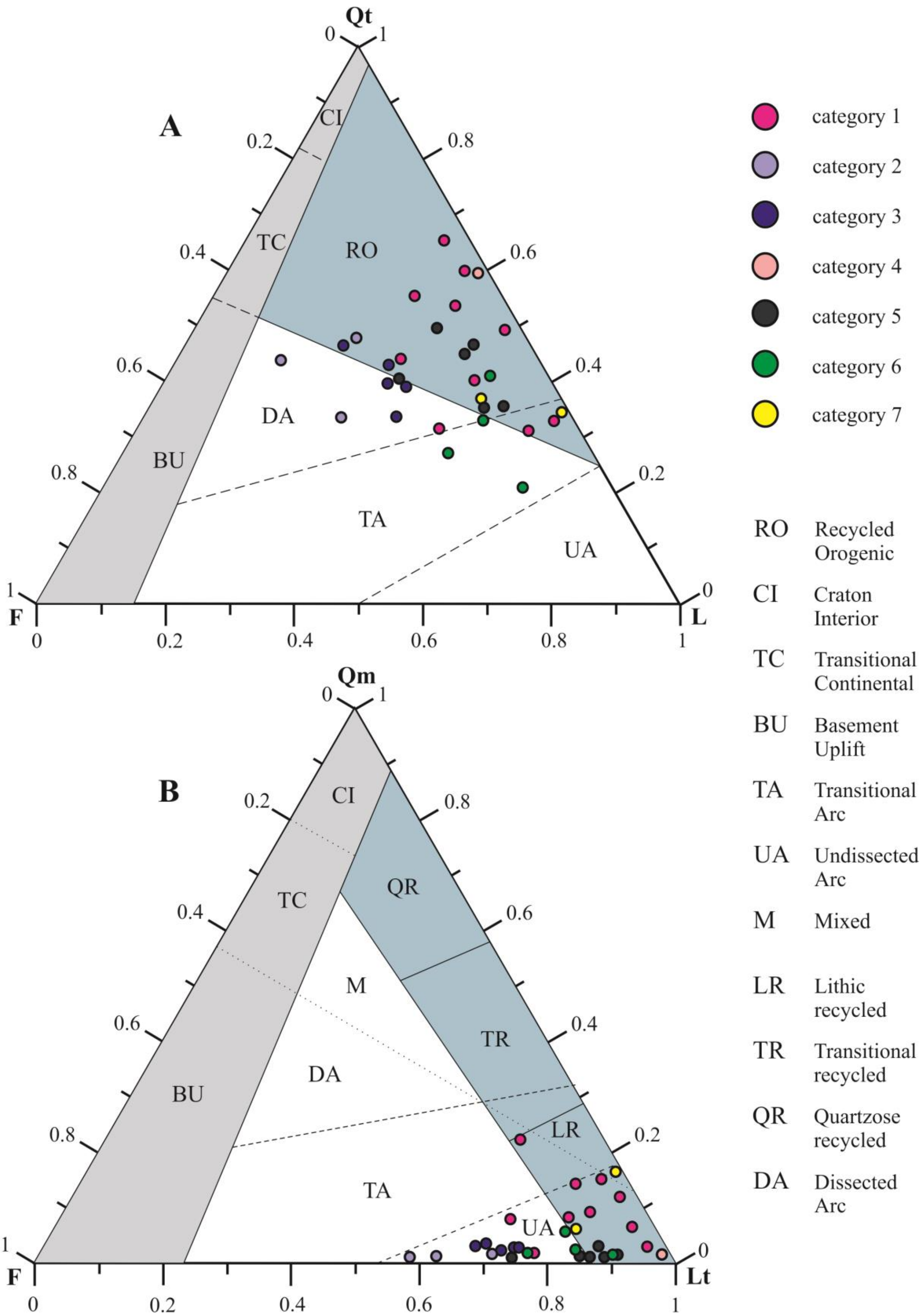

Figure 40: A: QtFL ternary diagram (after Dickinson, 1985) showing the distribution of the distinguished categories. The diagram shows the scatter of the samples including [Qt] total quartz, [F]total feldspar and [L] lithic fragments.

B: QmFLt ternary diagram (after Dickinson, 1985) showing the distribution of the distinguished categories explained in the legend. The diagram shows the scatter of the samples including [Qm]monocrystalline quartz, [F]total feldspar and [Lt]total lithic fragments.

The last defined category is category 7 (yellow colour). This category comprises a very high amount of fine-grained material. Not just the two main components carbonate (also crinoid remnants) and mica, but also high amounts of calcite cement were observed.

Worth mentioning are also remnants of echinoderms/crinoids that were found repeatedly in category 1 and category 7 (comprising mainly lithofacies 2, 3 and 10). Both, category 5 and category 6 (high amount of mica) comprises a lot of matrix. The high amount of fine-grained, deformed mica bands indicates an initially high amount of clay minerals which recrystallized due to metamorphosis.

10.4.5. RESULTS

Unfortunately the point scatters in both ternary diagrams are spread too wide to give a clear differentiation. Both diagrams show a high amount of measuring points in recycled areas (see Figure 40: A – area of recycled orogeny [RO] and B – lithic recycled [LR]). Also the area of transitional continental provenance can be excluded in both ternary diagrams. It is likely that the high amount of measuring points in the QmFLt-diagram in the area of dissected arc is due to metamorphism. This field holds no measuring points in the QtFL – diagram at all and is therefore an unlikely source for the samples. Combining the results it is most likely that the sediments originated from a recycled orogenic source.

Table 2: component distribution counted in thin sections.

The acronyms are: no number of grains, % percentage, S sample, U unit, F Fe oxide, Qm quartz, C calcite, CC calcite cement, D dolomite, M matrix mostly mica, QP quartzite. OP opaque phase, WM white mica, F feldspar, QU quartz with undulose extinction, CR echinodermata (crinoids?), HM heavy minerals.

S	U	F	Q	C	CC	D	M	QT	OP	WM	F	QU	CR	HM
WT15/1	no		22.0		67.0	87.0	29.0	65.0	1.0	15.0	6.0	8.0		
	%		7.3		22.3	29.0	9.7	21.7	0.3	5.0	2.0	2.7		
WT15/3	no	7.0	7.0		1.0	5.0	61.0	109.0	2.0	5.0	88.0	15.0		
	%	2.3	2.3		0.3	1.7	20.3	36.3	0.7	1.7	29.3	5.0		
WT15/7	no		21.0	48.0	123.0	39.0	7.0	27.0	2.0	2.0	5.0	8.0	18.0	
	%		7.0	16.0	41.0	13.0	2.3	9.0	0.7	0.7	1.7	2.7	6.0	
WT15/8	no		2.0	6.0		25.0	45.0	70.0	1.0	25.0	75.0	50.0		1.0

	%		0.7	2.0		8.3	15.0	23.3	0.3	8.3	25.0	16.7		0.3
WT15/12	no		13.0	25.0	135.0	19.0	15.0	45.0		2.0	21.0	6.0	19.0	
	%		4.3	8.3	45.0	6.3	5.0	15.0		0.7	7.0	2.0	6.3	
WT15/13	no		21.0	14.0	149.0	6.0	11.0	52.0	7.0	4.0	13.0	7.0	16.0	
	%		7.0	4.7	49.7	2.0	3.7	17.3	2.3	1.3	4.3	2.3	5.3	
WT15/14	no		8.0	9.0	169.0	22.0	4.0	54.0	2.0	2.0	5.0	16.0	9.0	
	%		2.7	3.0	56.3	7.3	1.3	18.0	0.7	0.7	1.7	5.3	3.0	
WT15/15	no	1.0	16.0			26.0	117.0	66.0	9.0	7.0	45.0	13.0		
	%	0.3	5.3			8.7	39.0	22.0	3.0	2.3	15.0	4.3		
WT15/16	no		14.0	1.0	215.0	10.0	23.0	11.0	17.0		1.0	3.0	5.0	
	%		4.7	0.3	71.7	3.3	7.7	3.7	5.7		0.3	1.0	1.7	
WT15/17	no	1.0	4.0		33.0	28.0	58.0	71.0	2.0	7.0	71.0	25.0		
	%	0.3	1.3		11.0	9.3	19.3	23.7	0.7	2.3	23.7	8.3		
WT15/18	no		1.0		49.0	23.0	43.0	63.0			71.0	50.0		
	%		0.3		16.3	7.7	14.3	21.0			23.7	16.7		
WT15/23	no	2.0		2.0	52.0	63.0	26.0	143.0	2.0		5.0	4.0		1.0
	%	0.7		0.7	17.3	21.0	8.7	47.7	0.7		1.7	1.3		0.3
WT15/24	no	11.0	2.0		12.0	25.0	17.0	77.0		58.0	70.0	28.0		
	%	3.7	0.7		4.0	8.3	5.7	25.7		19.3	23.3	9.3		
WT15/25	no	2.0	1.0		9.0	11.0	7.0	109.0	4.0	86.0	39.0	32.0		
	%	0.7	0.3		3.0	3.7	2.3	36.3	1.3	28.7	13.0	10.7		
WT15/26	no		4.0		142.0	28.0	16.0	62.0	2.0	26.0	5.0	11.0	4.0	
	%		1.3		47.3	9.3	5.3	20.7	0.7	8.7	1.7	3.7	1.3	
WT15/29	no				12.0	49.0	84.0	64.0	1.0	13.0	43.0	34.0		
	%				4.0	16.3	28.0	21.3	0.3	4.3	14.3	11.3		
WT15/30	no	17.0	2.0		4.0	15.0	69.0	117.0		32.0	27.0	17.0		
	%	5.7	0.7		1.3	5.0	23.0	39.0		10.7	9.0	5.7		
WT15/31A	no		3.0				65.0	87.0	6.0	80.0	29.0	30.0		
	%		1.0				21.7	29.0	2.0	26.7	9.7	10.0		
WT15/31B	no	82.0			17.0	13.0	57.0	78.0	3.0	2.0	31.0	17.0		
	%	27.3			5.7	4.3	19.0	26.0	1.0	0.7	10.3	5.7		
WT15/32	no	3.0			25.0	14.0	82.0	96.0		1.0	70.0	9.0		
	%	1.0			8.3	4.7	27.3	32.0		0.3	23.3	3.0		
WT15/35	no		1.0		116.0	13.0	18.0	69.0			77.0	6.0		

	%		0.3		38.7	4.3	6.0	23.0			25.7	2.0		
WT15/36	no	2.0	1.0		110.0	7.0	16.0	45.0		34.0	71.0	14.0		
	%	0.7	0.3		36.7	2.3	5.3	15.0		11.3	23.7	4.7		
WT15/37	no	4.0	2.0				24.0	74.0	1.0	113.0	68.0	14.0		
	%	1.3	0.7				8.0	24.7	0.3	37.7	22.7	4.7		
WT15/39	no		12.0		141.0	7.0	28.0	48.0		20.0	36.0	8.0		
	%		4.0		47.0	2.3	9.3	16.0		6.7	12.0	2.7		
WT15/40	no		14.0		236.0		5.0	20.0		8.0	9.0	1.0	7.0	
	%		4.7		78.7		1.7	6.7		2.7	3.0	0.3	2.3	
WT15/41	no		9.0		17.0	38.0	31.0	62.0	2.0	41.0	80.0	20.0		
	%		3.0		5.7	12.7	10.3	20.7	0.7	13.7	26.7	6.7		
WT15/42	no		6.0		11.0	15.0	59.0	106.0	1.0	54.0	32.0	16.0		
	%		2.0		3.7	5.0	19.7	35.3	0.3	18.0	10.7	5.3		
WT15/43A	no		11.0		111.0	10.0	18.0	50.0		68.0	25.0	7.0		
	%		3.7		37.0	3.3	6.0	16.7		22.7	8.3	2.3		
WT15/44	no	43.0	4.0		6.0	3.0	27.0	41.0	1.0	122.0	43.0	10.0		
	%	14.3	1.3		2.0	1.0	9.0	13.7	0.3	40.7	14.3	3.3		
WT15/45	no		1.0				57.0	66.0	5.0	88.0	70.0	12.0		1.0
	%		0.3				19.0	22.0	1.7	29.3	23.3	4.0		0.3
WT15/38	no		11.0	36.0	177.0	4.0		26.0		35.0	11.0			
	%		3.7	12.0	59.0	1.3		8.7		11.7	3.7			

11. X-RAY DIFFRACTOMETRY (XRD)

11.1. GENERAL DESCRIPTION

To get more detailed information about the samples mineralogy, whole rock x-ray diffraction analyses were conducted. The samples were analysed with a Panalytical X'Pert PRO (Cu Kα radiation, 40kV, 40 mA, step size 0.0167, 5s per step) diffractometer. The output of the diffractometer is a strip chart or diffraction pattern. The vertical scale shows the intensity (counts) of the diffracted peaks and the 2θ-angle increases from left to right on the horizontal scale. The minerals present in the sample can be identified by calculating the lattice spacing (d) out of the 2θ-angle applying Bragg's Law (Tucker, 1988): $2d \sin\theta = n\lambda$. For a qualitative analyses the x-ray diffraction patterns (Figure 41, Figure 42, Figure 43, Figure 44) were interpreted using the Panalytical software "X'Pert High score plus".

11.2. PREPARATION FOR THE XRD ANALYSIS

To prepare the altogether 13 samples for the XRD analysis it was necessary to produce a fine powder of a mean diameter between 5-10µm (Tucker, 1988) using a rock mill. To keep the contamination of the sample powder by iron as low as possible, considering that traces of metal interfere with the measurement and affect the signal, an agate bowl was used instead of a metal bowl to produce the powder. Since the samples have a high SiO2 content anyway, the additional SiO2 coming from the bowl doesn't change the overall result of the bulk analysis. The samples were loaded into the sample holders as non-oriented powder.

11.3. RESULTS

As already recognized in the thin sections on the optical microscope the occurrence of the components quartz, potassium-feldspar, plagioclase, mica, dolomite and calcite were confirmed by the XRD analysis. Additionally a clear signal for chlorite was found in the selected samples. Also worth mentioning is the mineral paragonite found in sample WT15/04. To get a better understanding for the overall composition and the relation to the profile the sample's chart records were placed in an order of their occurrence in the profile. Therefore the first three chart records shown (Figure 41, Figure 42, Figure 43, Figure 44) are those of the samples WT15/6B belonging to lithofacies 10 as the highest in the profile located sample analysed with XRD, WT15/34 belonging to lithofacies 13 and WT15/01 belonging to lithofacies 10. Under consideration of this chosen order all analysed samples were visualized.

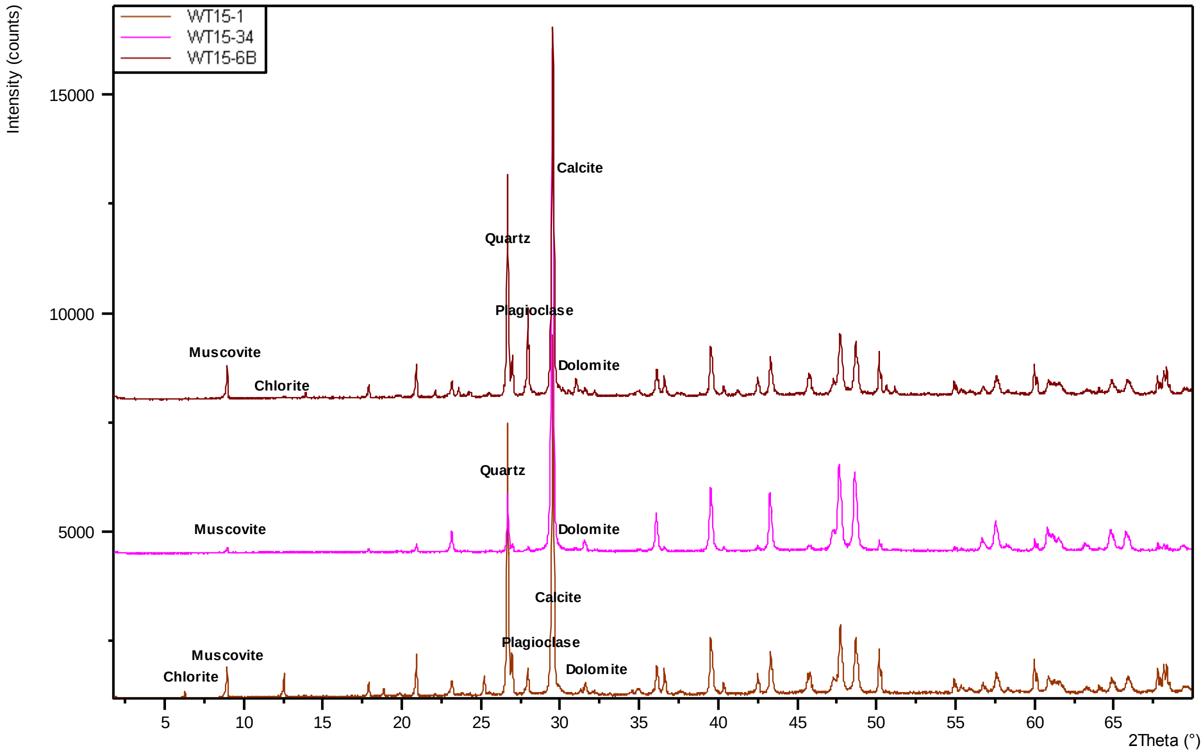

Figure 41: diffractogram of the samples WT15/6B, WT15/34 and WT15/01 showing x-ray diffraction patterns of the minerals muscovite, quartz, plagioclase, calcite and dolomite .The samples WT15/1 and WT15/6B also show the pattern of the mineral chlorite.

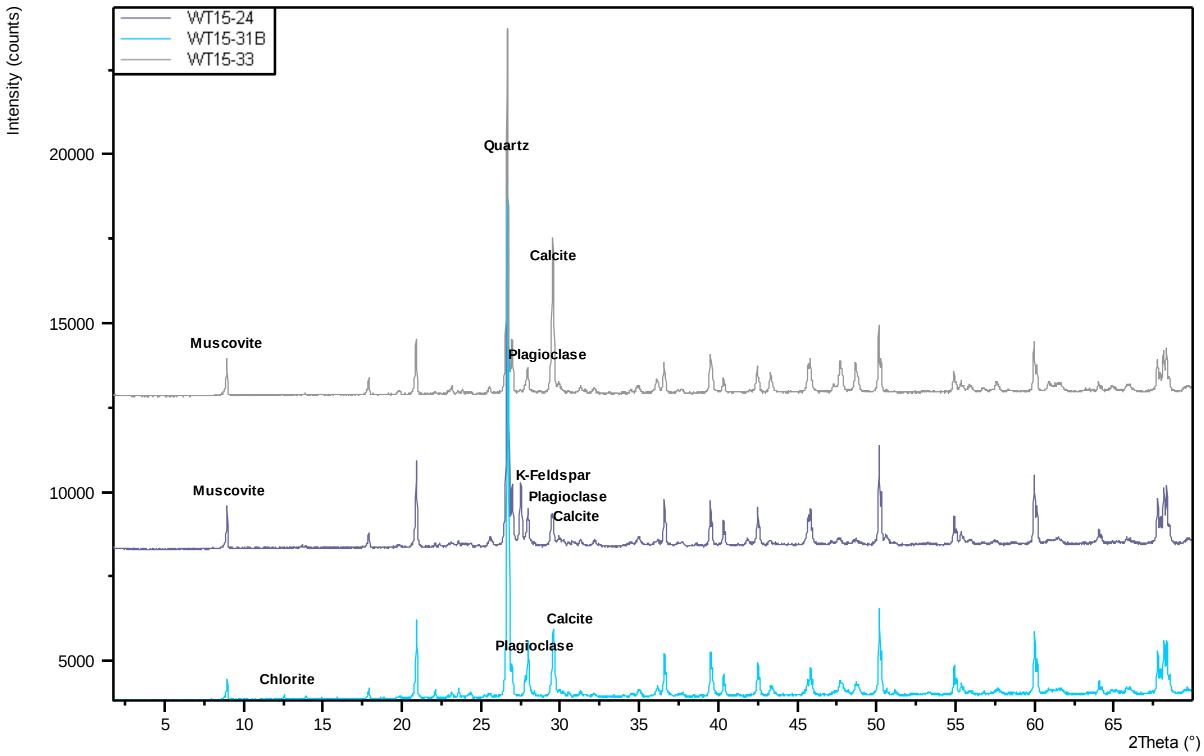

Figure 42: diffractogram of the samples WT15/24, WT15/31B, WT15/33 showing x-ray diffraction patterns of the minerals muscovite, quartz, plagioclase and calcite; sample WT15/24 also shows the pattern of potassium-feldspar; sample WT15/31B also shows the pattern of chlorite.

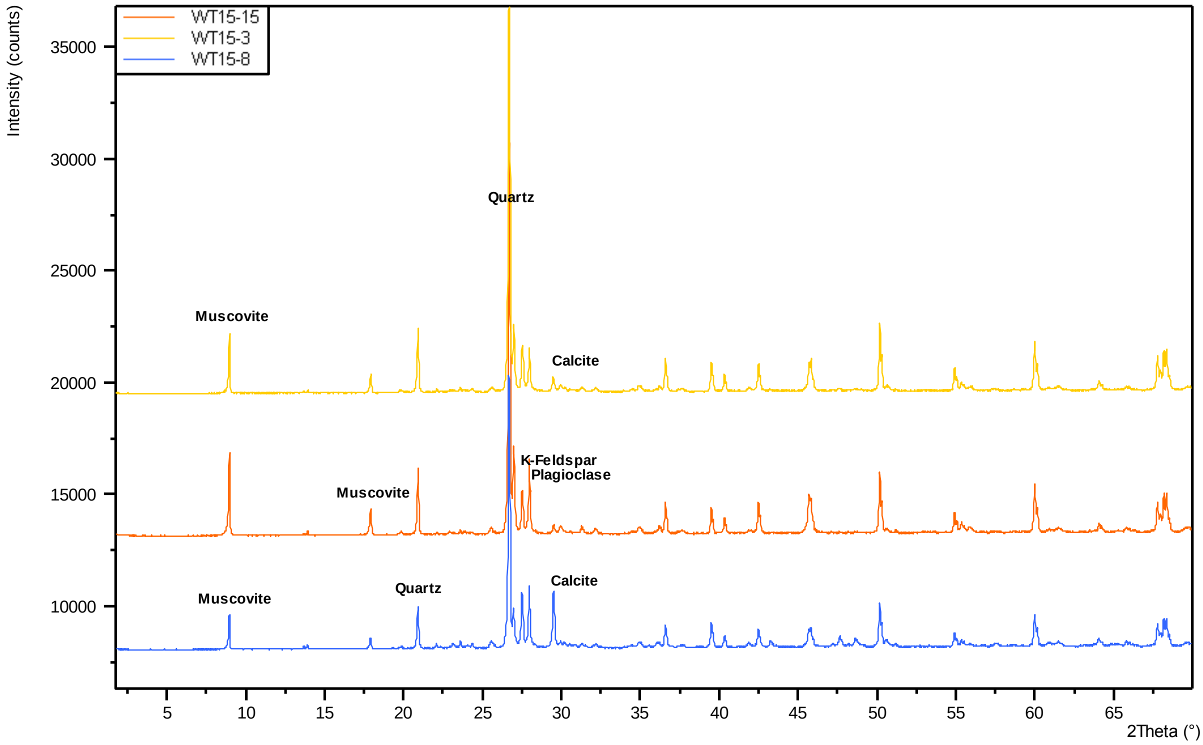

Figure 43: diffractogram of the samples WT15/15, WT15/3 and WT15/8 showing x-ray diffraction patterns of the minerals muscovite, quartz, calcite, potassium-feldspar and plagioclase;

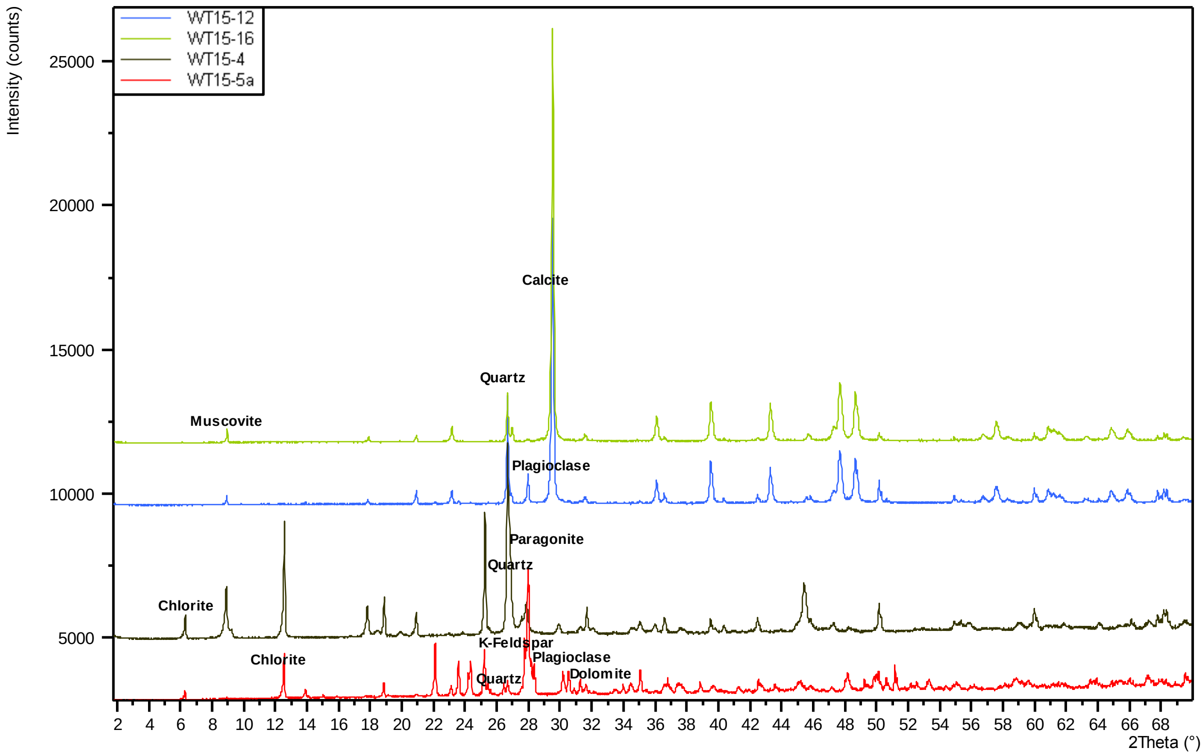

Figure 44: diffractogram of the samples WT15/12, WT15/16, WT15/4 and WT15/5a showing x-ray diffraction patterns of the minerals.

12. GEOCHEMISTRY: BULK ANALYSIS

12.1. SAMPLES AND PREPARATION

All together 13 samples were sent to the mineral laboratories of Bureau Veritas Commodities (www.bureauveritas.com/um), in Vancouver (Canada) to obtain geochemical bulk data (measured with an ICP-MS; see Table 3). When choosing the samples to be analysed, it was tried to get information of at least one sample per main lithofacies to get an idea of the geochemistry over the entire profile. From the bottom to the top following samples were chosen and prepared: WT15/5A (lithofacies 15), WT15/4 (lithofacies 1), WT15/12 (lithofacies 2), WT15/16 (lithofacies 3), WT15/8 (lithofacies 4), WT15/15 (lithofacies 5), WT15/3 (lithofacies 6), WT15/31B (lithofacies 8), WT15/24 (lithofacies 12), WT15/33 (lithofacies 14), WT15/1 (lithofacies 10), WT15/34 (lithofacies 13) and WT15/6B (lithofacies 10). Rock powder using a rock mill was produced (same procedure as explained in chapter "X-ray Diffractometry [XRD]"). It is important to keep in mind, that all samples have undergone metamorphosis. Therefore most of the results of the geochemical bulk analysis might not be fully reliably for the use of sedimentary provenance analysis. Analytical errors reported by Bureau Veritas are in the range of below ±1%.

Table 3: Data of the rock bulk geochemistry analysis

	Samples	WT 15/1	WT 15/12	WT 15/3	WT 15/4	WT 15/31B	WT 15/5A	WT 15/15	WT 15/24	WT 15/34	WT 15/33	WT 15/6B	WT 15/8	WT 15/16
Analyte	Unit	Rock Pulp	Rock Pulp	Rock Pulp	Rock Pulp	Rock Pulp	Rock Pulp	Rock Pulp	Rock Pulp	Rock Pulp	Rock Pulp	Rock Pulp	Rock Pulp	Rock Pulp
SiO2	%	38.19	25.04	81.54	54.7	69.38	57.15	79.31	77.53	9.33	59.98	37.6	71.11	11.92
Al2O3	%	4.92	2.26	8.27	23.35	5.48	19.33	10.14	8.19	1.08	6.27	5.23	8.89	1.05
FA2O3	%	1.99	0.84	1.01	5.97	2.44	7.36	1.59	1.06	0.31	1.28	1.2	0.95	1.49
MgO	%	1.33	0.58	0.52	2.68	0.81	2.4	0.64	0.56	0.8	0.88	1.54	0.41	0.48
CaO	%	27.74	38.97	1.62	0.98	9.84	1.96	0.7	3.53	48.58	15.08	27.57	6.9	46.59
Na2O	%	0.43	0.63	0.79	1.13	1.08	8.11	0.86	0.77	0.14	0.6	1.27	1.35	0.05
K2O	%	1.53	0.47	3.64	4.08	1.47	0.2	4.02	4.1	0.37	2.43	1.41	4.09	0.43
TiO2	%	0.18	0.06	0.18	0.94	0.1	0.83	0.26	0.18	0.03	0.16	0.11	0.18	0.04
P2O5	%	0.13	0.04	0.07	0.09	0.05	0.12	0.09	0.07	0.02	0.09	0.07	0.08	0.04
MnO	%	0.05	0.15	0.02	0.08	0.11	0.24	0.04	0.02	0.07	0.05	0.09	0.04	0.53
Cr2O3	%	0.004	0.002	0.004	0.019	0.002	0.017	0.002	0.003	0.002	0.003	0.002	0.003	0.002
Ba	ppm	146	61	377	506	158	50	457	452	55	188	268	340	41
Ni	ppm	21	<20	<20	41	<20	35	<20	<20	<20	<20	<20	<20	<20
Sc	ppm	5	2	3	22	4	18	6	3	<1	4	3	4	1
LOI	%	23.4	30.9	2.2	5.7	9.1	2.1	2.2	3.9	39.2	13.1	23.8	5.9	37.3
Sum	%	99.92	99.92	99.92	99.83	99.92	99.85	99.9	99.91	99.95	99.91	99.92	99.91	99.89
Be	ppm	<1	<1	1	5	<1	3	2	3	<1	2	<1	3	<1
Co	ppm	6	3	2.7	10	2.5	7.4	7.9	2.2	0.3	2.8	1.8	2.6	3.2
Cs	ppm	10	1.8	6.6	11.4	3.9	0.3	8.6	6.7	1.7	5.2	7.2	7.3	1.1
Ga	ppm	5.3	1.6	9.6	27.6	5.4	22.8	12.6	8.4	<0.5	5.8	4.6	10.6	0.8
Hf	ppm	1.2	0.7	2.6	4.5	1.6	5.3	3.6	3.4	0.4	2.1	1.2	3.2	0.6

Nb	ppm	3.7	1.4	6.2	18	3.9	16	9.2	6	0.7	4.2	2.9	7.3	0.8
Rb	ppm	64.8	18.6	129.7	169.4	50.5	5.7	201.2	143.2	11.9	93.2	55.9	173.2	19
Sn	ppm	1	<1	9	5	5	5	13	9	<1	4	1	13	<1
Sr	ppm	171.4	353.2	14.9	203.9	85.3	221.2	12.1	33.8	256.1	207.3	191.6	78.9	576.9
Ta	ppm	0.2	0.1	0.9	1.3	0.6	1	1.7	1.1	<0.1	0.5	0.3	1.5	0.1
Th	ppm	3.6	1.6	3.5	15.3	2.9	12.2	4.3	3.4	0.7	3.3	3.8	3.6	1
U	ppm	0.5	0.5	0.6	3.8	0.6	3.4	0.7	0.7	0.8	0.9	0.3	0.7	0.7
V	ppm	37	14	20	177	10	132	25	14	12	20	19	11	<8
W	ppm	1.1	0.5	2	1.3	1.1	2.7	3.3	2.1	<0.5	2.2	2.1	2.7	<0.5
Zr	ppm	40.6	24	88.8	160.7	49	190.5	120.9	123	16	73.6	42.8	112	19.1
Y	ppm	18.8	14.9	7.8	26	11.1	22	12.7	9.1	4.3	12.6	11	11.7	19.7
La	ppm	18.5	13	9.3	43.8	9.6	29.8	12.9	7.1	3.9	12	12.1	8.8	12.3
Ce	ppm	22.5	16	18.2	85.8	16.7	59.3	23.6	13.6	5.1	22.5	18.5	17.9	20.9
Pr	ppm	3.73	2.31	2.21	9.63	2.03	6.98	3.01	1.73	0.78	2.71	2.29	2.15	2.29
Nd	ppm	14.7	9.1	7.9	34.6	8	25.7	11.9	6.5	2.9	9.9	8.3	8.3	9.3
Sm	ppm	2.67	1.72	1.7	6.25	1.68	4.97	2.34	1.38	0.5	2.05	1.61	1.71	1.91
Eu	ppm	0.7	0.52	0.34	1.42	0.38	0.98	0.48	0.29	0.13	0.46	0.46	0.33	0.65
Gd	ppm	3.03	2.06	1.52	5.14	2	4.43	2.35	1.47	0.64	2.19	1.66	1.74	2.59
Tb	ppm	0.44	0.32	0.23	0.74	0.32	0.64	0.38	0.24	0.09	0.34	0.25	0.28	0.4
Dy	ppm	2.61	1.99	1.42	4.76	2.01	4.13	2.37	1.57	0.52	2.31	1.59	1.77	2.64
Ho	ppm	0.51	0.39	0.27	0.9	0.38	0.77	0.42	0.3	0.1	0.42	0.3	0.34	0.5
Er	ppm	1.45	1.13	0.87	2.72	1.06	2.43	1.26	0.92	0.3	1.19	0.9	1.01	1.36
Tm	ppm	0.21	0.14	0.12	0.44	0.16	0.35	0.19	0.14	0.04	0.17	0.13	0.17	0.19
Yb	ppm	1.25	0.85	0.85	2.7	1	2.3	1.24	0.92	0.28	1.08	0.87	1.1	1.17
Lu	ppm	0.21	0.13	0.12	0.4	0.15	0.38	0.2	0.14	0.04	0.17	0.14	0.16	0.15
TOT/C	%	6.5	8.99	0.38	0.97	2.26	0.06	0.2	0.82	11.23	3.42	6.65	1.53	10.64
TOT/S	%	<0.02	0.06	<0.02	0.06	<0.02	<0.02	<0.02	<0.02	<0.02	<0.02	<0.02	0.07	0.2
Mo	ppm	<0.1	0.3	0.3	0.2	0.3	0.5	0.2	0.2	<0.1	<0.1	0.1	0.3	0.3
Cu	ppm	9.6	4.6	4.2	46.2	3.9	9	10	3.7	9.7	10.8	30.9	5.8	2.8
Pb	ppm	4.8	7.9	11.9	6.7	20.4	1.1	11.9	11.5	4.8	14	5.7	12.2	10.6
Zn	ppm	18	4	3	89	16	147	25	5	4	3	11	4	6
Ni	ppm	15.3	6.1	2.6	41	5.5	38.1	10.5	2.6	0.4	1.3	2	3.8	5.6
As	ppm	<0.5	2.4	3	<0.5	3.6	1.5	5.6	2.3	<0.5	2.4	<0.5	2.8	5.7
Cd	ppm	0.2	<0.1	<0.1	<0.1	<0.1	<0.1	0.1	<0.1	<0.1	<0.1	0.4	<0.1	<0.1
Sb	ppm	<0.1	0.5	0.2	<0.1	<0.1	<0.1	0.4	0.2	<0.1	0.8	<0.1	0.1	0.6
Bi	ppm	0.1	<0.1	0.2	0.3	0.3	<0.1	0.2	0.3	<0.1	0.2	0.1	0.3	<0.1
Ag	ppm	<0.1	<0.1	<0.1	<0.1	<0.1	<0.1	<0.1	<0.1	<0.1	<0.1	<0.1	<0.1	<0.1
Au	ppm	<0.5	<0.5	<0.5	<0.5	<0.5	<0.5	<0.5	<0.5	<0.5	<0.5	<0.5	<0.5	<0.5
Hg	ppm	<0.01	<0.01	0.01	<0.01	<0.01	<0.01	0.01	0.01	<0.01	<0.01	<0.01	<0.01	0.01
Tl	ppm	0.1	<0.1	0.1	<0.1	<0.1	<0.1	0.2	<0.1	<0.1	<0.1	<0.1	0.1	<0.1
Se	ppm	<0.5	<0.5	<0.5	<0.5	<0.5	<0.5	<0.5	<0.5	<0.5	<0.5	<0.5	<0.5	<0.5
Cr	ppm	27.37	13.68	27.37	129.99	13.68	116.31	13.68	20.53	13.68	20.53	13.68	20.53	13.68

12.2. SEDIMENT CLASSIFICATION

The SandClass system (after Herron, 1988) is based on the relation of log (SiO2/Al2O3) versus log (FA2O3/K2O) and can be used to distinguish between different shale and sandstone types (see Figure 45). This diagram only includes sedimentary classifications, therefore the greenschist sample WT15/5B was not included. The yellow dots represent all sandstone and breccia samples analysed. They show a tight scatter in an area representing arkoses and litharenites. The black shale sample WT15/4 is marked as a black dot, plotting in the shale area of the SandClass system. These results indicate that even though the samples underwent metamorphism, their sedimentary nature can still be detected using geochemical analyses.

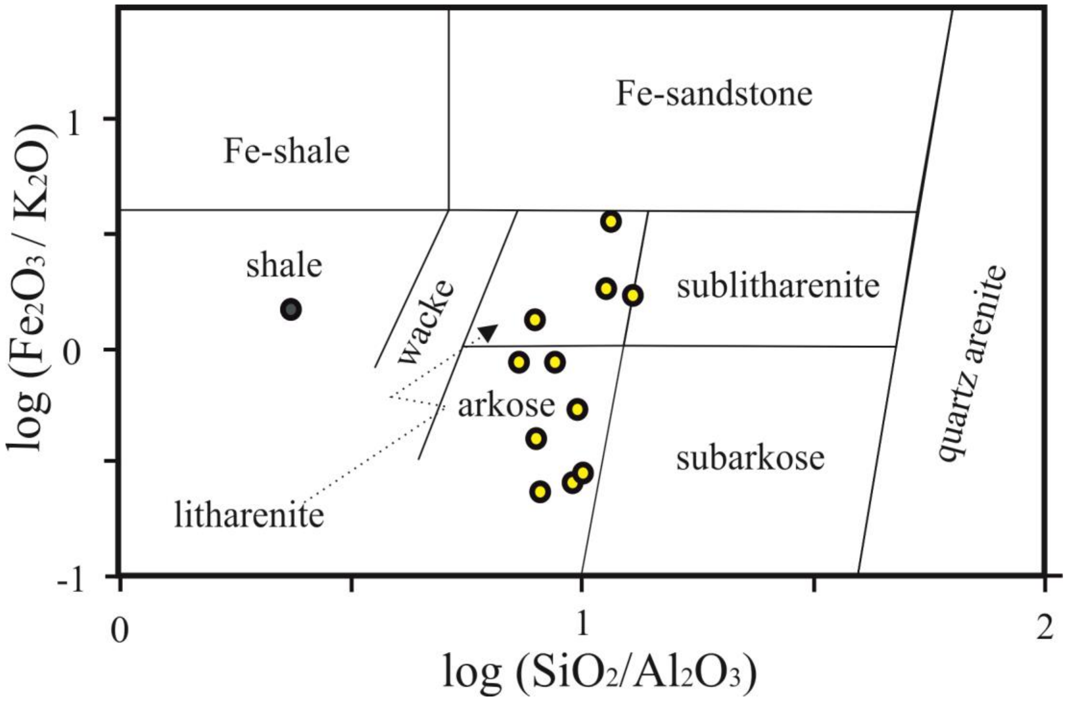

Figure 45: The SandClass system for geochemical classification of sediments (after Herron, 1988) based on the relation of log(SiO2/Al2O3) on the x-axes versus log(FA2O3/K2O) on the y-axis. The yellow measuring points show the sandstone samples, the black measuring point shows the shale sample WT15/4.

12.3. PROVENANCE

To determine the provenance of the sediments using geochemical data several approaches were done. Starting with the La/Sc versus Th/Co – diagram (after Cullers, 2002), which is used to make a basic differentiation between a basic source rock and a silicic source rock (see Figure 46). The sample points include all sandstone, breccia and shale samples analysed. Not included is the greenschist sample WT15/5B. The samples show a clear scatter in the area of silicic rock source.

Another diagram that was used is the Discrimination function diagram (see Figure 47) includes the major elements for sedimentary provenance (after Roser & Korsch, 1988). The functions are Discrimination function 1 = (1.773 x TiO_2) + (0.607 x Al_2O_3) + (0.760 x FA2O_3) + (-1.50 x MgO) + (0.616 x CaO) + (0.509 x Na_2O) + (-1.224 x K_2O) + (-9.090) and Discrimination function 2 = (0.445 x TiO_2) +(0.070 x Al_2O_3) + (-0.250 x FA2O_3) + (-1.142 x MgO) + (0.438 x CaO) + (1.475 x Na_2O) + (-1.426 x K_2O) + (-6.861). The four provenances distinguished by Roser & Korsch, 1988 are quartzose sedimentary provenance, felsic igneous provenance, intermediate igneous provenance and mafic igneous provenance. The sample points show a tight scatter in the area of quartzose sedimentary provenance. Both discrimination functions show relatively low values.

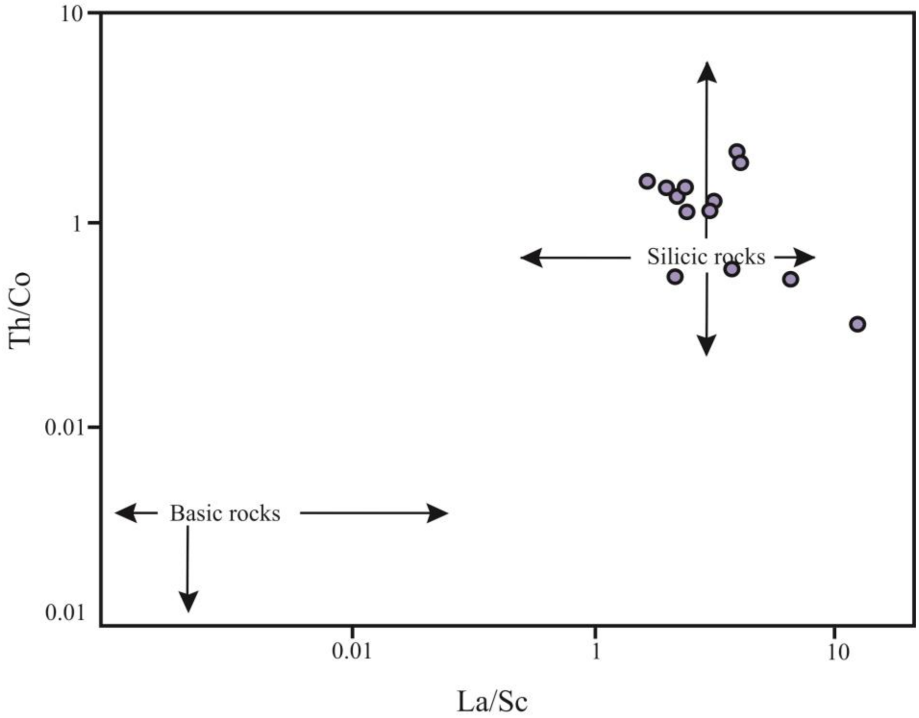

Figure 46: The La/Sc versus Th/Co diagram (after Cullers, 2002) is used to distinguish between samples deriving from basic source rocks or silicic source rocks. The sample points show a tight scatter clearly concentrated around the silicic source.

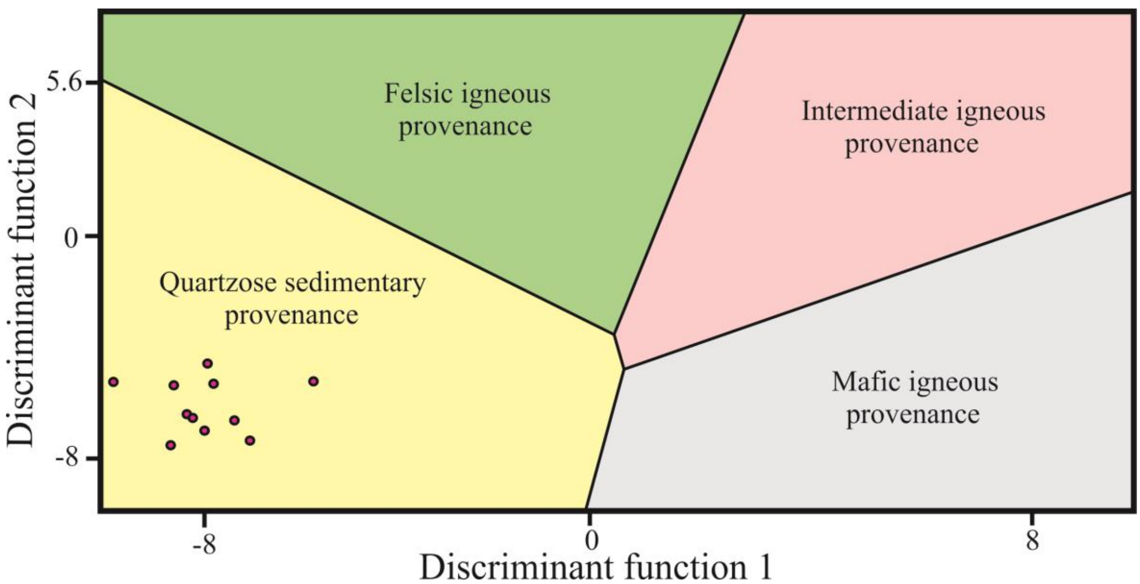

Figure 47: Discrimination Function diagram (slightly modified after Roser & Korsch, 1988) including the major elements for sedimentary provenances. The sample points show a clear recycled source in the area of quartzose sedimentary provenance.

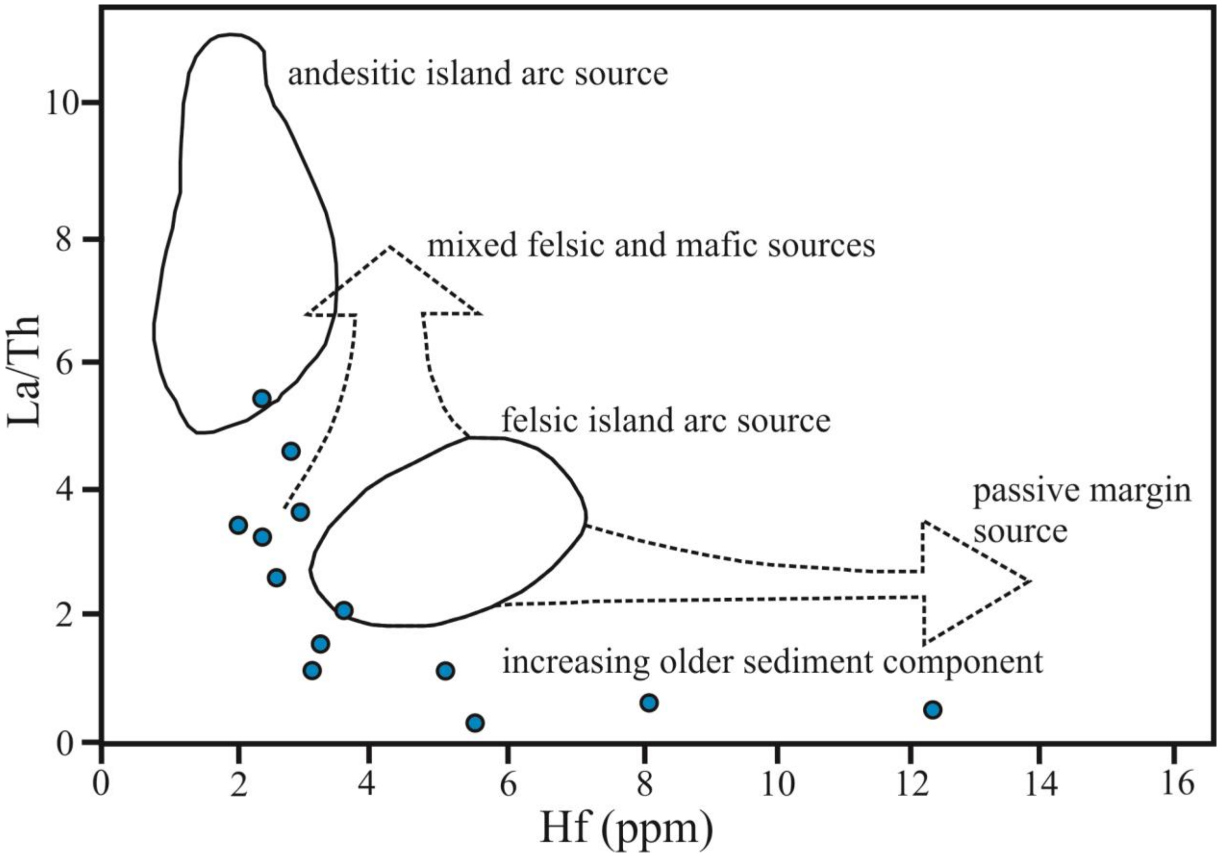

Figure 48: The ratio of La/Th versus Hf – diagram (after Floyd, 1987) for discrimination of provenance distinguishing between the four provenances: 1. andesitic island arc source, 2. mixed felsic and mafic source, 3. felsic island arc source and 4. passive margin source.

The Hf versus the ratio of La/Th diagram (after Floyd, 1987) is used to discriminate between different arc compositions. Most sample points show both, low La/Th ratios and low Hf values (Figure 48). Their distribution is closest to both the area of felsic island arc source and the mixed felsic and mafic sources. Unfortunately the values are too low and the distribution of sample points shows a too wide scatter over more than one field up to older sediment components and passive margin sources. Therefore it is not possible to determine an accurate provenance using this diagram.

According to Taylor & McLennan (1985), the Th/Sc ratio of the upper continental crust is >1. Apart from four samples, that lie close to a Th/Sc ratio of 1, all samples show a Th/Sc ratio slightly lower than 1 (see Figure 49), which could indicate an input from magmatic arc source (after McLennan et al, 1991, also see Bahlburg, 1998). There is strong indication of the samples being derived from a quartzose, sedimentary recycled source by combining the results of both the La/Sc versus Th/Co – diagram (see Figure 46; after Cullers, 2002), showing a tight scatter around the silicic rock area, and the Discrimination Functions diagram (see Figure 47; after Roser & Korsch, 1988), showing all samples in the recycled, quartzose sedimentary provenance area.

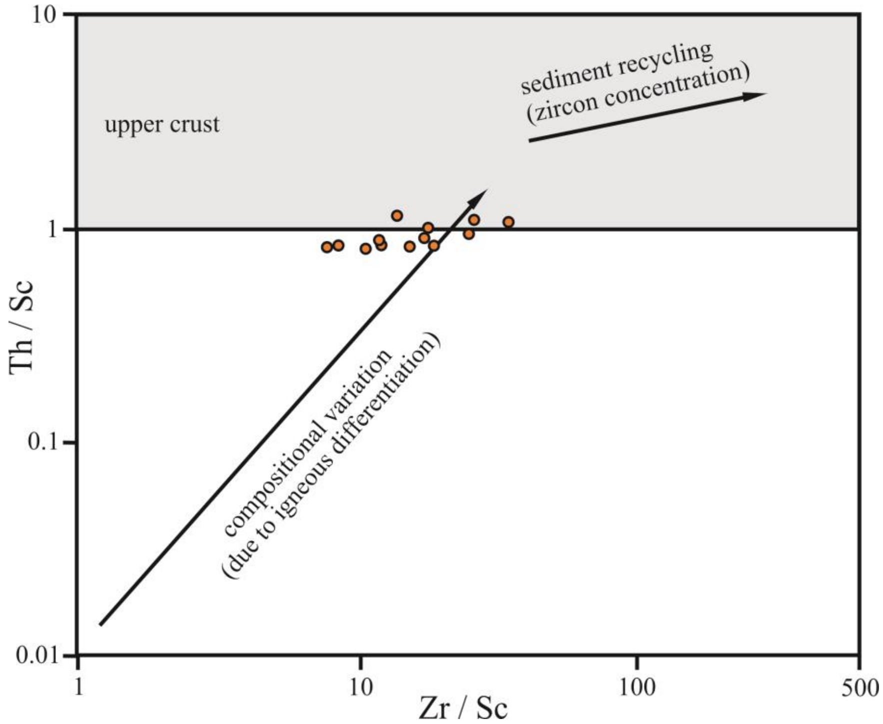

Figure 49: The Zr/Sc versus Th/Sc – diagram (after McLennan, 1993 and including slight modifications after Bahlburg, 1998) shows a horizontally sustained scatter of measuring points close to the border of the upper crust. The sustained form is due to the recycling trend of the samples, increasing towards the right which shows a higher Zr/Sc ratio and therefore an enrichment of zircon.

12.4. Chemical Index of Alteration (CIA)

The Chemical Index of Alteration (CIA, after Nesbitt & Young, 1982) gives information about the chemical changes within the sediments due to weathering.

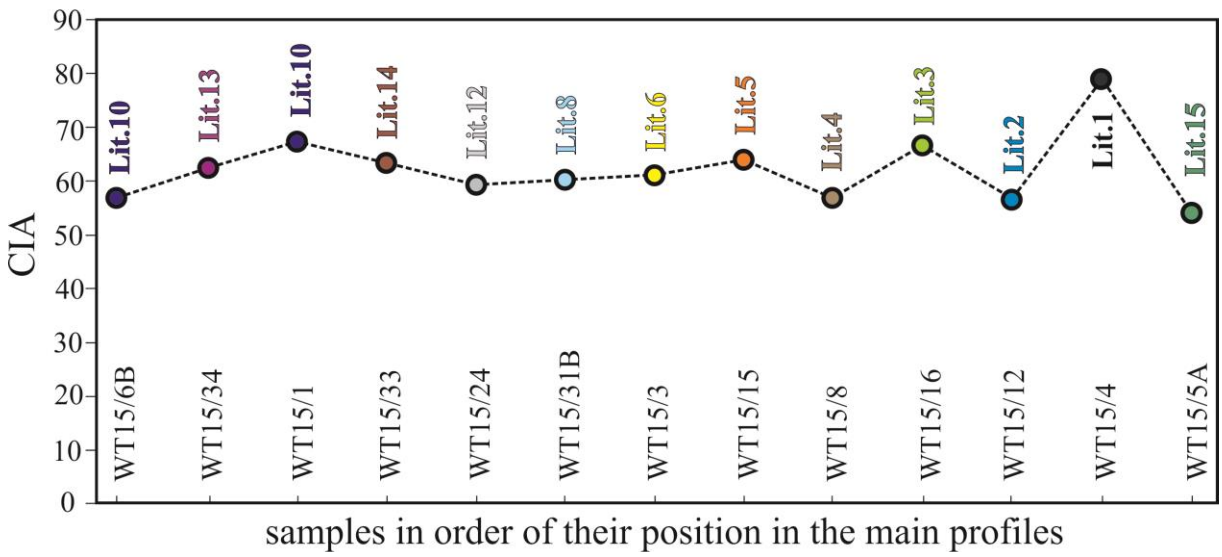

Figure 50: The Chemical Index of Alteration (CIA) (after Nesbitt & Young, 1982) of the selected samples shown in their order of occurrence in the main profiles. The lithofacies the samples were taken from are also marked and the sample points are shown in the colour they are also visualized in in the main profiles.

Whole rock chemical data of major element oxides (after Nesbitt & Young, 1982), given in molecular proportions, are used to calculate the CIA, which is defined as

$CIA = \left(\frac{Al_2O_3}{Al_2O_3+Na_2O+K_2O+CaO^*}\right) \times 100$ (Bahlburg & Dobrzinski, 2011).

CAO^* (after Fedo et al., 1995) only includes the CaO of silicate minerals. For this reason the CaO* of carbonate containing samples had to be corrected (after Fedo et al., 1995).The selected samples show bigger changes in the CIA at the bottom of the profile than at the top (see Figure 50). Starting off with the greenschist-sample WT15/5A which shows a low CIA, the CIA increased strongly at times of the deposition of Lithofacies 1 (WT15/4). The changes in CIA (and thus weathering) are getting less and less towards the top of the profile. All together most samples show a CIA between 55 and 65. Worth mentioning is the correlation of grainsize and the CIA. It is notable that especially the fine-grained shales of lithofacies 1 show higher values and thus higher apparent weathering. The grainsize increases towards the

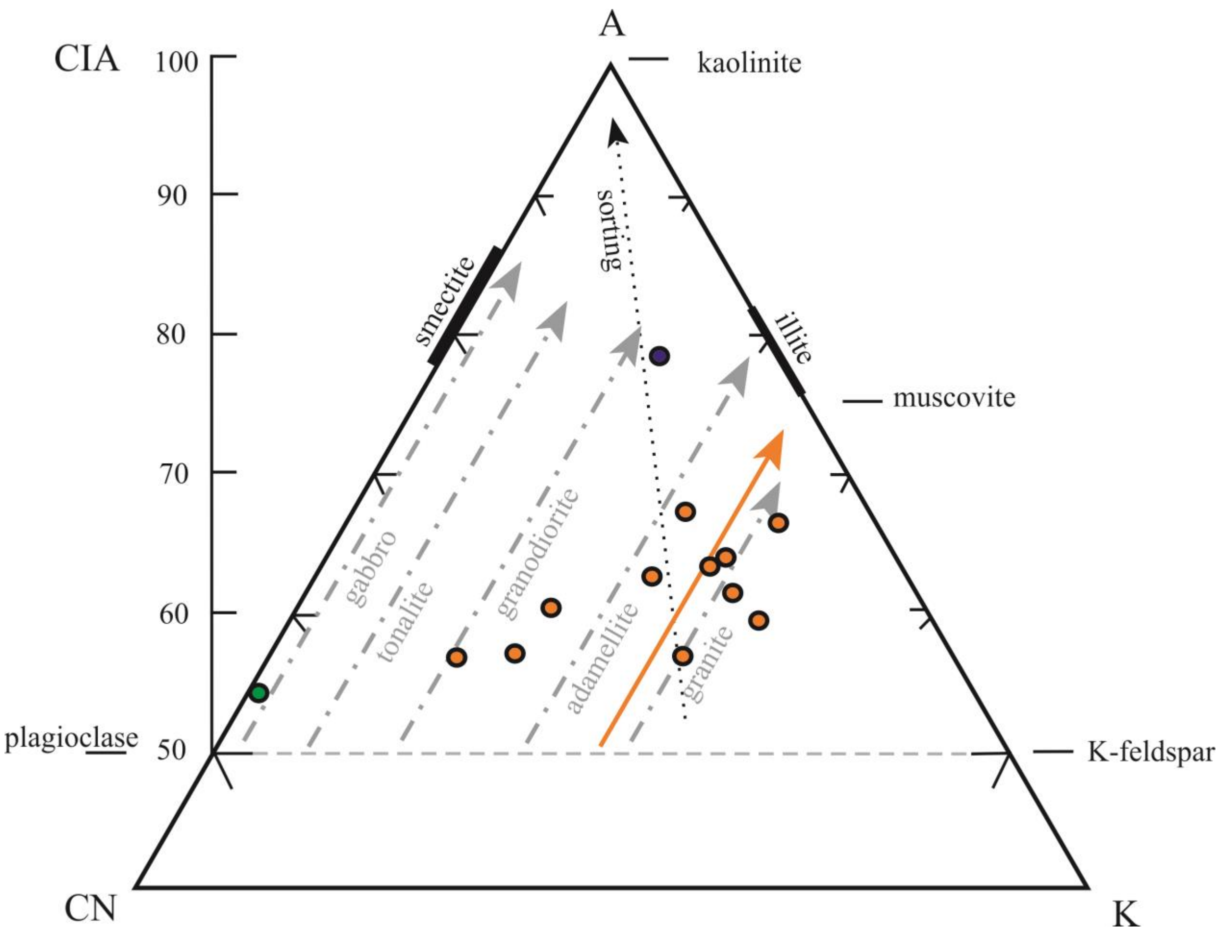

Figure 51: A [A] Al2O3 – [CN] CaO + Na2O – [K] K2O ternary diagram (slightly modified after Nesbitt & Young, 1984)including predicted weathering trends (dashed grey lines) of typical magmatic source rock types (after Fedo et al., 1995) indicates a mostly granitic source for the sandstone samples shown in orange colours. The orange arrow shows their mean weathering trend concerning. The green point shows the position of the greenschist sample. The dark blue point shows the position of the back shale sample that was analysed. It shows a higher CIA than all other samples and strong weathering. The black dotted line shows the trend of sorting of the material. The dashed grey lines show the weathering trends of certain rock types.

top and CIA decreases at the same time. The ACNK-ternary diagram (see Figure 51; after Nesbitt & Young, 1984) gives an idea about the source rock the samples derived from, based on the oxides Al_2O_3 [A], CaO + Na_2O [CN], K_2O [K] and the relation to the CIA of the samples. The predicted weathering trends of typical magmatic source rock types (after Fedo et al., 1995) are shown in Figure 51 in dashed grey lines. As expected the greenschist sample (WT15/5A) shows a very low CIA, which indicates low weathering and plots close to the gabbro line. Following the line of better sorting the blackshale sample of lithofacies 1 shows the highest CIA, therefor indicates higher weathering close to the Illit CIA values. The majority of the flysch sediment samples show moderate weathering. Their average value is marked with an orange line indicating a most likely granitic source rock.

12.5. TECTONIC SETTING

To find out the (plate) tectonic setting for the sediment's deposition, several diagrams for discrimination of tectonic settings (after Bhatia & Crook, 1986) were plotted (see Figure 53). Bhatia & Crook, (1986) distinguish between four main tectonic settings. The first tectonic setting is oceanic island arc [A], visualized in light red colour. The second tectonic setting is continental island arc [B], visualized in green colour in the diagrams. The third tectonic setting is active continental margin [C], visualized in blue colour. The fourth tectonic setting distinguished is passive margin [D], visualized in grey colour. Altogether Figure 53 includes five diagrams. Graphic E is a Th – Sc – Zr/10 – ternary diagram; graphic F is a Sc/Cr versus La/Y – diagram; graphic G is a La/Sc versus Ti/Zr-diagram; graphic H is a Th-Co-Zr/10-ternary diagram; graphic I is a Th-La-Sc-ternary diagram; The measured samples plot in various fields with a majority in continental island arc to passive margin areas. The average value plots in/or close to the tectonic setting B, the area of continental island arc.

A second approach for distinguishing between tectonic settings was done using a SiO2/ log (K2O/Na2O) - diagram (after Roser & Korsch, 1986; see Figure 52). Roser & Korsch (1986) distinguish between three tectonic settings, passive margin [PM], Active continental margin [ACM] and Island arc [ARC]. Unfortunately the sample points show a scatter over all separate areas of tectonic settings and it is therefore not possible to get clear information about the tectonic setting using this major element oxide compound diagram, probably due to element transport during metamorphism.

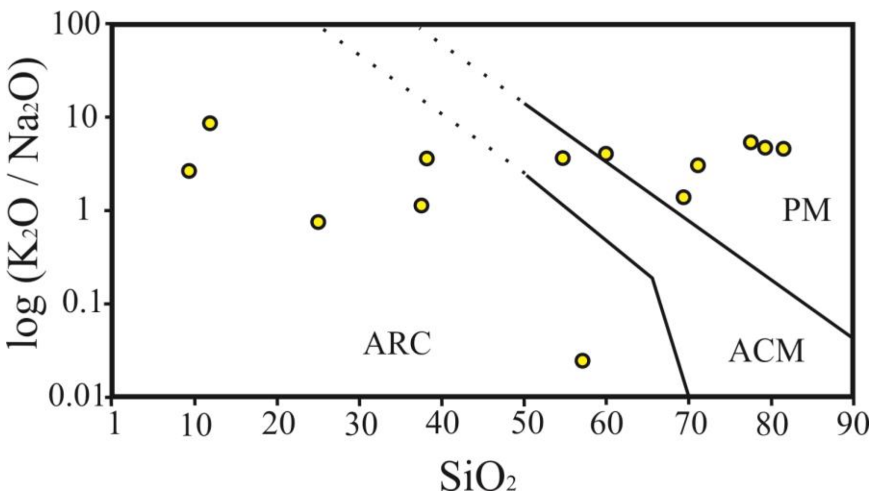

Figure 52: SiO2 versus log(K2=/Na2O)-diagram for discrimination of tectonic settings (after Roser & Korsch, 1986). Three main tectonic setting are distinguished: [PM] passive margin; [ACM] Active continental margin; [ARC] Island arc.

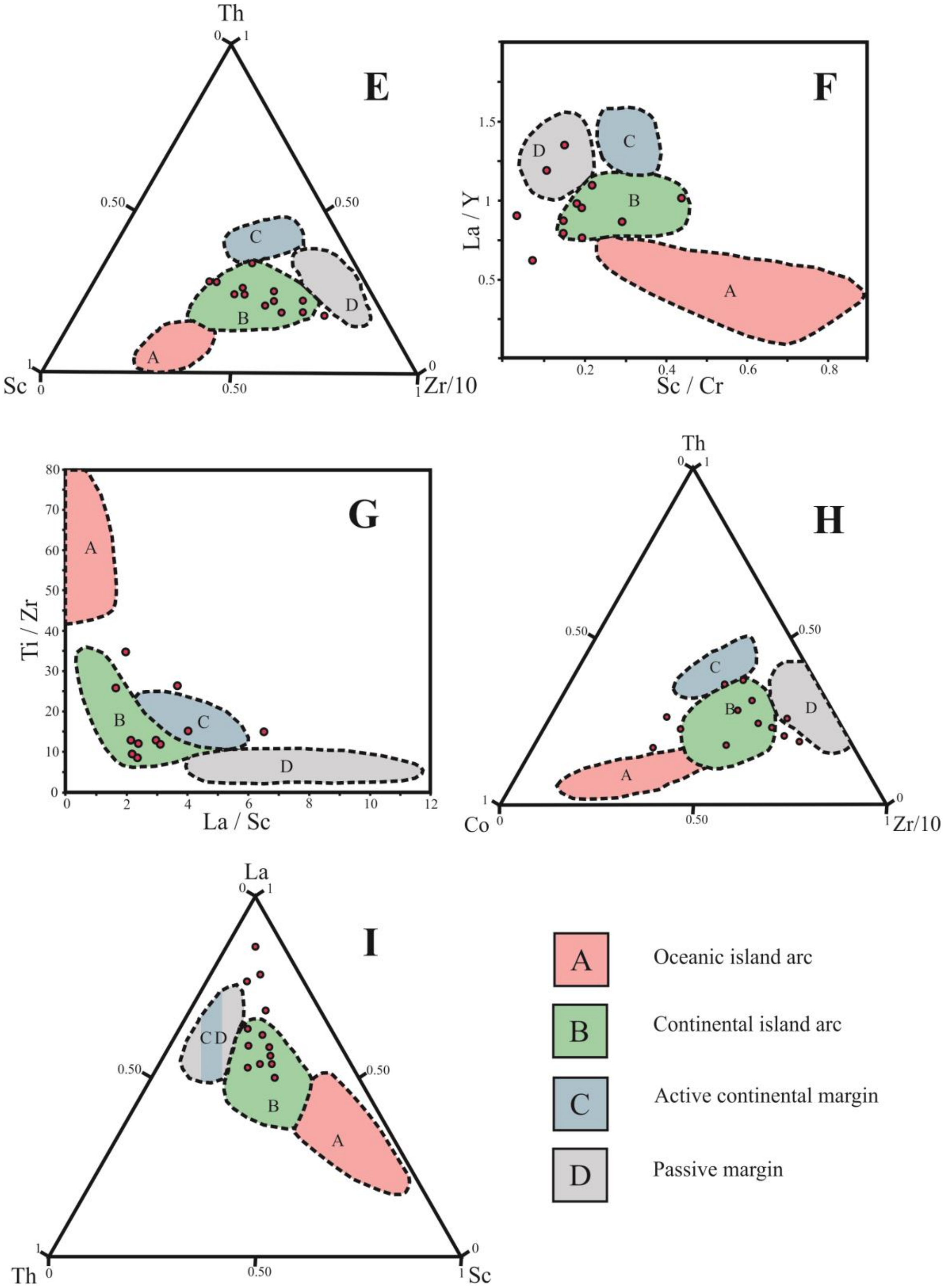

Figure 53: Diverse Plots used for discrimination of tectonic settings (after Bhatia & Crook, 1986). The four main tectonic settings distinguished are: Oceanic island arc [A] light red colour, Continental island arc [B] green colour, Active continental margins [C] blue colour and Passive margins [D] grey colour; Graphic E is a Th – Sc – Zr/10 – ternary diagram; Graphic F is a Sc/Cr versus La/Y – diagram; Graphic G is a La/Sc versus Ti/Zr-diagram; Graphic H is a Th-Co-Zr/10-ternary diagram; Graphic I is a Th-La-Sc-ternary diagram; The measured samples are shown in red dots. The average value plots in/or close to the tectonic setting B, the area of continental island arc.

12.6. PRINCIPAL COMPONENT ANALYSIS

The main purpose of the component analysis was to find out, if there was one source area or if there were several sources for all samples analysed. The statistical analyses were conducted using the program package PAST (PAleontological STatistics; after Hammer, 2001). A principal components analyses (PCA) (see Davis, 1986) as well as a hierarchical clustering (after Ward, 1963 requiring euclidean distances) were applied. Ordination in the PCA follows a variance-covariance matrix and establishes principal components (PC) according to the amount of variance explained within the data (that mainly control the chemical relations of all samples). The first three principal components explain more than 95 percent of variance. As an indication of a valuable analysis useful for provenance discrimination, it is preferable to have a well-balanced percentage of variance between the principal components.

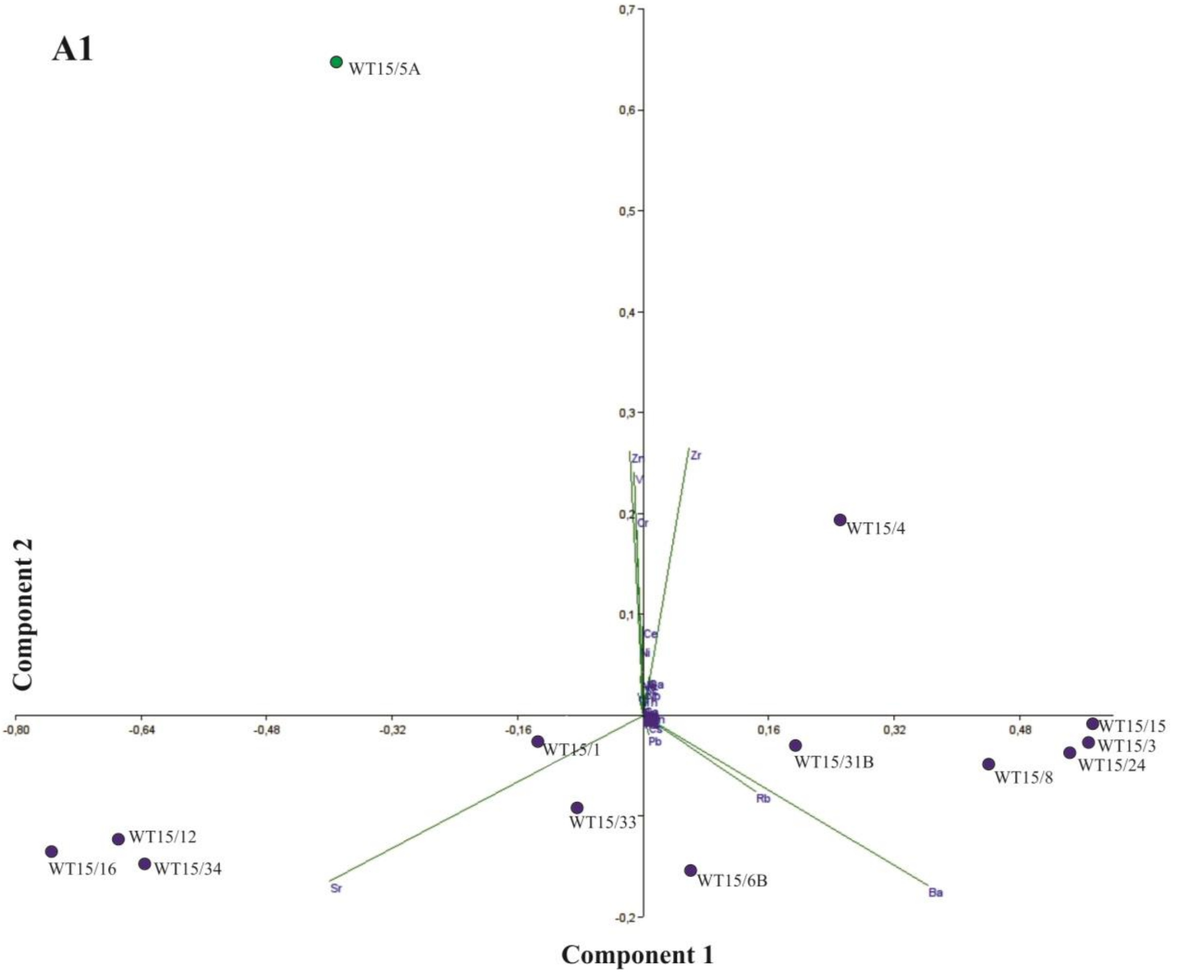

Figure 54: Principal component-analysis-plot (after Davis, 1986) based on single element data of all samples; PC1 is mainly depending on strongly positive values of Ba and Rb, and a strongly negative value of Sr; PC2 mainly depends on positive values of V, Zr, Zn and Cr and negative values of Ba, Sr and Rb.

As a first approach (A1) all samples, also including WT15/5A the greenschist sample and WT15/4 the black shale sample, were compared (see Figure 54). Raw data was standardized and transformed using a log-transformation. Only single element values were used, not including those only given as oxide compounds. In this first approach over 96% of all sample points are dependent of the principal component 1. A clear distance between the greenschist sample WT15/5A and the rest of the samples can be observed. It was taken in the area of the Glockner Nappe, at the base of the main profile A. The results of both the A1 and A2 show this clear difference of WT15/5A to the other samples. Also worth mentioning is the slight difference of the shale sample WT15/4 and the rest of the flysch samples. AT15/4 shows a higher dependence on PC2 inter alia strongly depending on Zr values.

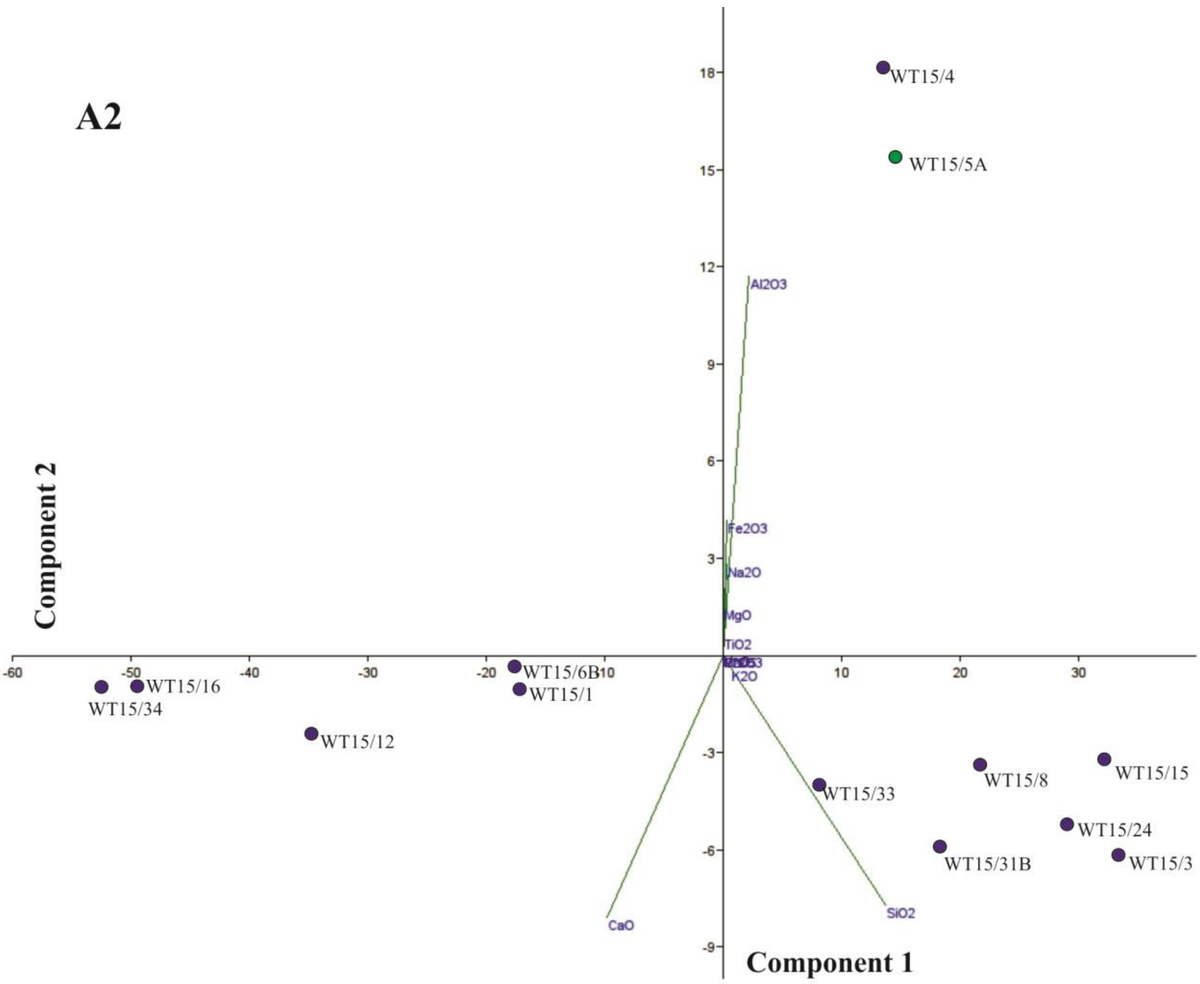

Figure 55: Principal component analysis plot (after Davis, 1986) based on raw data of oxide compounds of all samples; All flysch samples are fully dependent on PC1, which is controlled by a strongly positive value of SiO2, a slightly positive value of Al2O3 and a strongly negative value of CaO; PC2 depends on a highly positive value of Al2O3.

The second approach (A2) was based only on the raw data values of the oxide compounds of Al, Si, Fe, Mg, Ca, Na, K, Ti, P, Mn and Cr (see Figure 55). The distribution in A2 basically shows the same pattern as A1. Again, like in A1 the greenschist-sample (WT15/5A) and the black shale-sample (WT15/4) are separated from the flysch samples. All other sample points are more or less controlled by only one principal component, by PC1 (see Figure 56). WT15/5A and WT15/4 show dependence on both principal components.

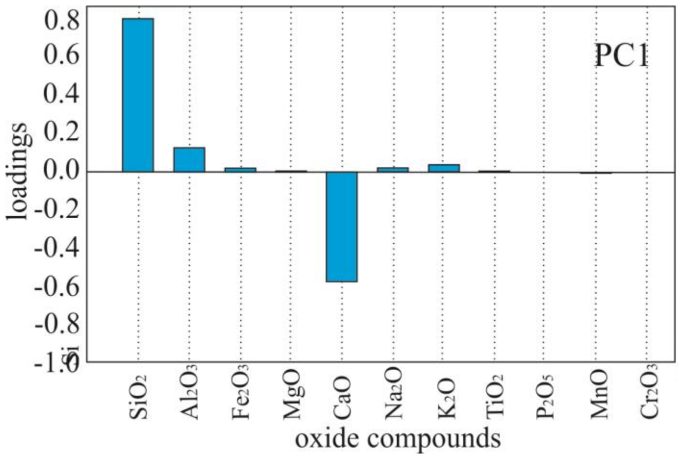

principal components	Eigenvalue	%
PC1	948.9650	93.685
PC2	59.5837	5.882
PC3	3.7500	0.3702
PC4	4.51E-01	4.45E-02
PC5	1.15E-01	1.13E-02
PC6	6.44E-02	6.36E-03
PC7	6.97E-03	6.88E-04
PC8	1.44E-03	1.43E-04
PC9	2.69E-04	2.66E-05

Figure 56: Exact register of oxide compound dependence of the first principal component PC1 used in the second approach A2. Also included is a listing of Eigenvalues and percentages of variance of all principal components.

Finally, the most accurate principal component analysis is the third one (see Figure 57 A). For this third approach only single element data of the geochemistry bulk data was used including those elements given as oxide compounds. Therefore the percentages of all given oxide compounds had to be converted to single element values, including Al, Si, Fe, Mg, Ca, Na, K, Ti, P, Mn and Cr. Afterwards the raw data and the calculated single element values were standardized and transformed using a log-transformation. The greenschist sample WT15/5B and the black shale sample WT15/4 are not included in this third approach. Their strong deviation of the other samples and (especially for WT15/5b) the high chance of separate provenances interfere with the calculations of the principal components. Excluding these two samples led to a better-balances percentage of dependence of variance of the first three principal components (see Figure 57). This balance of percentage of dependence of variance of all principal components is additionally visualized as a “broken stick”-diagram, representing the relation of Eigenvalue [%] on the y-axes versus principal components on the x-axes.

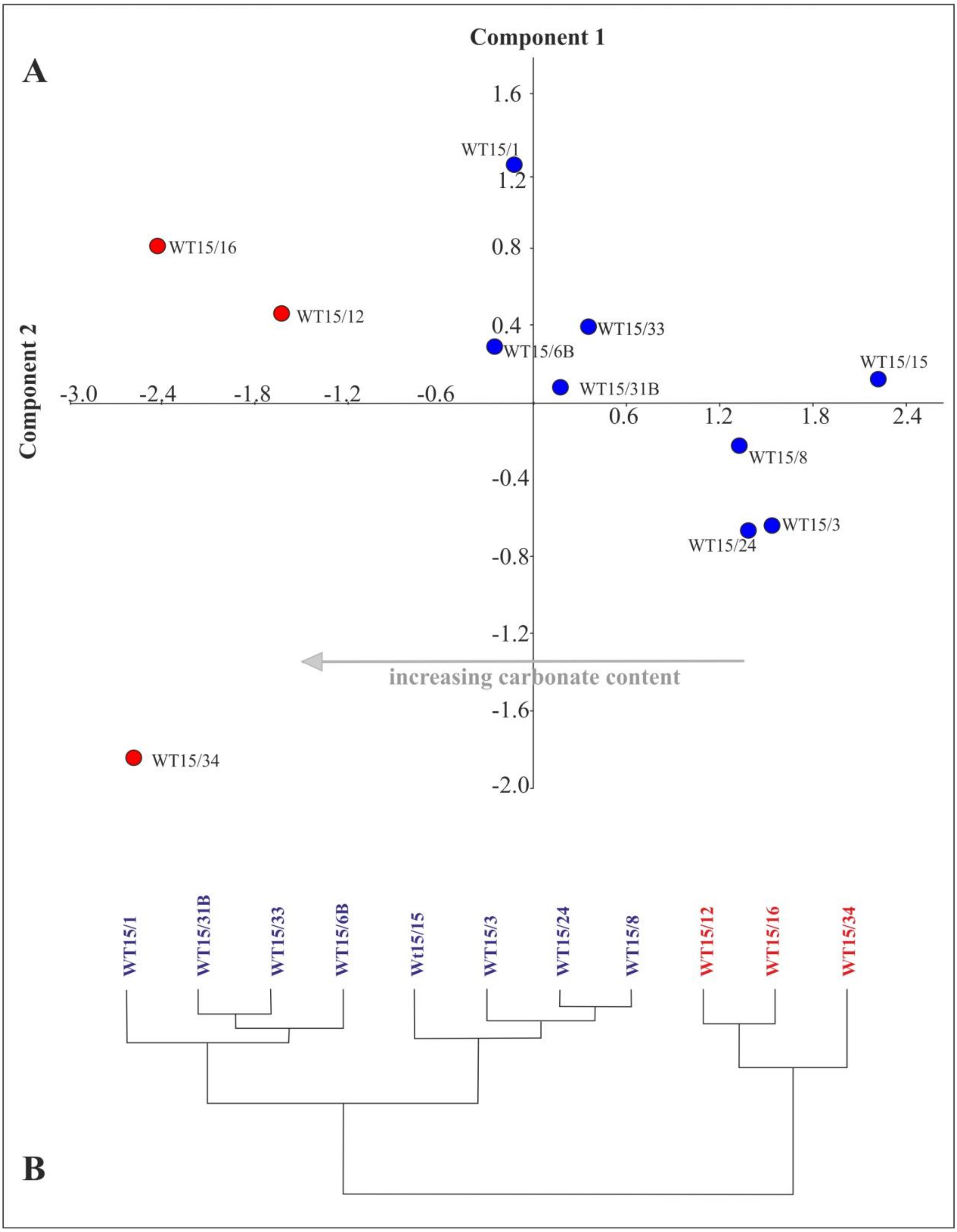

Figure 57: Graphic A shows a principal component-analysis (after Davis, 1986) including carbonate rich samples visualized in red colour and samples with low/no carbonate content visualized in blue colour.

Graphic B shows a hierarchical clustering-graphic (after Ward, 1963) visualizing the chemical relations of samples to each other based on their single element contents.

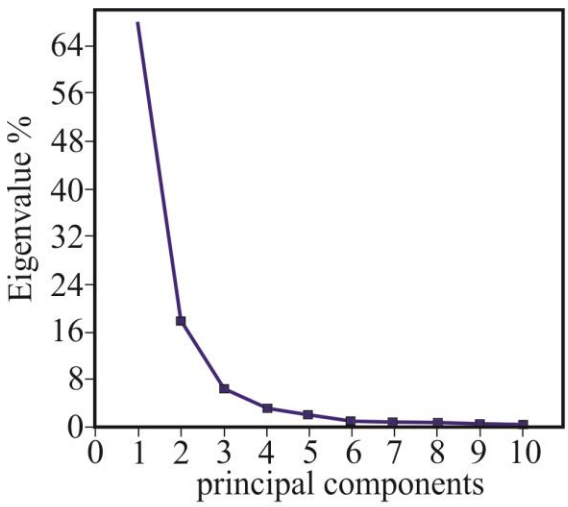

principal components	Eigenvalue	%
PC1	0.2363	78.453
PC2	0.0455	15.119
PC3	0.0113	3.7419
PC4	4.34E-03	1.4395
PC5	2.34E-03	0.7776
PC6	6.91E-04	0.2295
PC7	3.57E-04	0.1185
PC8	1.77E-04	0.0588
PC9	1.40E-04	0.0465
PC10	2.93E-05	0.0097
PC11	1.10E-05	0.0037

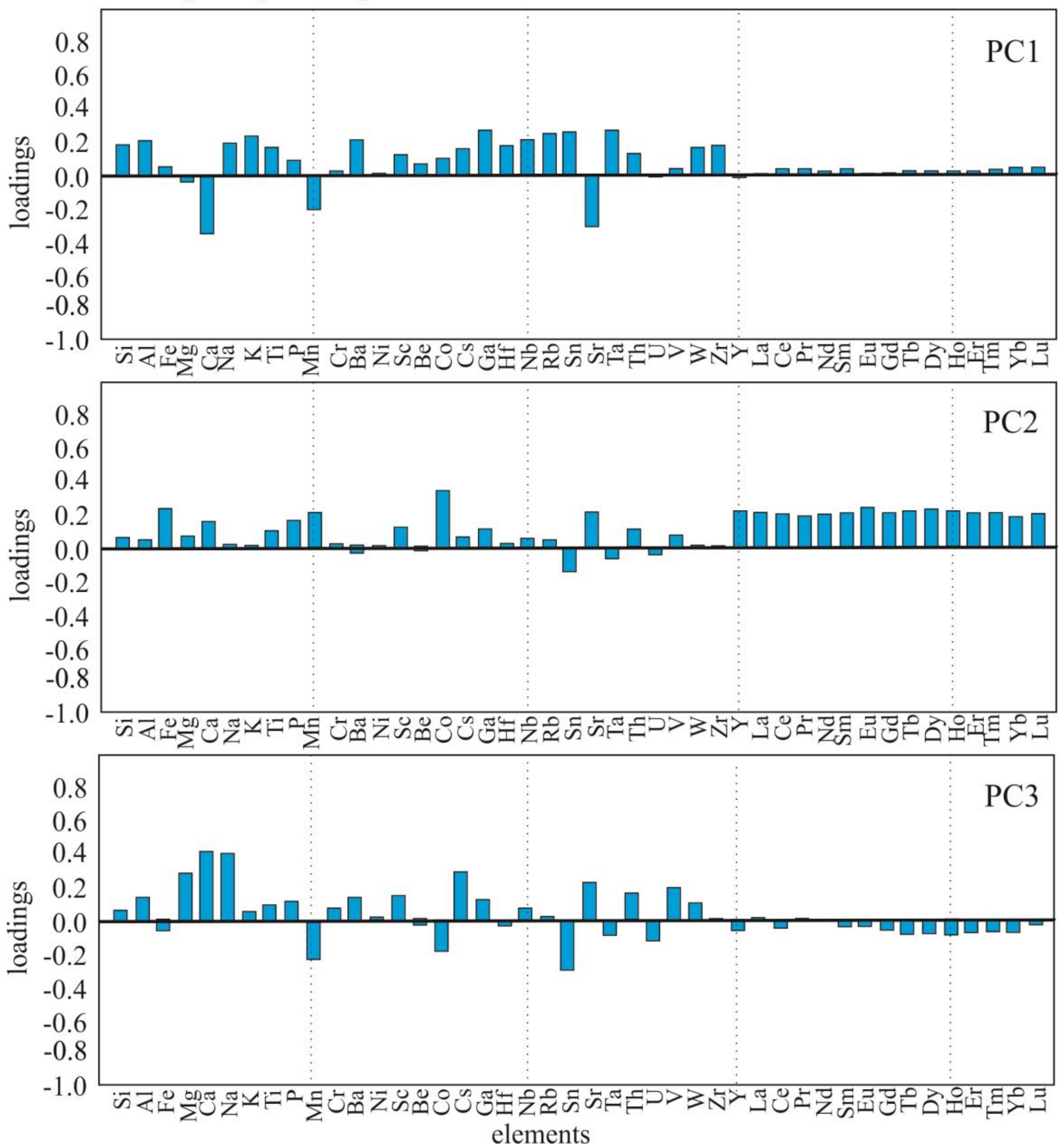

Figure 58: Exact register of element dependence of the first three principal components PC1, PC2 and PC3 including a listing of Eigenvalues and percentages of variance of all principal components and a "broken stick"-diagram of Eigenvalue [%] versus principal components.

The table shows that over 97 percent of sample relations can be explained with the first three principal components PC1, PC2 and PC3. An exact register of element dependence of these first three principal components is shown at the bottom of Figure 58. PC1 mostly depends on strongly negative values of Ca, Mn, Sr and strongly positive values of inter alia K, Ba, Ga, Rb, Sn and Ta. PC2 mostly depends on a negative value of Sn and strongly positive values of Fe, Co and Sr. It also shows dependence on positive values of REE. PC3 mostly depends on negative values of Mn, Sn and Co and strongly positive values of Mg, Ca, Na and Cs. For the third approach only the first two principal components PC1, explaining the relation of over 78 percent of the samples, and PC2, explaining the relation of over 15 percent of the samples, were used (see Figure 57 Graphic A).

The principal component analysis plot (Figure 57 Graphic A) shows two data point fields. This could indicate two separate source areas for the samples. To get better clearance on the information shown in the plot the components were first divided into two groups depending on their mineral composition. The carbonate-rich lithologies are visualized in red and the carbonate-poor/or -free lithologies are visualized in blue colours. The two data scatters observed first and this new sample division based on the mineral composition match perfect. The carbonate-rich samples shown in red colours form a scatter on the left (negative PC1 values) and the carbonate-free/or -poor samples form a scatter on the right side (positive PC1 values). WT15/1, WT15/6B, WT15/31B and WT15/33 also contain carbonates, but substantially less than the carbonate-rich samples shown in red. This four samples plot more or less in the middle, at PC1 values close to 0.

The second part of Figure 57 is Graphic B showing a hierarchical clustering-graphic (after Ward, 1963) visualizing the chemical relations of samples to each other based on their single element contents. The connecting lines show how closely related the samples are to each other. Three relation groups can be distinguished. The first group includes the samples WT15/1, WT15/31B, WT15/33 and WT15/6B. These four samples are those, which slightly contain carbonates. The second group includes the samples WT15/15, WT15/3, WT15/24 and WT15/8. All samples out of this second group are free of carbonates. The third group includes all carbonate-rich samples, shown in red colours, WT15/12, WT15/14 and WT15/32. This third group shows equal relations to both group 1 and group 2. Again, identically to Graphic A, the main difference controlling the relation grouping seems to be the carbonate content.

This last principal component analysis was calculated once again, including the CIA as an external controlling factor. No major change of sample distribution was observed. This indicates that weathering changes do not have a strong effect on the principal component analysis of these flysch sediments.

12.6.1. Results

Summarizing all information, it is not clearly discernible if there is more than one source for the deposits. Even though it is theoretically possible to divide the samples into two separate groups it is most likely, that their slight difference in geochemistry is based mainly on their carbonate content. This may either indicate two sources (a carbonate-bearing and a non-carbonate source) or may be only due to primary complex source area with some carbonates, and diagenetic and metamorphic alterations.

13. HEAVY MINERALS

13.1. INTRODUCTION TO HEAVY MINERAL ANALYSIS

In general minerals with a density higher than 2.9g/cm³ are grouped into heavy minerals. They can be used for provenance analysis (see Morton, 1985). Therefore both, the appearance or the lack of certain heavy minerals as well as the combination and relation of different heavy minerals to each other can give information about the source rock of the sediment (after Morton, 1999).

Table 4: average density and source reported for common heavy minerals (source: webmineral.com)

Heavy mineral	**Average density**	**Source**
Tourmaline	3,07	pegmatites, metamorphic rocks
Apatite	3,19	granite or other igneous rock
Hornblende	3,20	lower amphibolite facies
Titanite	3,48	granitic pegmatites, skarn, gneisses
Chloritoide	3,54	metamorphosed phyllites, schists and marbles
Garnet	3,95	Highly metamorphic rocks
Rutile	4,25	high pressure igneous rocks
Zircon	4,65	magmatic rocks, metamorphic rocks, pegmatites
Chrome spinel	4,79	mineral found in ultramafic and mafic rocks
Monazite	5,15	Granitic pegmatites

A large variety of factors, for instance the acidity/basicity of the rock’s environment, sorting or mixing of different source rocks controls and influences the heavy mineral distribution. Therefore, it is necessary to have more information about the area the samples come from. Another factor that has influence on the heavy mineral distribution is the grainsize chosen for the analysis of the material. It is important to keep in mind that different minerals form in different crystallographic classes and prefer different grainsizes. For example tourmaline, staurolite, kyanite and pyroxene usually form bigger grains than for instance rutile or zircon crystals, which occur increasingly in smaller grain fractions (after Mange et al., 1991). For reliable results, only literature data, which is based on analysis using heavy minerals of the same grainsize as your own, can be used for comparison. Furthermore, other factors influencing the heavy mineral assemblage after deposition (e.g. diagenesis, metamorphosis, etc.) have to be considered. These factors can cause possible dissolution of unstable heavy mineral species and therefore change the overall distribution of all heavy minerals in the deposits (after Morton, 2007).

13.2. Preparation for heavy mineral separation

Out of 49 samples taken in the field, 44 samples were used for heavy mineral separation. The samples were prepared for the production of the thin sections. Afterwards the remaining pieces were partitioned in a way that there was a piece of every sample left for later examination if necessary. Every single sample was crushed to a maximum grain size of 5 mm using a jaw crusher.

To get rid of organic material and carbonates within the samples, the crushed material was acidified. Therefore, a mixture of 200ml acetic acid with a concentration of 80% and 300ml deionized water was used. Each sample remained in the solution for a week and was properly stirred once a day. A week was chosen as a time frame, because it gives the sample enough time to dissolve eventual carbonates, but doesn't dissolve less acid-stable heavy minerals, like for instance apatite.

To get the requested grainsize of 0.04 mm to 63µm for the heavy mineral analysis, the samples were wet sieved. Before drying them in the compartment drier, the samples were additionally rewashed with deionized water to get rid of eventually remaining shale minerals and micas that would block the filters during the heavy mineral separation.

13.3. HEAVY MINERAL SEPARATION

For the main heavy mineral separation the heavy liquid LST Fastflow was used. LST Fastflow is a light yellow coloured, water-soluble 80% sodium-heteropolytungstate in our case used with a density above 2.85g/cm³. After a separation the LST Fastflow had to be cleaned using a Buchner-funnel and a vacuum pump. The liquid got filtered first using a 1µm - 2µm filter paper and second using a carbon filter. By vaporizing the liquid with a maximum temperature of 100°C on a hotplate, the wanted density can be regained. When storing the heavy liquid it is important to keep it in a closed bottle, otherwise in contact with air it continues to vaporize and crystallizes.

Two slightly different ways of the experimental assembly were used during the separation process, due to the fact that not a lot of experiments with this heavy liquid have been done in the lab beforehand.

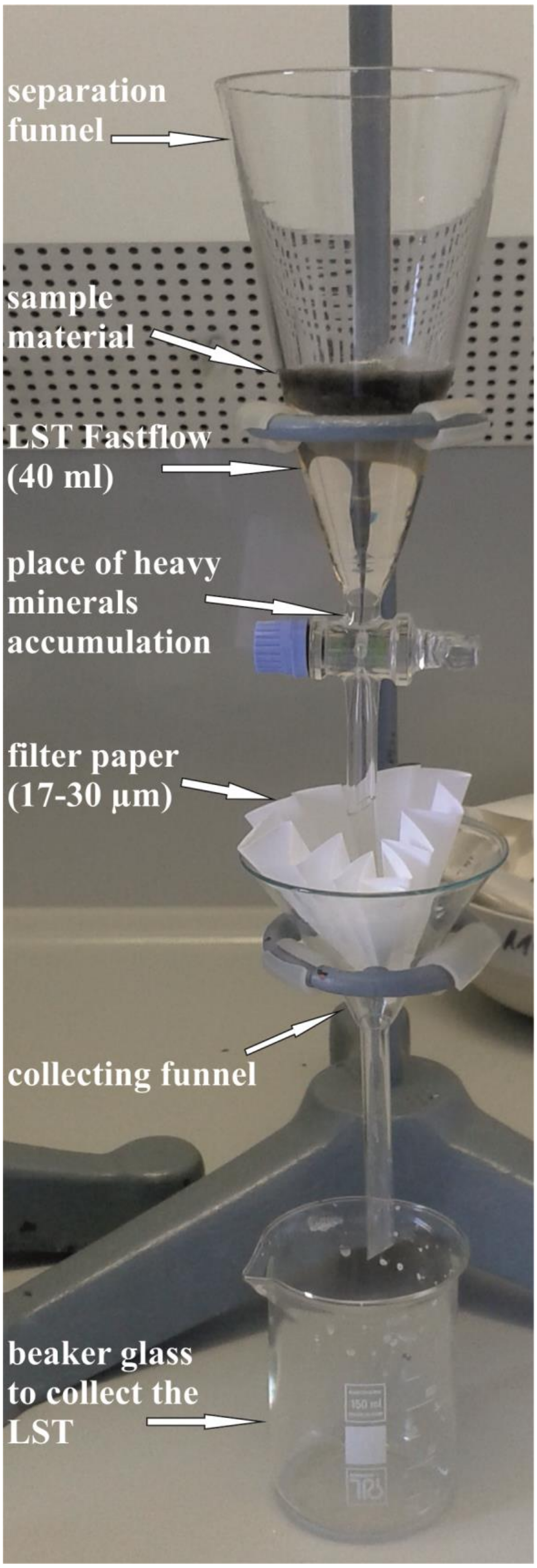

Figure 59: Experimental assembly of a heavy mineral separation using LST Fastflow.

For the heavy mineral separation of 30 samples a 250ml separation funnel, filled up with 200ml heavy liquid for each sample, was used. First the cold liquid was filled into the funnel. Afterwards two small spoons of dry material were put into the funnel. Then the separation funnel was carefully turned in an angle a few times, so the sample was well spread over the entire heavy liquid's surface. The separation funnel was positioned vertical on the holder, closed with a plastic cork and left for two hours so the heavy minerals could sink towards the bottom of the separation funnel. At the end of the separation the accumulated heavy mineral grains at the bottom were carefully let out of the funnel into another small funnel, holding a 17µm – 30µm pleated filter. The filter paper was washed several times with boiling deionized water. The samples were ready to get dried in the compartment drier as soon as there was no sign of remaining LST Fastflow within the heavy mineral grains or the filter paper. This method allowed the separation of two samples at the same time, due to the capabilities in our laboratory.

The second experimental assembly (see Figure 59) was used to separate the heavy minerals of 14 samples. Therefore, a smaller separation funnel holding 40ml of LST Fastflow per sample was used. The same way as with the other method first the heavy liquid was filled into the funnel. Afterwards two spoons of sample material were put into the funnel. The mixture then was stirred with a thin glass rod to loosen up the material within the liquid and to spread it out over the entire heavy liquid's surface. Then the separation funnel was covered with a watch glass and left for 15 minutes. Afterwards the stirring process got repeated several times. The separation using this method should also take two hours, but unfortunately the LST Fastflow is highly temperature dependent and tends to crystallize quickly when in contact with air. This is problematic for a reliable separation over two hours. For this reason the separation using the smaller separation funnel took an hour the longest. Afterwards the heavy mineral grains were taken out, washed and dried the same way as with the first method. The use of the smaller separation funnels allowed a separation of four samples at the same time.

As soon as the samples were dried completely, they were filled into small capsules and stored until they were needed to produce strew slides using a natural resin called Canada Balsam.

13.4. HEAVY MINERALS OF THE TAUERN FLYSCH

Heavy minerals in general can be grouped in various ways for instance due to their stability in general (after Pettijohn et al., 1973), resistance in general (after Pettijohn, 1941), their stability towards acidity or immersion (after Morton, 1985). The heavy mineral distribution of the Tauern Flysch shows an enrichment of ultra-stable heavy minerals like rutile, zircon and tourmaline and of stable heavy minerals for instance apatite (after Pettijohn et al., 1973).

13.4.1. Zircon

Zircons can be clearly distinguished from all other heavy minerals due to their lack of colouring in PPL and their strong relief. With crossed polarisers they show high, very intense interference colours. Their crystal shape in general is idiomorphic. Within the samples of the Tauern Flysch some elongated forms were observed, mostly, however, slightly rounded small zircons can be found.

13.4.2. Tourmaline

Tourmalines in general show very strong pleochroism, which is most likely their most dominant characteristic. The tourmalines observed within the samples of the Tauern Flysch mostly include colouring from brown to green-brown to being translucent. They occur mostly in prismatic grains, rarely, however, also radial aggregates were observed. They show high, intense interference colours in XPL.

13.4.3. Rutile

Rutiles occur as small, idiomorphic grains, with a thick, strong relief and show orange to red to brown colour. The inherent colour of rutile is very dominant. It outshines and overlies it’s interference colours when using XPL completely. It is for that reason that rutile more or less looks the same using PPL or XPL.

13.4.4. Apatite

Apatite occurs as translucent, mostly rounded grains, showing a thin, weak relief compared to zircon. When using XPL the grains show a light grey to light blue colouring. They have a very low tolerance for acidic environments (see Morton, 1985). Therefore, it is important to know what acid was used to prepare heavy minerals for the separation. Hydrochloric acid for instance dissolves apatite, which leads to an alteration of the overall heavy mineral distribution.

13.4.5. Garnet

Garnets only occur rarely in the samples of the Tauern Flysch. They mostly occur as translucent, idiomorphic grains with a thick, strong relief. In general, garnets can show weak colouring of rose to rose-brown (see Mange, 1991). However, no colouring and no pleochroism can be observed. All garnets analysed are isotropic when using XPL. The sometimes occurring etching marks, which can be characteristic for some garnets, cannot be found.

13.4.6. Titanite

Titanite can solely be observed as crystal aggregates and it does not occur frequently. Even though the single grains of titanite are translucent, the aggregates seem slightly brown-coloured. This appearance could be caused by surface etching marks (after Mange, 1991). It shows high, very intense interference colours when using XPL.

13.5. COUNTING OF HEAVY MINERALS

For the counting of heavy minerals it was tried initially to count around 300 grains per slide. Unfortunately many of the samples don't contain that many heavy minerals. For this reason, only strew slides of samples containing at least 100 heavy minerals were used for further analysis and bar charts (Table 5; Figure 60).

Table 5: Calculated heavy mineral distribution of strew slides containing more than 100 heavy minerals (in percent [%]). The acronyms are: L lithofacies, S sample, Zir zircon, Apa apatite, Tou tourmaline, Rut rutile, Chl chloritoid, Tit titanite, Gar garnet, Dis disthene, Amp amphibole, O others.

L	S	Zir	Apa	Tou	Rut	Chl	Tit	Gar	Dis	Amp	Others
15	WT15/5B	15.8	8.6	14.4	1.4	18.9	0.0	0.0	7.7	32.4	0.9
11	WT15/10	13.2	16.1	2.3	61.5	0.0	0.0	0.0	0.6	0.0	0.0
2	WT15/12	36.8	19.5	9.8	4.5	2.3	0.0	27.1	0.0	0.0	0.0
	WT15/13	26.3	12.3	56.1	2.3	0.0	0.0	2.9	0.0	0.0	0.0
	WT15/14	9.2	47.7	19.2	7.7	7.7	0.0	1.5	0.8	0.0	0.0
5	WT15/15	57.1	19.4	0.0	18.6	2.0	0.0	1.6	0.0	0.0	0.0
	WT15/19	41.1	41.6	1.1	11.9	3.2	1.1	0.0	0.0	0.0	0.0
	WT15/43	42.1	37.2	0.0	18.3	1.2	0.0	1.2	0.0	0.0	0.0
4	WT15/8	66.0	23.8	0.7	8.2	1.4	0.0	0.0	0.0	0.0	0.0
	WT15/17	64.7	15.7	0.8	17.4	0.8	0.3	0.3	0.0	0.0	0.0
8	WT15/31A	24.3	33.7	32.9	8.2	0.4	0.0	0.4	0.0	0.0	0.0
	WT15/31B	17.8	30.5	36.6	13.2	0.6	0.0	1.2	0.0	0.0	0.0
6	WT15/45	45.1	9.6	15.4	29.9	0.0	0.0	0.0	0.0	0.0	0.0
	WT15/7	35.3	35.9	10.5	5.2	6.5	0.0	1.3	5.2	0.0	0.0
	WT15/25	32.6	48.0	1.5	17.8	0.0	0.0	0.0	0.0	0.0	0.0
	WT15/32	59.3	8.2	1.2	31.3	0.0	0.0	0.0	0.0	0.0	0.0
	WT15/44	66.3	7.6	10.3	15.2	0.0	0.0	0.0	0.0	0.0	0.0
	WT15/3	27.7	31.3	4.5	4.5	5.4	26.8	0.0	0.0	0.0	0.0
10	WT15/1	13.0	28.4	14.2	6.2	13.0	21.6	0.0	2.5	0.0	1.2
	WT15/6B	13.6	52.7	16.4	3.6	13.6	0.0	0.0	0.0	0.0	0.0
	WT15/27	53.2	16.0	10.1	20.7	0.0	0.0	0.0	0.0	0.0	0.0
12	WT15/24	28.7	50.2	0.0	16.6	4.0	0.0	0.4	0.0	0.0	0.0
14	WT15/33	28.8	61.2	1.2	8.8	0.0	0.0	0.0	0.0	0.0	0.0
13	WT15/34	18.6	60.2	9.7	10.6	0.0	0.0	0.9	0.0	0.0	0.0

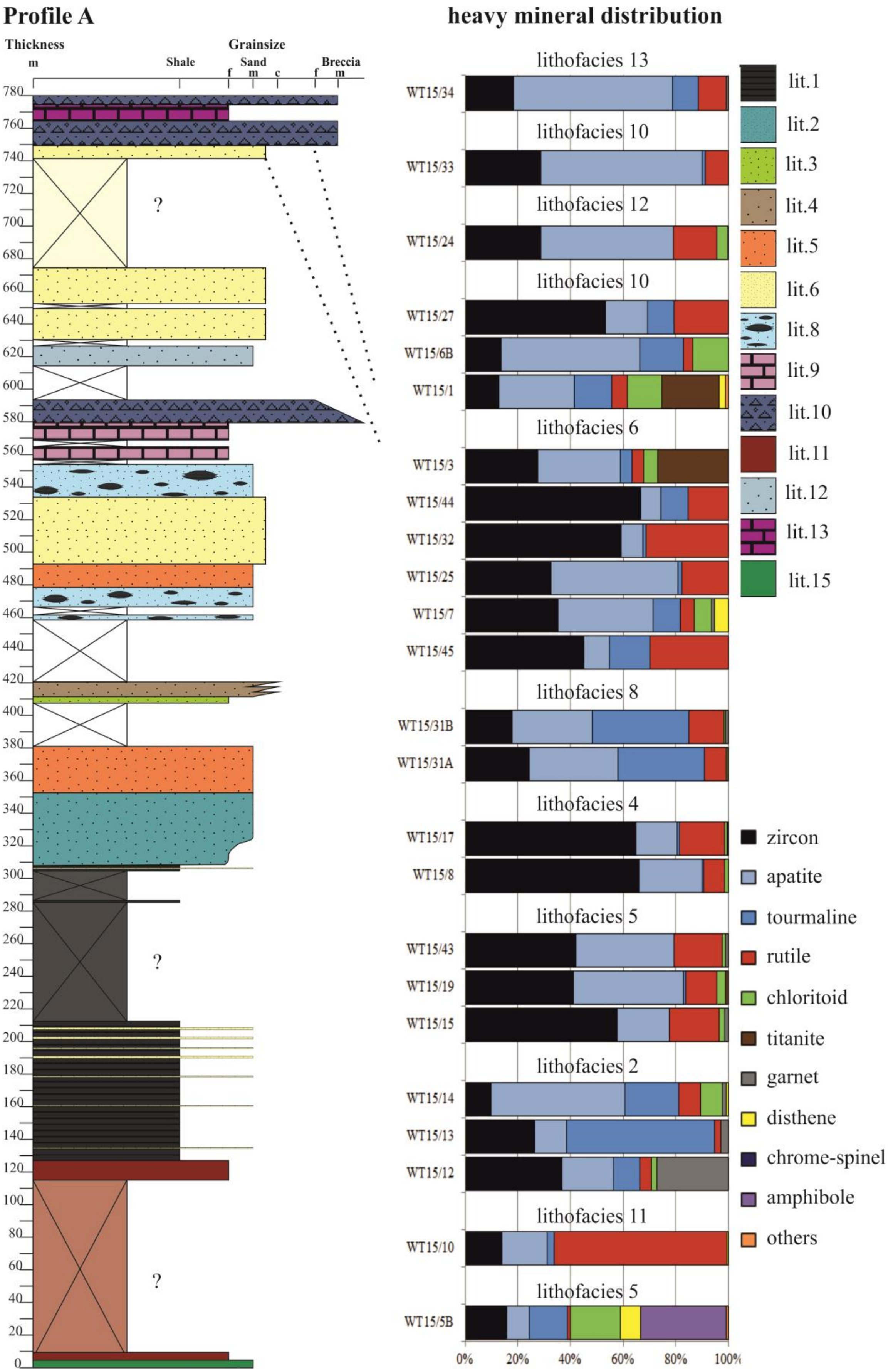

Figure 60: Heavy mineral distribution of all strew slides containing more than 100 heavy minerals combined with profile A.

The heavy mineral samples are arranged in the order of their occurrence in the main profiles. Two dotted lines show the position of the two samples WT15/1 (lithofacies 10) and WT15/3 (lithofacies 6). All other samples are arranged in their order in profile A. As visualized in Figure 60 the composition of heavy minerals is dominated by the ultra-stable heavy minerals zircon, rutile, tourmaline and the stable heavy mineral apatite (compare Pettijohn et al., 1973). Rarely also garnet, chloritoid, and titanite occur. Sample WT15/5b represents the greenshist sample at the base of the main profiles and shows a clearly different heavy mineral distribution including high amounts of amphibole and chloritoid. Several other phases, not relevant for the heavy mineral distribution where observed, like white mica, chlorite, dolomite and pyrite. These phases were recognized and classified, but not counted. The highest amounts of garnet were observed in samples of lithofacies 2 (WT15/12, WT15/13 and WT15/14). It is worth mentioning that these samples are 3 out of only a few samples containing crinoids as well. Sample WT15/12 was analysed in the course of the component analysis as well and is one of those carbonate-rich samples, which could represent a second source area.

13.6. RESULTS

The distribution of heavy minerals shows an enrichment of extremely stable heavy minerals, especially zircon, with a ZTR value of 64%. The main source rock was probably a granitic pegmatite, or slightly metamorphic. The enrichment in zircon gives indication to the grade of recycling. It is likely that the sediments underwent more than one sedimentation cycle, i.e. were reworked from older (meta-)sediments.

Table 6: Total distribution of heavy minerals in percent.

heavy mineral	%
zircon	36.6
apatite	28.3
tourmaline	11.0
rutile	16.8
chloritoid	2.7
titanite	1.4
garnet	1.1
disthene	0.6
amphibole	1.3
epidote	0.1
others	0.1

heavy mineral	%
zircon	36.6
apatite	28.3
tourmaline	11.0
rutile	16.8
others	7.3

9.4 MICROPROBE ANALYSIS

The microprobe analysis was conducted by Wolfgang Knierzinger, using a Cameca SXFive instrument (equipped with 5 WDS spectrometers). In the course of this microprobe analysis 6 samples (WT15/6b, WT15/27, WT15/31, WT15/35, WT15/40, WT15/45) were tested using an EDX (Energy-dispersive X-ray spectroscopy) - system providing quantitative chemical analyses of single minerals. The main aim was to get more detailed information about the chemical composition of heavy minerals. However several other minerals with a density of less than 2,9g/cm³, like dolomite, calcite and feldspar were analysed as well (see Table 9).

Table 7: raw data of the chemical composition in [%] of rutile grains; The acronym MV stands for the mean value of all samples, accept sample WT15/40.

[%]	**SiO2**	**Al2O3**	**TiO2**	**FeO**	**Nb2O5**	**ZrO2**	**Ta2O5**	**WO3**	**Total**	**sample**
rutile	0	0.156	63.568	6.994	18.504	0.05	2.868	2.052	94.192	40
	0	0.175	63.039	6.921	18.011	0.024	2.791	2.199	93.161	40
	0.015	0.038	98.367	0.215	0	0.038	0	0.007	98.68	35
	0.031	0.001	97.722	0.186	0.013	0.024	0.079	0	98.057	45
	0.02	0.013	97.523	0.222	0.014	0.042	0	0.081	97.913	27
	0.039	0.022	97.996	0.22	0.019	0.052	0	0.02	98.368	45
	0.01	0.013	97.056	0.312	0.082	0.016	0	0	97.488	41
	0.191	0.056	96.452	0.228	0.102	0	0	0	97.03	35
	0.031	0.022	97.448	0.225	0.111	0.022	0	0.178	98.039	31
	0.045	0.028	97.359	0.235	0.111	0.014	0	0	97.792	45
	0.04	0.058	97.4	0.216	0.12	0	0	0.169	98.004	6b
	0	0.018	97.383	0.311	0.123	0.035	0	0	97.87	41
	0.366	0.086	96.237	0.238	0.128	0	0	0.004	97.059	35
	0.003	0.025	97.591	0.177	0.135	0.003	0.02	0.1	98.053	41
	0.024	0.026	96.998	0.284	0.143	0.036	0.09	0	97.6	45
	0.116	0.034	97.013	0.279	0.163	0.01	0	0	97.616	35
	0.107	0.04	97.419	0.283	0.196	0.002	0	0.023	98.069	6b
	0.002	0.022	97.691	0.244	0.288	0.018	0.079	0.108	98.449	41
	0.313	0.063	95.936	0.644	0.549	0.015	0.087	0.548	98.154	6b
	0.012	0.023	97.169	0.32	0.654	0.004	0.051	0.076	98.308	45
	0.038	0.02	95.571	0.504	2.473	0.014	0.126	0.044	98.79	45
MV	0.074	0.032	97.175	0.281	0.285	0.018	0.028	0.071	97.965	all

Sample WT15/45 shows high amounts of pyrite, feldspar and apatite. Also zircon and monazite were recognized. Some zircons contain inclusions of pyrite and monazite. WT 15/6b contains high amounts of dolomite, zircon and apatite. Apatites contain several inclusions inter alia of rutile at times. WT15/27 contains inter alia pyrite and apatite. The apatite in this sample displays faint dissolution features. Apatite grains seem partly acidified, which could be an effect of the preparation for the heavy mineral separation, because of its lack of tolerance towards acid and acidic environments. WT15/40 contains a significant amount of tourmaline and zircon. Both of these stable heavy minerals contain inclusions of pyrite. WT15/31 shows a similar picture as WT15/40, it however also contains high amounts of apatite. The tourmaline analysed in this sample occurs in large number and often contains pyrite inclusions. WT15/35 did not contain a high amount of heavy minerals altogether, the minerals measured are quartz, calcite, and a lot of carbonates, both calcite and dolomite. Within the few heavy minerals WT15/35 contains, monazite was detected. Almost all analysed samples contain phengite.

The analysed rutile grains (see Table 7) as expected show high amounts of TiO2 with a mean value (not including sample WT15/40) of 97,2 percent. However the results of the analysis of sample WT15/40 differs from all other rutiles measured. They show a depletion of TiO2 compared to the mean value of 33-34%. Other oxides like FeO, Nb2O5, Ta2O5 and WO3 are significantly enriched in the rutile grains of this sample.

Table 8: raw data of the chemical composition in [%] of tourmaline grains;

[%]	SiO2	MgO	F	Na2O	Al2O3	K2O	TiO2	MnO	CaO	FeO	Total	sample
tourmaline	36.08	6.664	0.056	1.943	33.611	0.017	0.783	0	0.715	6.43	86.298	41
	36.449	4.875	0.014	1.618	34.988	0.014	0.235	0.011	0.23	8.239	86.673	6b
	36.158	7.492	0.246	2.776	32.296	0.002	0.476	0.015	0.095	6.33	85.886	40
	34.98	1.532	0.441	1.847	35.057	0.038	0.071	0.192	0.064	13.126	86.673	40
	36.911	7.97	0.256	2.702	32.688	0	0.336	0	0.088	6.213	85.886	40
	36.081	5.972	0.151	2.084	34.49	0.02	0.821	0.005	0.391	6.724	87.348	40
	36.983	7.713	0.146	2.58	32.805	0.021	0.784	0.018	0.268	5.406	87.166	40
	37.656	7.874	0.287	2.861	32.085	0.016	0.231	0.022	0.081	6.179	86.74	40
	36.902	7.327	0.108	2.636	32.607	0	0.25	0.007	0.068	6.655	86.724	41
	36.809	7.606	0.257	2.783	31.902	0.017	0.456	0.008	0.079	6.403	87.291	41
	34.795	0.4	0.54	1.987	35.259	0.043	0.153	0.258	0.079	14.326	86.559	31
	35.056	0.209	0.23	1.394	36.219	0.026	0.16	0.188	0.084	13.477	86.32	31
	36.008	5.832	0.049	2.679	31.714	0.009	0.622	0	0.04	9.337	87.842	31
	36.627	6.448	0.024	2.665	32.203	0.011	0.136	0.012	0.025	8.352	87.043	31
	35.166	0.872	0.441	1.608	35.936	0.023	0.249	0.222	0.064	13.052	86.289	31
	34.475	1.011	0.475	1.973	35.402	0.025	0.457	0.164	0.138	13.34	86.503	31
	36.434	6.58	0.07	2.615	31.975	0.018	0.327	0	0.037	8.082	87.632	31
	36.581	6.708	0.098	2.785	32.093	0.003	0.154	0.006	0.016	8.094	87.46	31

The chemical composition of tourmaline grains (see Table 8) can give indication of their host rock type (after Henry, 1985). The elements used for the discrimination of are Fe_{tot} (including both $FA2^{+}$ and $FA3^{+}$), Mg and Ca. For this, the share of the element (Mg, Fe, Ca) within the molecule (MgO, FeO, CaO) is needed. To illustrate this calculation the molecular proportion of Mg in MgO will be explained using the data of sample WT15/6b.

This tourmaline shows values of 4.875 % MgO, 8.239 % FeO and 0.23 % CaO. For the Mg share within the MgO the mass proportions of Mg to O are needed. The molar mass of MgO is approx. 40.304 g/mol, the atomic weight of Mg is ~24.31g/mol and the atomic weight of O is ~15,99g/mol. As the ratio of Mg:O in the molecule MgO is 1:1. The mass proportion of Mg can be calculated using its atomic mass (24.31g/mol) divided by the total mass of MgO (40.304 g/mol) and multiplied with 100 for percent. This leads to the molecular proportion of 60,3 percent for Mg in MgO and therefore a conversion factor [CF] of 0.603. This factor can be used for further calculation (see Mortimer, 2007). The percent value of MgO can simply be multiplied with the CF to receive the molecular proportion of Mg in the tourmaline.

This means applied on the chosen example of sample WT15/6b that the molecular proportion of Mg is 4,875% (MgO) x 0.604 (CF) = 2.945%. The adjusted molecular proportions for Mg, Fe and Ca are visualized in Table 9 on the left side.

Table 9: Adjusted molecular proportions of the elements Mg, Fe and Ca using the conversion factor of 0.604 for Mg, 0.780 for Fe and 0.714 for Ca; The normalized values on the right are necessary for plotting the results in a ternary diagram.

Adjusted values of elements by CF			Normalized values (total of 1) of elements			sample
Mg	Fe	Ca	Mg	Fe	Ca	
4.025	5.015	0.511	0.421	0.525	0.054	41
2.945	6.426	0.164	0.309	0.674	0.017	6b
4.525	4.937	0.068	0.475	0.518	0.007	40
0.925	10.238	0.046	0.083	0.913	0.004	40
4.814	4.846	0.063	0.495	0.498	0.006	40
3.607	5.245	0.280	0.395	0.574	0.031	40
4.659	4.217	0.192	0.514	0.465	0.021	40
4.756	4.820	0.058	0.494	0.500	0.006	40
4.426	5.191	0.049	0.458	0.537	0.005	41
4.594	4.994	0.056	0.476	0.518	0.006	41
0.242	11.174	0.056	0.021	0.974	0.005	31
0.126	10.512	0.060	0.012	0.983	0.006	31
3.523	7.283	0.029	0.325	0.672	0.003	31
3.895	6.515	0.018	0.374	0.625	0.002	31
0.527	10.181	0.046	0.049	0.947	0.004	31
0.611	10.405	0.099	0.055	0.936	0.009	31
3.974	6.304	0.026	0.386	0.612	0.003	31
4.052	6.313	0.011	0.390	0.608	0.001	31

The ternary diagram using normalized values of Mg, Fe and Ca from tourmaline geochemical data, shows 6 areas of possible source rocks the tourmalines could have derived from. Field 1 represents Li-rich granitoid pegmatites and aplites, field 2 represents Li-poor granitoids and associated pegmatites and aplites, field 3 represents Ca-rich metapeliutes, metapsammites and calc-silicate rocks, field 4 represents Ca-poor metapelites, metapsammites and quartz-tourmaline rocks, field 5 metacarbonates and field 6 represents Metaultramafites (after Henry, 1985).

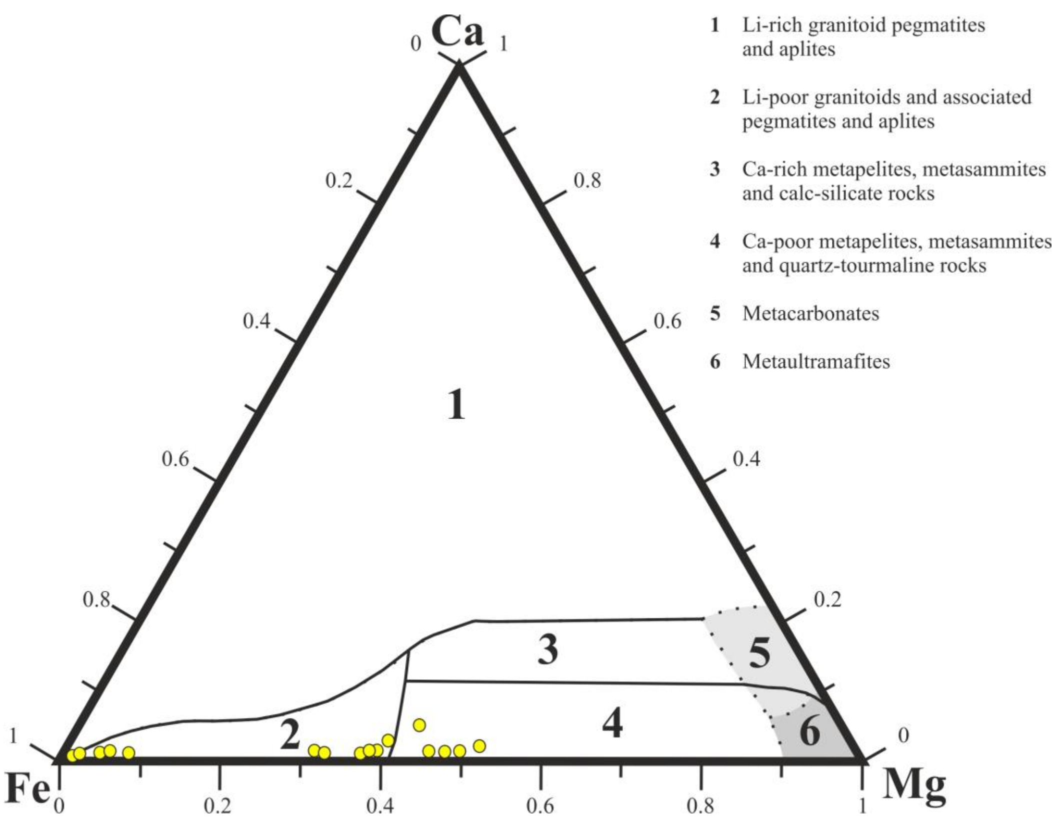

Figure 61:A Fe-Mg-Ca- ternary diagram, which is used on tourmaline geochemical data for source rock distribution (after Henry, 1985).

The sample points show two groups, one tight sample group in the Fe-rich area of field 2 and one in the balanced Fe:Mg area between field 2 and field 4. This could indicate two separate (original) source areas. Most of the sample points are positioned in field 2 the Li-poor granitoids and associated pegmatites and aplites. A few sample points show higher Mg levels at the expense of the Fe. These points plot in the field 4, the field of Ca-poor metapelites, metapsammites and quartz-tourmaline rocks.

14. STRUCTURAL PART

14.1. RESEARCH QUESTION

The main purpose of adding this structural part to the work is to clarify if there are structural interferences with the sedimentological sequences. For instance folding in the scale of 10 meters or more can cause layers to occur several times within one profile in reverse order. Another question was, whether traces of the SEMP (Salzachtal – Ennstal – Mariazell - Puchberg) – fault (see i.a. Rosenberg et al., 2008) can be detected in the area.

14.2. MEASUREMENTS AND STRUCTURES

The structural analysis of the area indicates three stages of deformation (1) a ductile, (2) a ductile-brittle and (3) a brittle stage. Each one of these stages caused characteristic structures, which were combined and visualized within stereo plots (Figure 62, Figure 65, Figure 66) created using Tectonics FP.

The first stage, deformation stage 1 (ds1) and therefore the oldest deformation is a ductile deformation, causing isoclinal folds (see Figure 63) and stretching lineations (see Table 10), which were observed within all lithofacies (27 data; see Figure 62). They show an ESE - WNW - stretching direction and match the fold axes of the isoclinal folds (Figure 62).

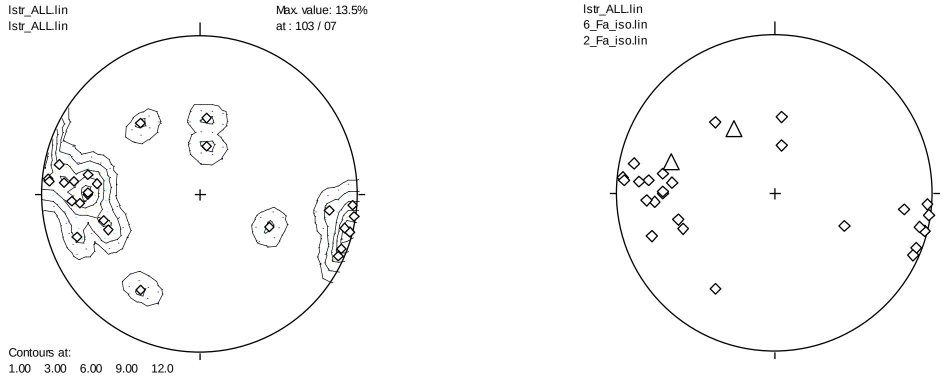

Figure 62: Stereo plots showing all stretching lineations visualized as diamonds and the fold axes of isoclinal folds, visualized as triangles.

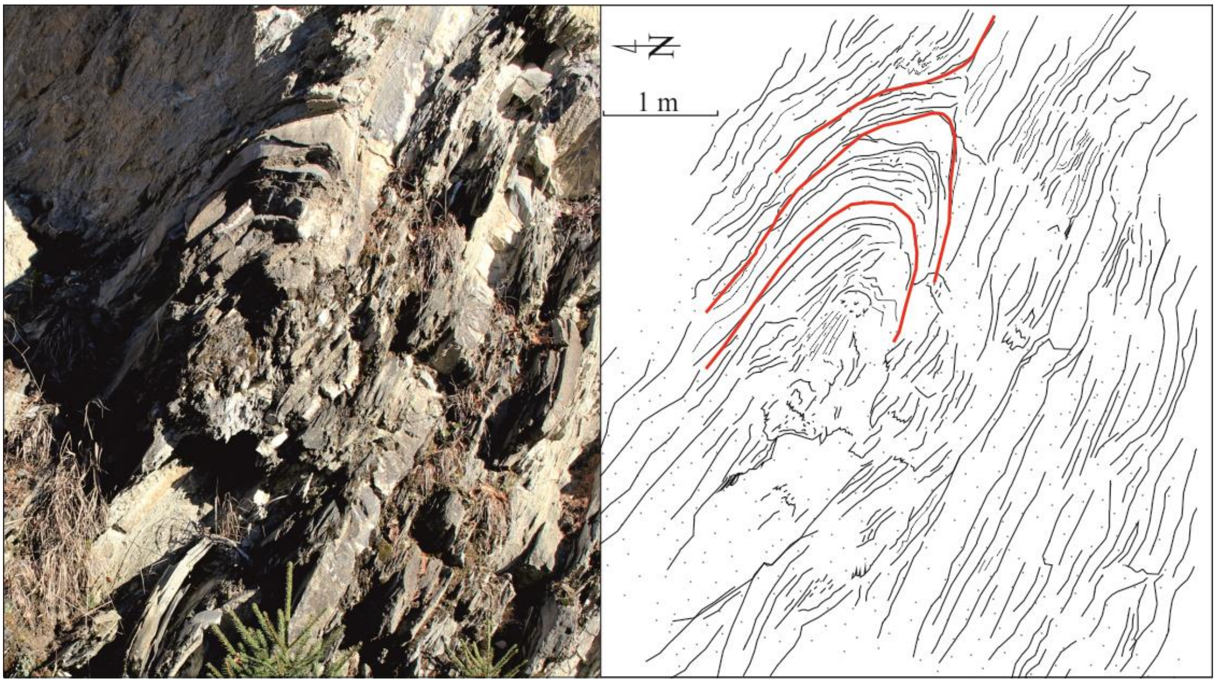

Figure 63: Photograph (left side) and sketch (right side) of an isoclinal fold of carbonate rich sandstone layers of lithofacies 2 – main profile A.

The second stage of deformation, deformation stage 2 (ds2) is a ductile - brittle deformation. This stage is responsible for asymmetric, open metre-scale folds (lithofacies 1; see Figure 64), crenulation lineation and foliation. The best-fit great circle is indicative for folding around NNE-dipping fold axes, which are younger than the isoclinal folding and stretching lineation of ds1. The crenulation lineation is indicative for NE-SW-directed shortening which is kinematically compatible with sinistrale shearing in a hypothetical "SEMP shearzone". The normal fault, which separates lithofacies 11 and lithofacies 1 in profile A (129m) matches also a hypothetical "SEMP-shearzone".

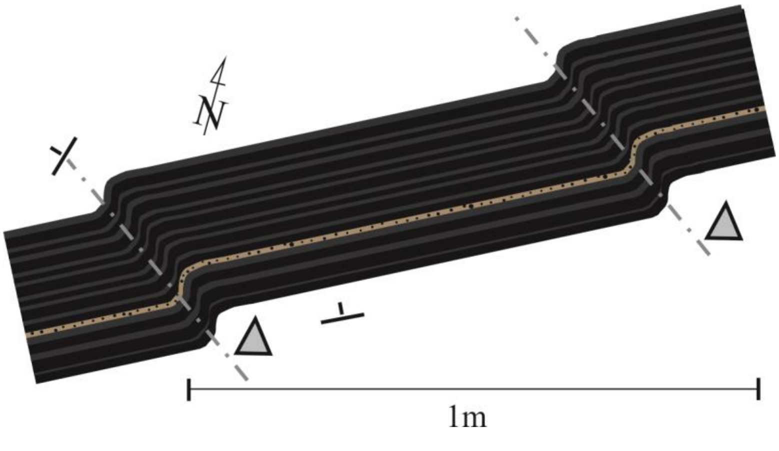

Figure 64: Sketch of asymmetric, open, metre-scale folds of lithofacies 1 observed in the riverbed of the Wolfbach.

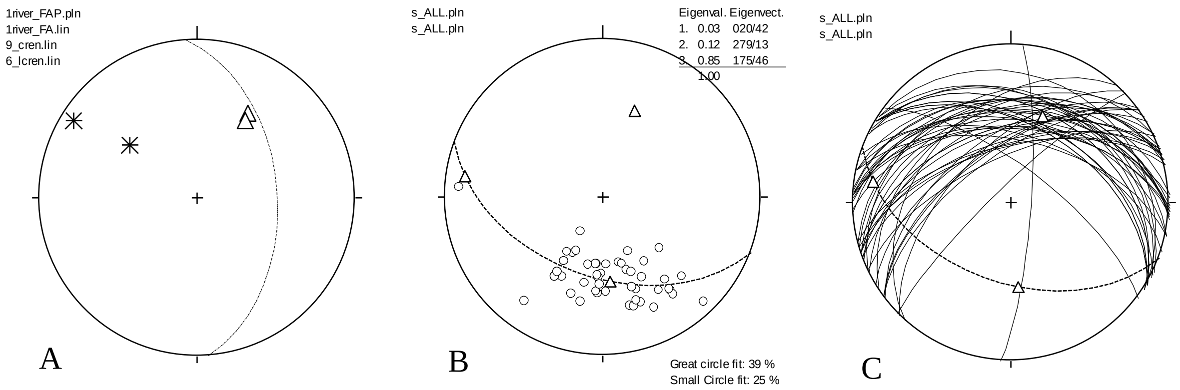

Figure 65: Stereo plots showing [A]crenulation, visualized as stars and the fold axes of asymmetric, open metre-scale folds, visualized in big triangles, [B] all poles of foliation, visualized in circles and the three calculated best fit fold axes, visualized as small triangles, and [C]all foliation great circles (solid lines) and again the three calculated best-fit fold axes.

The last and youngest stage of deformation, deformation stage 3 (ds3) is brittle, causing slickensides and strike-slip faults. The NW-SE-directed extension is kinematically compatible with sinistrale shearing in a hypothetical “SEMP shearzone” like the crenulation. The strike-slip faults are indicative for NNW-SSE-directed shortening, which is not compatible with the SEMP-fault.

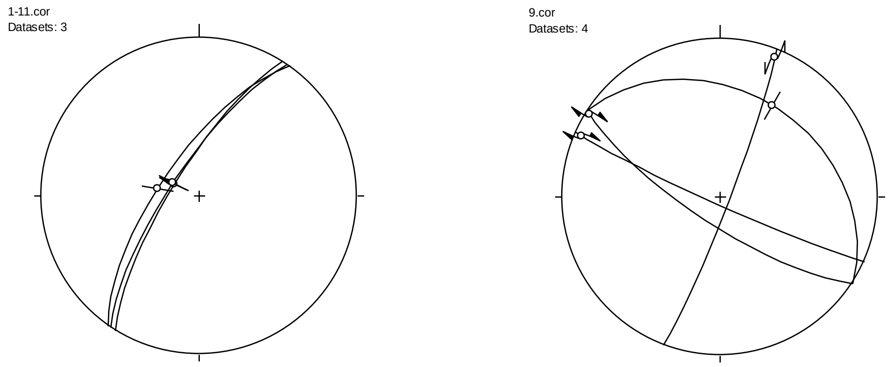

Figure 66: stereo plots showing slickensides and strike-slip faults. Small arrows show the shearsence.

Other structures observed are a variety of faults, kink faults (see Figure 69), a variety of σ-clasts and veins, which partly show boudinage and influence of both, brittle and ductile deformation , folding veins and shearing them brittle. Additionally a variety of tension gashes (for example Figure 68, Table 1) was observed. Kink faults (Figure 69) form in the course of low temperature deformation after stretching.

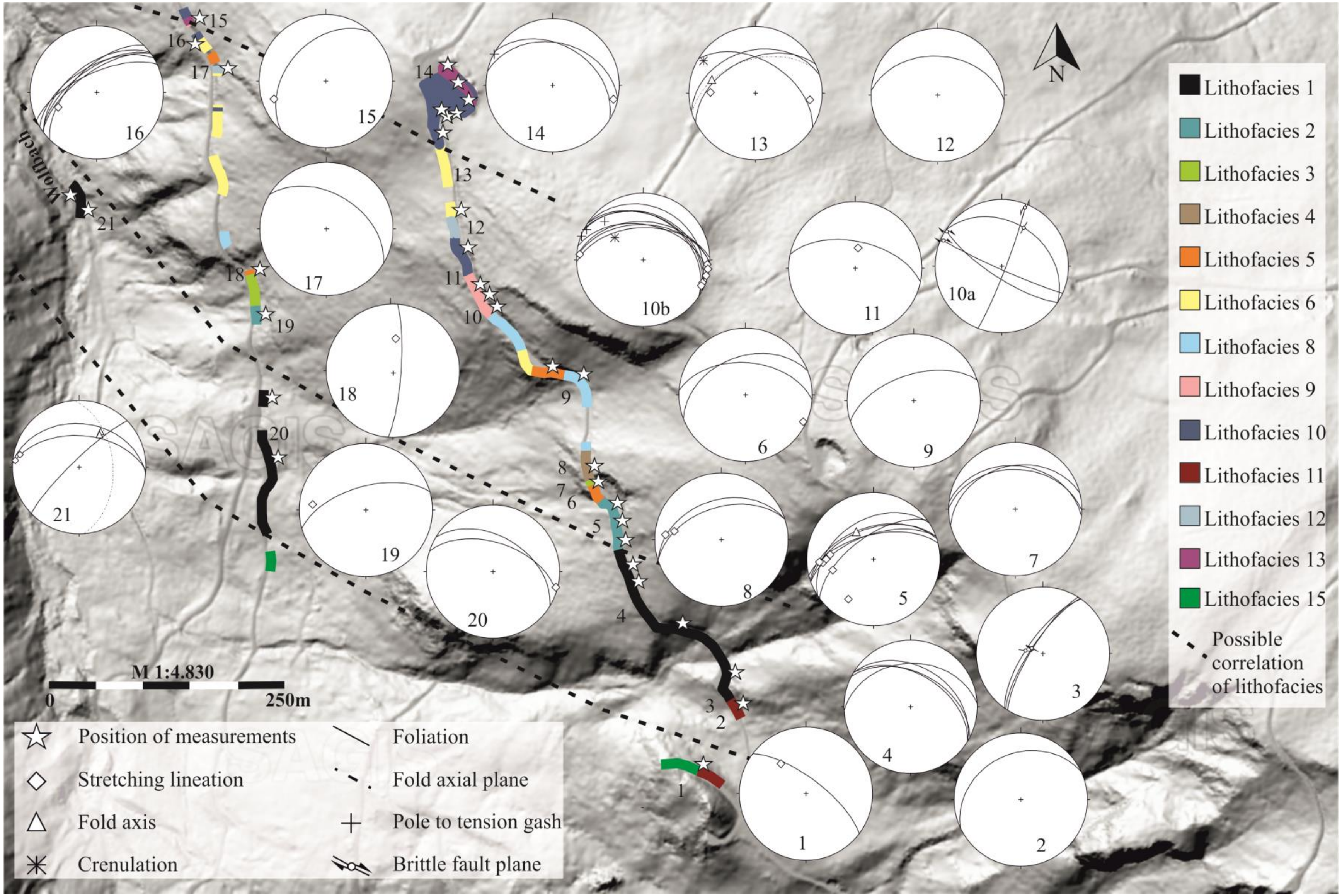

Figure 67: A variety of structural features measured along the profiles shown on a laser scan map of the Wolfbachtal (SAGIS online).

Table 10: All measurements of the area sorted in lithofacies of both main profiles A and B.

Lithofacies	foliation	Slicken slide	Isoclinal fold	Asymmetric open fold	Stretching Lineation	Crenulation	Shear sense	Tension gash
1upper	027/47							
	031/39							
	031/49							
	357/35							
1 lower	018/54				104/03			
	031/46							
1 river	316/81			031/38	276/04			
	003/51			032/42	282/10			
	005/35							
1/11 upper		302/76			297/71		Normal	
		302/75			298/72			
		302/70			278/70			
2 upper	327/40		328/50		276/35			
	324/62				255/37			
	340/52				266/25			
	342/50				267/20			
	340/60				270/30			
	346/60				212/30			
2 lower	344/61				276/21			
3 upper	346/35							
	001/40							
	006/35							
4 upper	342/40				275/17			
	342/50				280/29			
5 upper	339/42				115/50			
	004/50							
5 lower	094/80				005/50			
6 upper	031/49		287/32		097/19,	302/09		
	334/47		342/48		271/33			
	344/36							
8 upper	342/58							
9 upper	028/33	028/33			111/05	308/45	Dextral	111/89
	026/31	026/31			104/03		Dextral	118/86
	012/46	012/46			094/04			
	033/21	204/86			114/05;		Dextral	135/71
	033/34	213/76			297/05		Dextral	
	358/50	111/85			302/03			
	003/42	033/34			021/06		Dextral	
	002/46				030/29		Sinistral	
					275/05			
					098/02			
9 lower	312/40				251/19			
9/10 upper	012/57				008/65			
10 upper	031/39				103/07			118/89
	012/36							
11 upper	335/31							
12 upper	004/41							
12 lower	031/46							
14 lower	315/60				249/38			
	324/65							
	335/66							
	329/58							
	323/55							
	324/61							
15 upper	037/71				320/41			

They match the direction of the asymmetric, open metre-scale folds of ds2. Figure 68 shows tension gashes with a maximum width of 1cm, which (mainly the smaller ones) are partly formed en echelon. The mineral fibres filling up these tension gashes are oriented parallel to the stretching direction and therefore parallel to the stretching lineation (Figure 68).

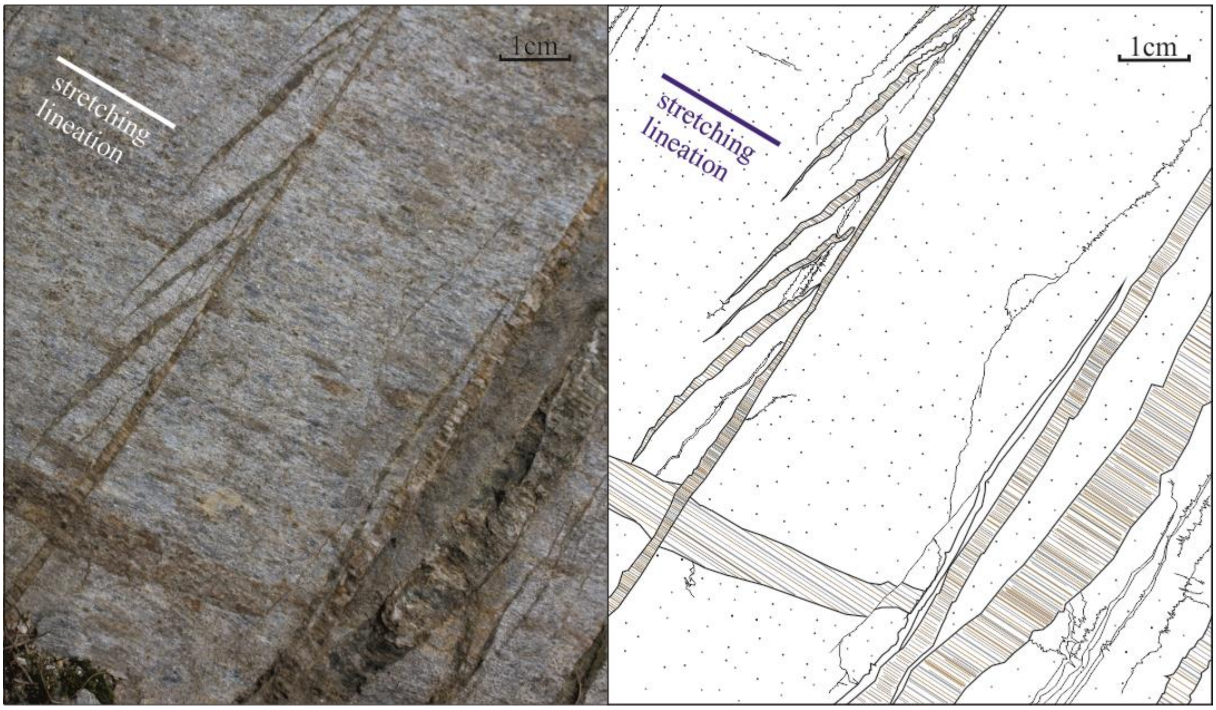

Figure 68 tension gashes shown as a photograph on the left side and a sketch (visualized using Corel Draw X5) on the right side.

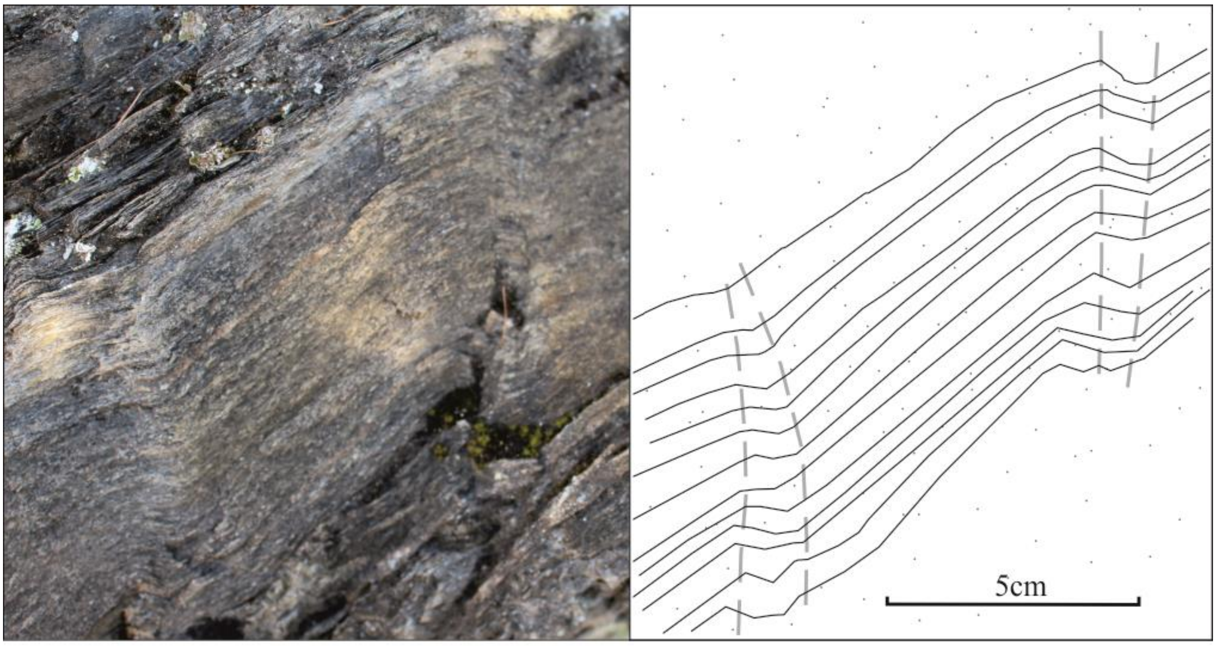

Figure 69: Kink faults within sandstone bed shown as a photograph on the left side and as a sketch (visualized using Corel Draw X5) on the right side.

15. DISCUSSION

15.1. DEEP-WATER FACIES AND CYCLES

The main profiles A and B of the upper and the lower forest road at Wolfbachtal show a consistent picture of a continuous stratigraphic succession. All in all the grain size increases and the carbonate content increases towards the (apparent) stratigraphic top of the composite section. If observable, grading and sole marks point to a normal position of beds throughout, with the exception of a few and short, locally inverted parts. The base of the profiles is represented by greenschists (lithofacies 15, metamorphic basic magmatic rocks, (Pestal et al., 2009) and a fine-grained siliceous rock (lithofacies 11, probably meta-chert or meta-radiolarite).

The studied profiles of the meta-sediments of the Tauern Flysch all indicate characteristics of turbidites and related mass-flows, and a flysch-like appearance, such as grading of sandy layers as already noted by previous authors (e.g. Prey 1975, 1977). Facies types are ordered according to their sandstone content (from low to high) and carbonate content in the following discussion.

15.1.1. LITHOFACIES 1

Lithofacies 1 consists predominantly of black shales (black phyllites), sometimes laminated, with thin (<10 cm) beds of silt and sandstones, partly graded; sandstone/shale ratios are from 1:50 to 1:20. The black colour comes from graphite and pyrite. This lithofacies can be interpreted as comprising at least partly pelagic to hemipelagic sedimentation in a deeper-water environment. The high amount of organic material (now graphite) points to dysoxic to anoxic bottom-water conditions, the overall carbonate-free pelitic lithology to deposition below the regional calcite compensation depth. Siliciclastic input is low, but constant, depicted by silt laminae and thin sandstone layers. Regarding deep-water turbidite facies models, this lithofacies can be classified as a transition from basin plain pelagic fine-grained shales to outer fan thin-bedded classical turbidites (Walker, 1979). According to the detailed facies classification of Pickering et al. (1986) (see Figure 70) these organized mud and silt deposits can be classified as E2.2 (laminated muds and clays), D2.3 (thin regular silt and mud laminae), D1.2 (muddy silts) and E1.1 (structureless muds). Contourites of bottom-water currents may be also present, especially in the thin silt layers.

A Gravels, muddy gravels, gravelly muds, pebbly sands, ≥5% gravel
- A1 Disorganized gravels, muddy gravels, gravelly muds and pebbly sands
  - A1.1 Disorganized gravel
  - A1.2 Disorganized muddy gravel
  - A1.3 Disorganized gravelly mud
  - A1.4 Disorganized pebbly sand
- A2 Organized gravels and pebbly sand
  - A2.1 Stratified gravel
  - A2.2 Intensively graded gravel
  - A2.3 Normally graded gravel
  - A2.4 Graded-stratified gravel
  - A2.5 Stratified pebbly sand
  - A2.6 Intensively graded pebbly sand
  - A2.7 Normally graded pebbly sand
  - A2.8 Graded-stratified pebbly sand

B Sands, ≥80% sand grade, <5% pebble grade
- B1 Disorganized sands
  - B1.1 Thick/medium-bedded, disorganized sands
  - B1.2 Thin-bedded, coarse grained sands
- B2 Organized sands
  - B2.1 Parallel-stratified sands
  - B2.2 Cross-stratified sands

C Sand-mud couplets and muddy sands, 20-80% sand grade, <80% mud grade (mostly silt)
- C1 Disorganized muddy sands
  - C1.1 Poorly sorted muddy sands
  - C1.2 Mottled muddy sands
- C2 Organized sand-mud couplets
  - C2.1 Very thick/thick-bedded sand-mud couplets
  - C2.2 Medium bedded sand-mud couplets
  - C2.3 Thin-bedded sand-mud couplets
  - C2.4 Very thick/thick-bedded, mud-dominated sand-mud couplets

D Silts, silty muds, and silt-mud couplets, >80% mud, ≥40% silt, 0-20% sand
- D1 Disorganized silts and silty muds
  - D1.1 Structureless silts
  - D1.2 Muddy silts
  - D1.3 Mottled silt and mud
- D2 Organized silts and muddy silts
  - D2.1 Graded-stratified silt
  - D2.2 Thick irregular silt and mud laminae
  - D2.3 Thin regular silt and mud laminae

E ≥95% Mud grade, <40% silt grade, <5% sand and coarser, ≥25% biogenics
- E1 Disorganized muds and clays
  - E1.1 Structureless muds
  - E1.2 Varicoloured muds
- E2 Organized muds
  - E2.1 Graded muds
  - E2.2 Laminated muds and clays

F Chaotic deposits
- F1 Exotic clasts
  - F1.1 Rubble
  - F1.2 Dropstones and isolated ejecta
- F2 Contorted/disturbed strata
  - F2.1 Coherent folded and contorted strata
  - F2.2 Brecciated and balled strata

G Biogenic oozes (>75% biogenics), muddy oozes (50-70% biogenics), biogenic mud (25-50% biogenics) and chemogenic sediments, <5% terrigenous sand and gravel
- G1 Biogenic oozes and muddy oozes
  - G1.1 Biogenic ooze
  - G1.2 Muddy oozes
- G2 Biogenic muds
  - G2.1 Biogenic mud
- G3 Chemogenic sediments

Figure 70: Turbidite facies classification from Pickering et al. (1986).

15.1.2. Lithofacies 2

This facies comprises predominantly calcareous sandstones alternating with black and grey shales, sandstone/shale ratios are around 4:1. Grading occurs, as well as pure limestone beds. Echinoderm remains are present, as well as mica-rich beds. Bedding types resemble medium-bedded calcareous sandy classical turbidites (Walker, 1979) and facies C2.2 of Pickering et al. (1986). Limestone beds may either also have been of turbiditic origin or of (hemi)pelagic origin. Given the facts that (1) sandstones do show already high carbonate contents throughout, (2) intervening shales are non-calcareous, (3) no clear turbidite-hemipelagite rhythm of a sandy turbidite interval grading into a turbiditic shale bed and a carbonate pelagic interval on top, and (4) limestone beds show sharp bases without any transition from shales to limestone, the limestone beds are interpreted as turbidites. This may point to two sources for the turbiditic material, a siliciclastic source and a (biogenic) carbonate source.

15.1.3. Lithofacies 6 and 8

Lithofacies 6 includes thin-bedded, non-calcareous sandstones whereas lithofacies 8 comprises sandstones with rip-up clasts, both characterized by sandstone/shale ratios of about 1 or slightly higher than 1. Transitions to lithofacies 5 (medium- to thick-bedded sandstones) do exist. Lithofacies 6 is classified as classical thin-bedded turbidites (Walker, 1979) and turbidite facies C2.3 (thin-bedded sand-mud couplets, Pickering et al., 1986) with thin (<30cm) black shale intervals that may include facies E2.2 (laminated muds and clays). Lithofacies 8 corresponds to C2.2 (medium-bedded sand-mud couplets, Pickering et al., 1986).

The rip-up clasts were formed by reworking from the immediately underlying fine-grained sediment of the former flow, as pelitic chips were ripped off the ground during the turbidity current flow. These clasts were transported together with other material and accumulated downflow.

15.1.4. Lithofacies 3, 5 and 12

These facies types include relatively thick-bedded coarse-grained sandstones (lithofacies 3), non-calcareous coarse-grained sandstones (lithofacies 5) and calcareous coarse-grained sandstones (lithofacies 12). Successions are always sandstones-rich, and provide sandstone/shale ratios of 6:1 to 12:1 to 50:1. Subordinate lithologies include both black and grey shales. Beds are 10-60cm in thickness, grading, rip-up clasts and horizontal bedding are present in lithofacies 3 and 5, thus those are interpreted as classical thick/medium-bedded turbidites (facies C2.2 of Pickering et al., 1986) with dominantly/solely siliciclastic sources. Relatively concentrated turbidite flows were capable of ripping up mud chips. Lithofacies 12 comprises thicker, more massive beds of B1.1 (thick/medium-bedded, disorganized sands), probably of highly-concentrated turbidite flows or sandy grain flows/debris flows.

15.1.5. Lithofacies 4

Amalgamated sandstones of lithofacies 4 comprise the highest sandstone/shale ratios with intervals of virtually no shales layers and thus >98% sandstones (sandstone/shale ratio >

100:1). Grading is present throughout and horizontal lamination is present both within and on top of beds, resembling parts of the Bouma-sequence of turbidites (layers Tb and Td), classified as B2.1 (parallel-stratified sands of Pickering et al., 1986).

The occurrence of amalgamated beds indicates a relatively proximal environment or deposition of material in a deep-water channel system. This kind of rapid turbidite accumulation could only happen if the turbidity currents, depositing the material, were so strong and frequent that the accumulation of pelitic layers in between the turbidity currents is hindered. There was no time for fine-grained clay for deposition or the clay was eroded immediately. This explains the complete absence of shale layers in this facies.

15.1.6. Lithofacies 9, 10 and 13

These facies types comprise pure limestones (lithofacies 9), limestones containing clasts (lithofacies 13) and carbonate breccias (lithofacies 10). These facies are transitional to one another, and concentrated at the top of the profiles. Sandstone+breccia/shale ratios (if applicable) are about 10:1, some coarse-grained thin-bedded (siliciclastic) sandstones and black shales are interbedded.

These facies can be interpreted as coarse proximal mass-flows including debris flows, grain flows and mud flows. Limestones with dispersed clasts may have been originally matrix-supported debris flows where the original micritic matrix is fully recrystallized. More densely packed breccias resemble clast-supported conglomerates. The facies can be classified as a continuum of different gravelly deep-water facies types such as A1.1 (disorganized gravel), A1.2 (disorganized muddy gravel), A1.3 (disorganized gravelly mud), A2.4 (graded-stratified gravel), A2.5 (stratified pebbly sand) of Pickering et al. (1986). Pure limestones may also have been originally pelagic limestone/micrite beds (facies G - biogenic oozes of Pickering et al., 1986), but due to recrystallization this cannot be proven or falsified. The feldspar-rich breccia seems to be a single mass-flow event bed, characterized by dominance of feldspar clasts instead of carbonates.

15.1.7. Cycles And Sequences

Lithofacies 1 shows a coarsening- and thickening-upwards trend within a predominantly shaly black shale succession as more and more sandstone layers occur. The single profiles of lithofacies 2 show two different types. The sandstone beds of the single profile A7, which is lower positioned in the section of lithofacies 2, show a thickening-upwards trend. According to turbidite fan models this may be associated with lobe deposits.

A14, which is positioned close to the transition to lithofacies 5 in profile A, shows thinning upwards and increasing carbonate content. All lithofacies overlying lithofacies 2 show thinning- and fining upwards. Lithofacies 4, including amalgamated thick-bedded graded sandstone beds, represents most probably a channel fill succession.

With respect to the depositional environment, these characteristics match Walker's model for a submarine fan stratigraphic sequence produced by fan progradation (see Walker, 1979,

Figure 71). This model is used to describe and classify whole submarine fans. However, the Tauern Flysch is only of limited thickness and could not represent a full-developed large-scale submarine fan. It is more likely that the deposits represent one out of many smaller fans or sub-fans, which resemble the stratigraphic sequence of the main submarine fan (after Zhang, 2017). The characteristics are the same, but the sequence occurs on smaller scale. The overall properties of the main profiles correlate to this model, as coarsening upwards over the entire profile can be observed. The coarsening upwards sequences at the bottom of the main profile include lithofacies 1 and 2 in segments of 0.5 – 2.5 metres. The change of gradation takes place at the top of lithofacies 2, after which the following sequences show fining upwards and thinning upwards trends (dashed line). These cycles may be interpreted as channel-fill successions (Walker, 1979).

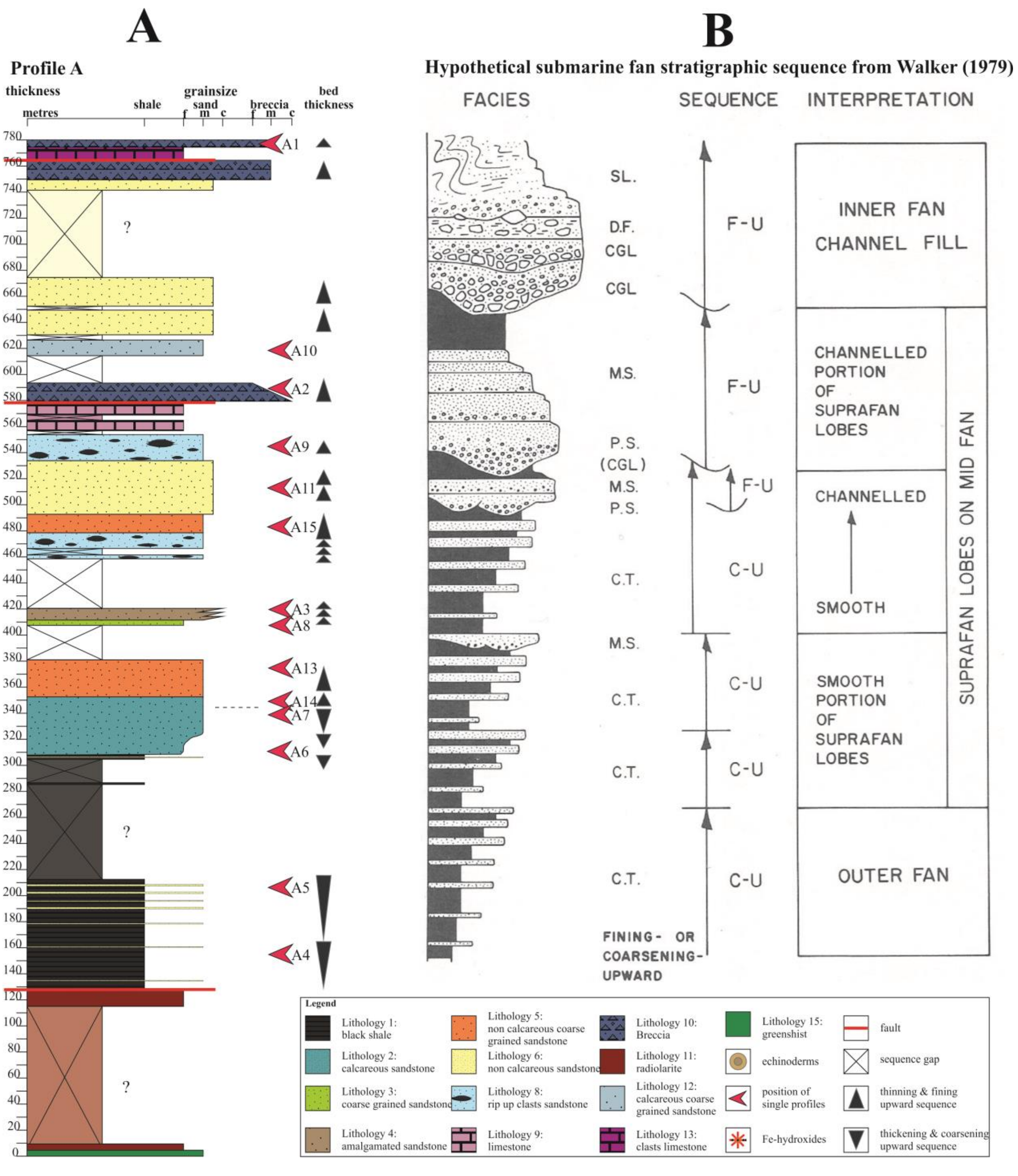

*Figure 71: **A** shows profile A (upper forest road) of the Wolfbachtal. The dark grey triangles show thinning/fining-upward sequences and thickening/coarsening-upward sequences. B shows the model of a hypothetical submarine fan stratigraphic sequence formed by fan progradation (from Walker, 1979). The thinning/fining-upward sequences and thickening/coarsening upward sequences are marked with arrows and the abbreviations [C-U] for thickening and coarsening-upward sequences and [F-U] for thinning and fining upwards.*

15.2. Stratigraphy and Provenance

15.2.1. Stratigraphy

The profiles indicate flysch-like characteristics, such as grading. All in all the grain size increases towards the top of the composite section, which is comparable to parts of the successions of the Rhenodanubian Flysch Zone (Faupl & Wagreich, 2000). This resemblance may limit the sedimentation age to the Cretaceous-Palaeogene, even though a sedimentation age could not be discerned due to lack of palynology or other fossil evidence. Published age indications give mainly Early Cretaceous, up to Aptian ages based on a few foraminifera and ichnofossils from similar carbonate-rich sediments along the northeastern margin of the TW (Höck et al., 2006; Slaczka et al., 2011) and palynology from dark phyllites reported by Reitz et al. (1990). Thus, a Lower Cretaceous part of the Tauern Flysch can be assured, however, no unambiguous Upper Cretaceous or Paleogene ages could be detected so far for the Tauern Flysch.

15.2.2. Provenance

The presence of dolomite clasts indicates in general a southern source area and therefore a depositional position at the **southern margin of the Penninic Ocean** (compare Figure 73). The source area had to comprise a sufficient amount of dolomite, therefore an Austro-Alpine provenance is most likely. If the deposits had derived from a northern source at the northern margin of the Penninic Ocean, material had to derive from the Bohemian Massive or equivalent Variscian units, which does not comprise a sufficient amount of dolomite. In the stratigraphically upper part of the main profiles breccia layers occur to an increasing degree (see lithofacies 10). This deposition of coarse-grained material could be interpreted as part of the Sandstein-Brekzien Decke (Braumüller, 1939). Olistoliths have been described in this area (Hoeck et al., 2006). Olistoliths are formed as slide deposits, often containing isolated blocks of e.g. limestones or dolomites in otherwise fine-grained sediments like sandstones or shales (after Reading, 1996). Equivalent olistoliths containing sequences are not described in the Rhenodanubian Flysch Zone. This indicates that, in the case of a common source area, the Tauern Flysch is closer to the (Austro-Alpine) source than the typical Rhenodanubian Flysch successions.

The heavy mineral distribution, showing a dominance of stable heavy minerals such as zircon, tourmaline and rutile, does not fully match heavy mineral distributions of the Eastern Alpine flysch sediments from the literature. The ZTR reaches 64%. However, the lack of garnet and chrome spinel, and the high amounts of apatite complicate the allocation of the heavy mineral distribution to data from the literature (heavy mineral distribution of several flysch units from Faupl, 1996). The heavy mineral distribution (Figure 72) would fit the published assemblages of the Palaeogene of the Kaumberg-Nappe best, however, no age indications for Palaeogene were ever found.

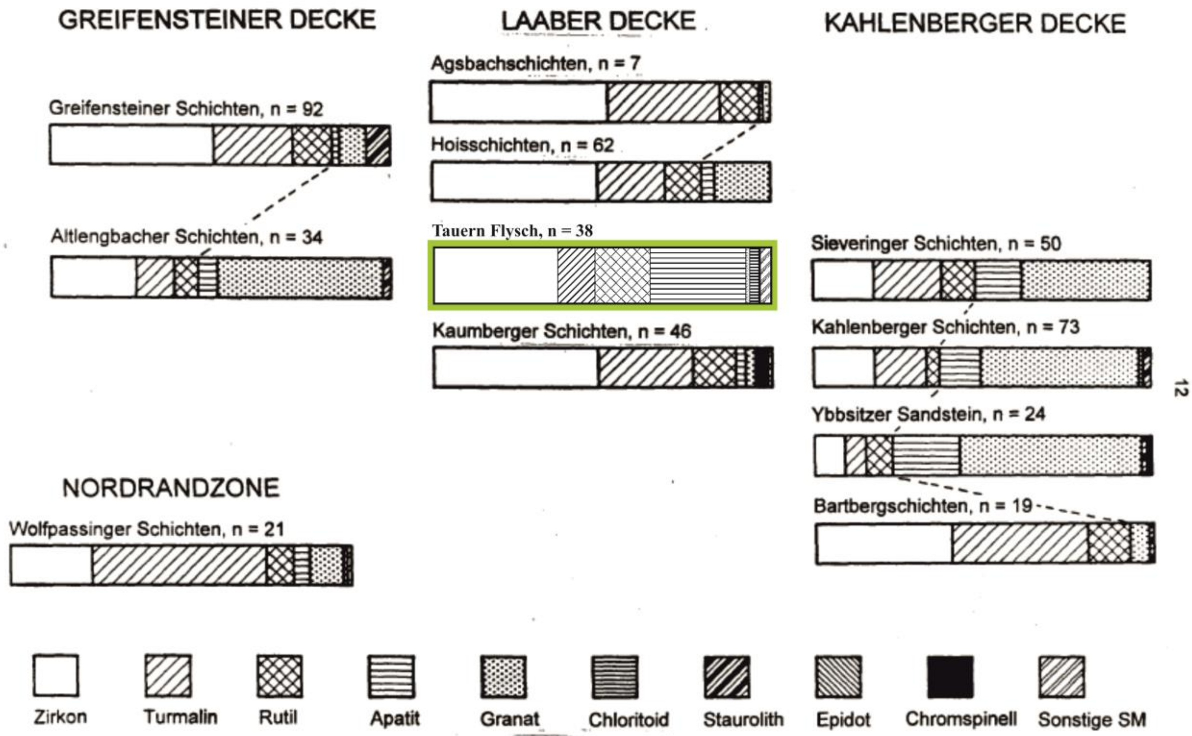

Figure 72: Comparison of the total distribution of heavy minerals of the Tauern Flysch and known Flysch heavy mineral distributions from the literature (from Faupl, 1996).

Heavy mineral assemblages from southern Penninic non-metamorphic flysch units like the Ybbsitz Zone (Homayoun and Faupl, 1992) and the continuation into equivalents of the Kahlenberg Nappe (Schnabel, 1992; Faupl and Wagreich, 1992; Wagreich, 2008) also bear either chrome spinel and/or significant garnet contents in contrast to the Tauern Flysch. From the Lower Cretaceous flysch units of the **Ybbsitz Zone** only parts of the **Haselgraben Formation** of Aptian-Albian age (Homayoun & Faupl, 1992: Hubegggraben) show heavy mineral assemblages with high ZTR, medium apatite and very low garnet, but, in contrast, low but conspicuous amounts of chrome spinel. However, the turbidite facies of these units, including black shales and classical turbidites (C2.1, C2.2, C2.3 of Pickering et al., 1986) and the presence of fine-grained breccias including dolomite clasts and echinodermal fragments resembles parts of the Tauern Flysch.

The presence of various dolomite clasts up to the size of olistoliths (Ślączka et al., 2011) and echinodermal fragments relates the Tauern Flysch to the **Austro-Alpine realm** where Triassic dolomites such as the Hauptdolomit Formation are ubiquitous. Comparing heavy minerals with data from other flysch units, especially the Rhenodanubian Flysch Zone in eastern Austria (Faupl, 1996) places the depositional area of the Tauern Flysch somewhere (close to) the Kaumberg basin and thus the Laab Nappe and the **Ybbsitz Zone** (Figure 73). All other nappes contain lithounits with significant amounts of garnet, minor, but conspicuous chrome spinel, and only very little amounts of apatite. The base of the main profile A is the only section containing notable amounts of garnet. In the upper part of the profiles no garnet has been observed. Titanite also only occurs in a short section in the higher part of the main profile between lithofacies 6 and 10. Thus, two principal sources for the heavy minerals and thus the siliciclastic material of the Tauern Flysch may be interpreted: (1) ZTR-rich assemblages point to strong and multiple **sediment recycling** of a principally silic basement source. Within this broad source, tourmaline gives indications of at least 2 sub-sources, (1a) Li-poor **granitoids** and (1b) Ca-poor **metapelites and metapsammites**; (2) garnet-bearing assemblages in the lower part of the profile indicate also higher grade **metamorphic rocks** in the source area.

The Dickinson (1985) method shows various possible sources. The QtFL-ternary diagram indicates a recycled orogenic, the QmFLt-ternary diagram indicates a **lithic recycled source**. Both diagrams show a high amount of data points in recycled areas. However metamorphism caused strong recrystallization of the quartz grains. Polycrystalline quartz grains belong to the total lithic components and are therefore most likely the reason for the strong shift of the scatter towards the lithic components. Combining the results it is most likely that the sediments originated from a **recycled orogenic source**.

The bulk geochemistry analysis shows, that even though the deposits are meta-sediments, their sedimentary origin can still be detected. The sediment classification diagram (after Herron, 1988) classifies these meta-sandstones as **litharenites** to **arkoses**. Several geochemical plots indicate a **strongly recycled, granitic source**. The diagram for rock source classification (after Cullers, 2002) shows a clear tight scatter in the field of **silicic** source rock. The Discrimination Function diagram (after Roser & Korsch, 1988), including the major elements for sedimentary provenances, shows a clear recycled source in the area of **quartzose sedimentary provenance**. The ratio of La/Th versus Hf – diagram (after Floyd, 1987) for discrimination of provenance does not show a tight scatter in any area. Most of the scatter points follow the field of a mixed felsic and mafic source. The Zr/Sc versus Th/Sc – diagram (after McLennan, 1993, including slight modifications from Bahlburg, 1998) displays a horizontally distributed scatter of sample points close to the limit of the upper crust field. The sustained form is due to the **recycling trend** of the samples, increasing towards the right which shows a higher Zr/Sc ratio and therefore an enrichment of zircon (also recognized in the heavy mineral assamblages). The position of the scatter close to the limit of the upper crust field indicates input from a **magmatic arc source** (after McLennan et al, 1991, also see Bahlburg, 1998). Even though the geochemical plots after Roser & Korsch (1986) indicate a sedimentary setting of a **volcanic island arc**, the most likely geological setting would be a **passive margin**.

The principal component analysis and the microprobe analysis of tourmalines indicate the possibility of **two separate sources**. This would indicate that most likely lithofacies 2 is not derived from the same source area as the rest. However the chemical distribution recognized in the principal component analysis is most likely caused by the varying carbonate content of the samples (non-calcareous versus calcareous sandstones) and not by two separate source areas.

All in all this points to a source including: (1) continental crust (silicic, granitic, quartzose) with granitoids, meta-sediments and minor metamorphics including recycling trends, and (2) a dolomitic/carbonate sedimentary cover, again with recycled siliciclastics probably. In principle, Austroalpine basement (including Paleozoic metasediments) and its Mesozoic cover may provide such a source area. The partly immature character of the sediments (presence of breccias, arkoses, high amounts of detrital mica and matrix) points to relatively nearby sources without long-distance river transport or strong coastal reworking, and fast transport into the deep-sea sedimentary system.

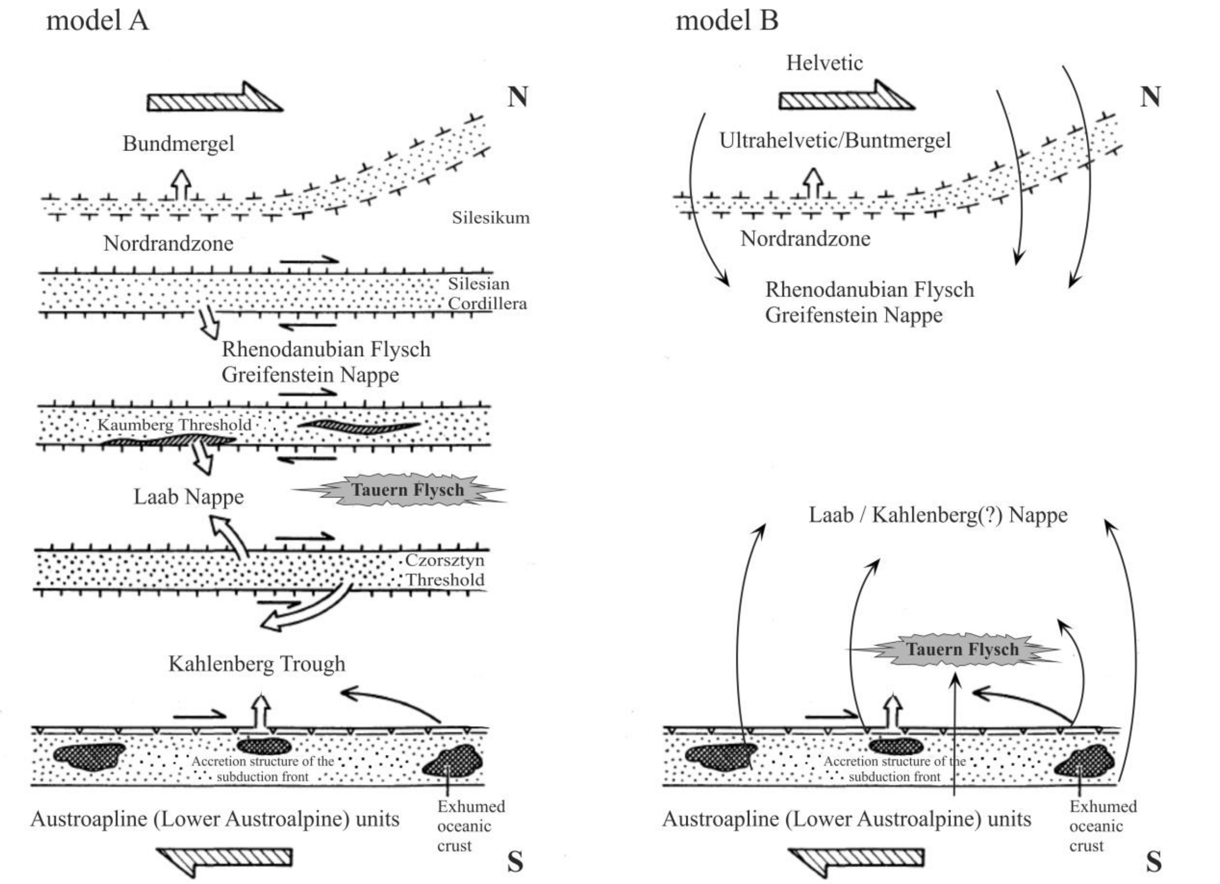

Figure 73: Hypothetical paleogeographic model (partly modified after Faupl, 1996) showing the possible position of the Tauern Flysch. Model A includes the middle Penninic unit. Model B shows a simplified version of the model only distinguishing between a northern and a southern source within a single Penninic Ocean (Alpine Tethys of Handy et al., 2015).

15.3. TECTONIC ATTRIBUTION

The age of the Tauern Flysch and associated units is still strongly debated, i.e. Jurassic (Plasienka et al., 2012: based on the distinct succession from shales to sandstones to carbonate breccias including dolomite fragments similar to inferred Penninic units of the Western Carpathians and the Lower Austroalpine of Austria) or Early Cretaceous (Tollmann, 1977) or Late Cretaceous to Paleogene (e.g. Prey, 1977; based on apparent similarities to the Rhenodanubian Flysch Zone). Unfortunately there is no new fossil evidence of the sedimentation age but indications for an Early Cretaceous age of at least parts of the succession including carbonate-rich intervals (Reitz et al., 1990; Höck et al., 2006).

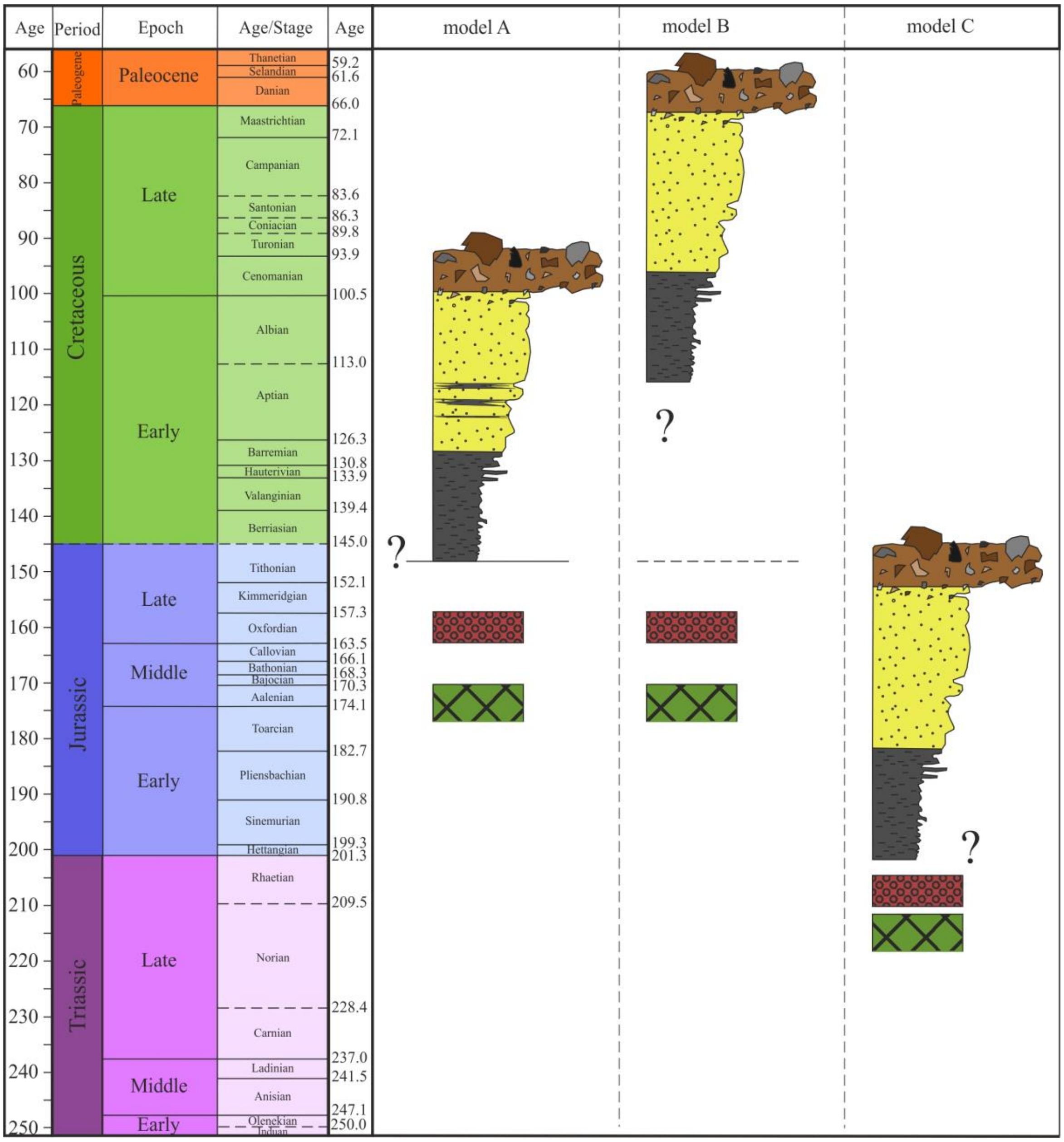

Figure 74: Three possible models for the stratigraphic disposition of the Tauern Flysch.

Three possible stratigraphic models (see Figure 74) for the Tauern Flysch are used to evaluate the sequence of the Tauern Flysch for its paleogeography and tectonic attribution.

Model A represents a position within the southern part of the Penninic Ocean (Tollmann, 1977 based on underlying Jurassic strata). The greenschists at the bottom of the profile represent an early to middle Jurassic age as representative for the Penninic Nappe System, i.e. the Glockner Nappe and related units up to ophiolites (Pestal et al., 2009). The chert (radiolarite) (lithofacies 11) overlying stratigraphically the greenschists, would then correspond to the wide-spread Tethyan siliceous sedimentation during the Late Jurassic (Oxfordian?). No Upper Jurassic limestones are present in the Wolfbach profile, however, elsewhere in this zone along the northern margin of the TW, some indications for a Late Jurassic age of limestones are known (Kleberger et al., 1981). The actual siliciclastic and turbiditic deposition then started between the end of the Late Jurassic and the Early Cretaceous, continuing through the Early Cretaceous. Ubiquitous black shales (black phyllites) then correlate well to the widespread Cretaceous Anoxia including Oceanic Anoxic Events, mainly during the Aptian / Albian. The following sandy Tauern Flysch succession of a prograding fan may compare to Lower Cretaceous flysch units of Rhenodanubian Flysch and the Ybbsitz Zone. The deposition of the breccias at the top of the profile may stop during the mid-Cretaceous (Cenomanian/Turonian?) as no indications for a Late Cretaceous or Paleogene age were ever found, similar to Arosa Zone flysch units (Winkler, 1988) and other units along the Austroalpine/Penninic suture. This model is in accordance with the sparse biostratigraphic data, the facies correlations with black shale and siliciclastic deposition, and the provenance of clasts such as dolomites. However, heavy mineral data, i.e. the lack of chrome spinel, is in contradiction to this model.

Model B allocates the Tauern Flysch in a similar stratigraphic position to the main **Rhenodanubian Flysch Zone** (see e.g. Prey, 1977). This would represent a **northern Penninic position**. The greenschists (Early - Middle Jurassic) and the chert/radiolarite lithofacies (Late Jurassic) may still be interpreted as representative for the same age as in model A. The turbiditic deposition may then have started during the Aptian/Albian, represented by the thick black shales of lithofacies 1. Neocomian would then be missing in the Wolfbach profile (but may be present in *Aptychus* limestone lithofacies elsewhere in this unit). The siliciclastic flysch sedimentation continues through the Late Cretaceous, up to the Cretaceous/Paleogene boundary, alike more southern units of the Rhenodanubian

Flysch Zone (e.g. Kahlenberg Nappe) and the related Ybbsitz Zone (Schnabel, 1992), or even represent Paleogene "wildflysch". This model is in accordance with the black shale stratigraphy and the Rhenodanubian Flysch Zone stratigraphy in general, also proposed Bertle (2004) and Prey (1977). However, there is no indication, like fossil evidence of for instance orbitoids or nummulites, of a depositional age of the Tauern Flysch continuing into the Late Cretaceous and Paleogene. In contrast, especially the sparse biostratigraphic data for the upper, limestone- and breccia-rich part of the Tauern Flysch succession still suggests an Early Cretaceous age and thus contradict this model.

Model C positions the flysch deposits in their entirety into the Jurassic. This model is based on successions in the Western Carpathians (see Plasienka et al., 2012) and corresponds to a (more) **northern Austroalpine position** similar to the metamorphic Lower Austroalpine units containing Jurassic breccias (e.g. Häusler, 1988). Consequently, the position of the basal greenschists and cherts/radiolarites would then be older than Jurassic (Triassic?) or these units may even be not part of stratigraphic succession at all and belong to a different tectonic unit. The black shale/turbiditic section starts with the beginning of the Early Jurassic and continues through the Jurassic. Early Jurassic ages of black shales may thus correspond to the Toarcian Oceanic Anoxic Event. The breccia lithology would then be of Late Jurassic to earliest Cretaceous age, corresponding to Lower Austro-Alpine breccias like the Schwarzeck breccia (Häusler, 1988). Although the stratigraphic positions of black shales and breccias in this model may show conformity to global events and corresponding successions, the huge quantity of siliciclastic flysch during Middle and Late Jurassic remains inexplicable - no related flysch succession is known from nearby tectonic units (except Neotethyan Jurassic flysches far away from the Penninic Ocean to the south of the Austroa-Alpine, Gawlick et al., 2009). Furthermore, Tethyan-wide events like the Late Jurassic (Oxfordian) siliceous sedimentation and the Tithonian-Neocomian *Saccocoma*/*Calpionella*/*Aptychus* pelagic limestone sedimentation would remain totally unrecorded. Such a Jurassic age would also contradict the sparse biostratigraphic data.

16. CONCLUSION

The sedimentology of the Tauern Flysch at the northern margin of the Tauern Window was investigated using various field and lab methods. The single profiles indicate characteristics of turbidites, related mass flow and flysch-like appearance. All in all the grain size and the carbonate content increase, and the shale content decreases towards the top of the main profiles. The succession in the main profiles show the characteristics of a prograding, small submarine fan, fitting the model of a hypothetical small submarine fan stratigraphic sequence formed by fan progradation (after Walker, 1979).

The mineralogy indicated that the source area had to comprise a sufficient amount of dolomite (Hauptdolomit?) and therefore an Austro-Alpine provenance, on top of the Penninic-Austro-Alpine accretionary wedge, presumably in a part where ophiolites are missing, is most likely. Indication for two (original) separate sources is given by the succession of lithofacies 2 (siliciclastic source and a (biogenic) carbonate source), the results of the principal component analysis, the heavy mineral distribution (e.g. occurrence of garnet) and geochemical microprobe data of tourmalines (mostly Li-poor granitoids and associated pegmatites and aplites, with varying Mg/Fe levels). Both petrographic and geochemical analysis indicate a recycled, siliceous source.

Out of the three possible stratigraphic models for its paleogeography and tectonic attribution, model A is most likely. The base of the profile in the Wolfbachtal is represented by greenschist (inferred Early to Middle Jurassic age) and fine-grained siliceous rocks (meta-chert? of inferred Late Jurassic age, Oxfordian?). The actual siliciclastic and turbiditic deposition started between the end of the Late Jurassic and the Early Cretaceous, continuing through the Early Cretaceous. Indication for an Early Cretaceous age of at least parts of the succession including carbonate-rich intervals, is also given by the black shale, which represent a partly pelagic to hemipelagic deep-water sedimentation and could not have been deposited in such thickness e.g. during the Late Cretaceous. Microstructural analysis, such as non-recrystallized micritic dolomite clasts and recrystallized feldspar grains, indicate metamorphic conditions of up to 450°C. Pressure solution was determined as the main deformation mechanism. Three stages of deformation were distinguished. However, no clear indication of deformation directly connected to the SEMP-strike-slip-fault was detected.

17. APPENDIX

KURZFASSUNG

Die Herkunft und der stratigraphische Zusammenhang der metamorphen Flysch-ähnlichen Sedimente am Nordrand des Tauernfensters (Penninikum der Ostalpen, Salzburg; u.a. nach Braumüller, 1939; Prey, 1977; Ślączka, 2011) stellt ein ungelöstes Problem der Gebirgsbildung der Ostalpen dar. Unterschiedliche Modelle versuchen eine Zugehörigkeit dieser Tiefwasser-Mass-Flow-Sedimente zu finden. Diese Masterarbeit beschäftigt sich mit der Herkunft des Tauern Flyschs und damit einhergehend mit der Beantwortung der Frage nach dessen paläogeographischen und paläotektonischen Zuordnung. Hierfür wurden vor allem Schwermineralverteilungen und Bulk-Geochemie Analysen herangezogen. Eine weitere Forschungsfrage widmet sich dem Metamorphosegrad dieser Flysch Ablagerungen und dem möglichen tektonischen Einfluss der SEMP (Salzach–Ennstal–Mariazell–Puchberg; Rosenberg et al., 2008) –Störung auf diese.

Die Geländearbeit beinhaltete sedimentologische Aufnahme von zwei Hauptprofilen (das erste 780m, das zweite 400m lang) und 18 Einzelprofilen im Bereich des Wofbachtals (südwestlich von Taxenbach, Salzburg). Die beinahe durchgehenden Aufschlüsse von metamorphen Flysch-Ablagerungen befinden sich entlang zweier Fortstraßen im Höferwald und im Bachbett des Wolfbachs. Die Ablagerungen beinhalten Meta-Tonschiefer, (teilweise) turbiditische Meta-Sandstein, Meta-Brekzie und Marmor. Insgesamt 50 Proben wurden genommen und analysiert. Zu den Analysen zählt petrographische Mikroskopie, XRD-Analysen, Schwermineralanalyse, Mikrosonden Messungen der Schwerminerale, Bulk-Geochemie Analysen und Principal Component Analysen. Die mikrostrukturelle Analyse der Dünnschliffe ergibt höhere Metamorphose Bedingungen als erwartet (obere Grünschieferfazies, mit Temperaturen von 450°). Diese Bedingungen sind verantwortlich dafür, dass die geochemischen Analysen nicht völlig vertrauenswürdig sind und daher keine eindeutigen Ergebnisse liefern. Da es sich bei dem Hauptdeformationsmechanismus um Drucklösung handelt, können Sedimentstrukturen (beschrieben von Prey, 1977), welche die Zuteilung zum „Flysch“ bestätigen, trotz Metamorphose beobachtet werden. Die Abfolge der Hauptprofile (Modell nach Walker, 1979) lässt auf eine Bildung durch einen progradierenden, submarinen Schwemmfächer schließen. Es gibt wiederholte Hinweise auf zwei ursprünglich separate Herkunftsgebiete. Das erstellte wahrscheinlichste stratigraphische Modell zur

paläogeographischen und tektonischen Zugehörigkeit dieser Metasedimente ordnet jene überwiegend der Unterkreide zu.

ABSTRACT

The provenance and the stratigraphic correlation of the metamorphic flysch-like sediments at the northern border of the Tauern Window (Penninic unit, Salzburg; i.a. Braumüller, 1939; Prey, 1977; Ślączka et al., 2011) represent a conundrum of the orogeny of the Eastern Alps. There are several models trying to explain Alpine palaeogeography and the derivation and stratigraphc position of these deep-water-mass-flow-sediments. Provenance of the Tauern Flysch may help to solve the question of its palaeogeographic and palaeotectonic position, mainly by making comparisons of heavy mineral associations and bulk geochemistry analysis data. Another research question is the degree of metamorphosis and how strong the possible influence of the SEMP (Salzach–Ennstal–Mariazell–Puchberg; Rosenberg et al., 2008) Fault is on these flysch deposits.

The fieldwork included the sedimentological logging of two main profiles (1st 780m, 2nd 400m in length) and 18 single profiles in the area of the Wolfbachtal (southwest of Taxenbach, Salzburg). Almost continuous outcrops of metamorphic flysch deposits along forest paths and the Wolfbach streambed can be found, including meta-black shales, turbiditic meta-sandstones, meta-breccias and marbles. Analysis-methods used on altogether 50 samples include petrographic microscope analysis, x-ray diffraction, heavy mineral associations, micro-probe analysis of heavy minerals, rock bulk geochemistry analysis and principal component analysis.

Microstructural microscope analysis (i.a. recrystallized feldspar grains and brittle deformed non-recrystallized dolomite grains in a fully recrystallized calcite matrix) indicates higher metamorphic conditions than previously reported (with upper Green-schist facies and temperatures around 450°C). Due to these conditions the results of the bulk geochemistry analysis are not fully reliable and don't give straightforward results. Nevertheless sedimentary structures (described by Prey, 1977), confirming the flysch-like nature of these meta-sediments, can be observed, due to the main deformation mechanism being pressure solution. The succession of the profile in the Wolfbachtal was formed by a prograding, small submarine fan (fitting the model of Walker, 1979). There is an enhanced possibility of two (originally) separate sources. The most likely stratigraphic model for the paleogeography and tectonic attribution of these meta-sediments indicates that the deposition started during the end of the Late Jurassic and continued mainly throughout the Early Cretaceous.

Appendix 1: Table of all lithofacies distinguished, including a summary of their characteristic features

lith.	name	calcite	grainsize	rip up clasts	bedding	mica	black shale	sandstone/ shale ratio	clasts	samples	single profiles	comment
1	**black shale**	+	fine	-	max. 0.5 cm	~	black	02 / 98	-	2,4,28,11sst,	A4,A5,	sandstone layers max 2.5 cm
2	**calcareous sandstone**	+	middle-coarse	-	thin	+	silver, black	80 / 20	-	12,?13,14,39,40	A6,A7,A14	
3	**coarse grained sandstone**	~	coarse	-	thin-thick	~	silver, black	85 / 15	-	16,	A8,	
4	**amalgamite**	~	fine-middle	-	thick	~	-	100 / 0	-	8,17,18,41	A3	
5	**non-calcareous coarse grained sandstone**	-	coarse	~	thick	~	black	92 / 8	black shale, calcite	15,19,35,36,42,43	A13,A15, B16	small black shale - rip up clasts
6	**non-calcareous sandstone**	-	middle-coarse	-	thin-middle	~	black	60 / 40	-	32,25,3,7,30, 37u,44, 45	A11, B12, B17	
8	**rip up clasts-sandstone**	+	middle-coarse	+	thin-middle	~	black	50 / 50	-	31ab, 29	A9,	rip up clasts of silver and black shale
9	**limestone**	+	fine	-	thin-massive	-	black	97 / 3	-	21,20	-	
10	**breccia**	+	coarse	-	thin-middle	-	black	90 / 10	dolomite, quartz	1,26,23,?6ab,22, 27,	A1,A2,	rip up clasts of silver and black shale
11	**radiolarite**	-	-	-	massive	-	-	-	-	9,10,	-	
12	**calcareous coarse grained sandstone**	+	middle-coarse	-	thin-middle	-	black	98 / 2	-	24,	A10	
13	**clasts-containing - limestone**	+	fine	-	middle-massive	-	~ clasts black	97 / 3	dolomite, black shale	34,38u	-	
15	**greenshist**	-	fine	-	massive	-	-	-	-	5a,5b,	-	

Appendix 2: Figure 75: The positions of all single profiles of Profile A and B shown on a laser scan map of the Wolfbachtal (SAGIS online).

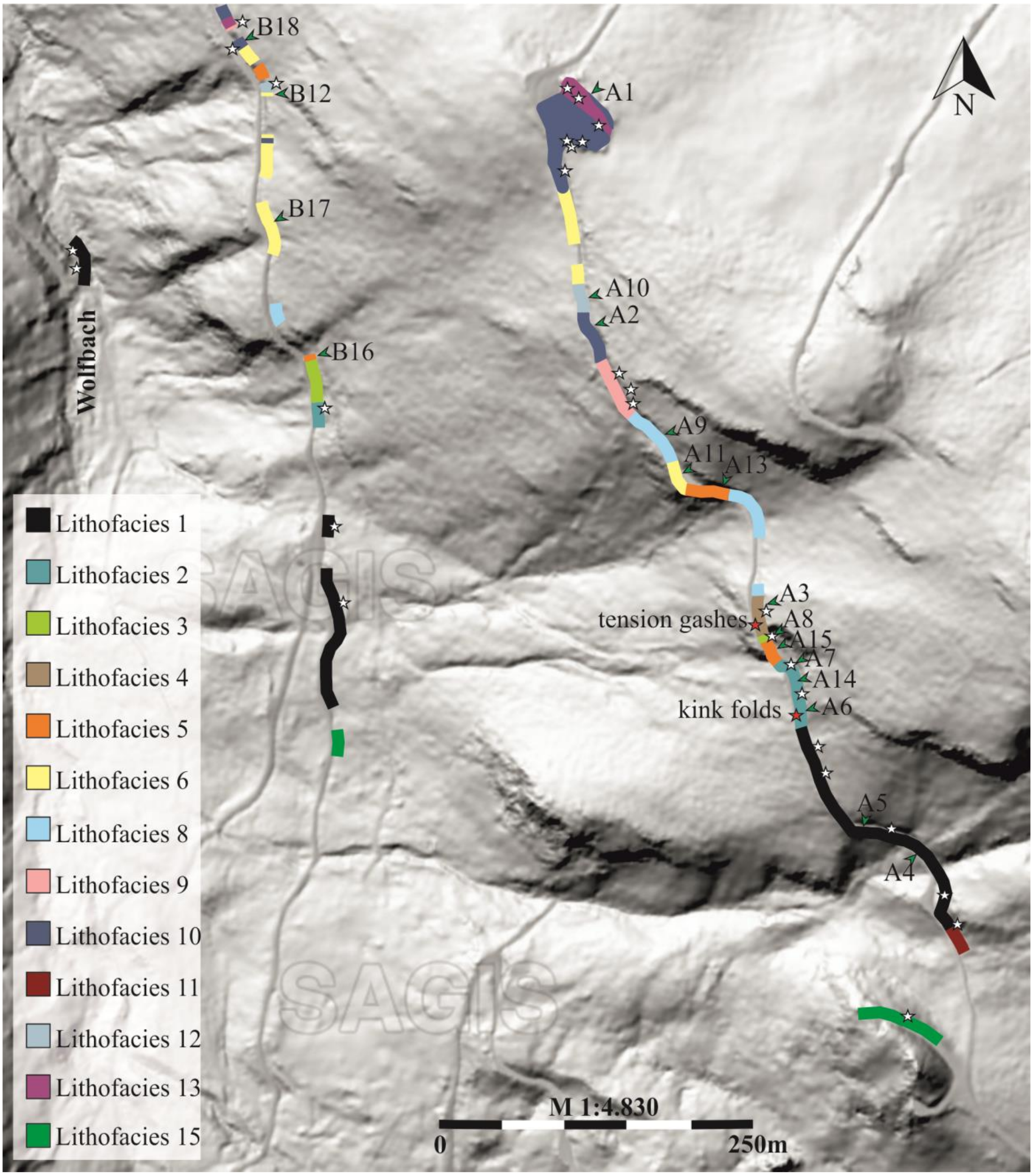

Appendix 3: Diagram of heavy mineral analysis of all analysed samples, including those with less than 100 grains counted.

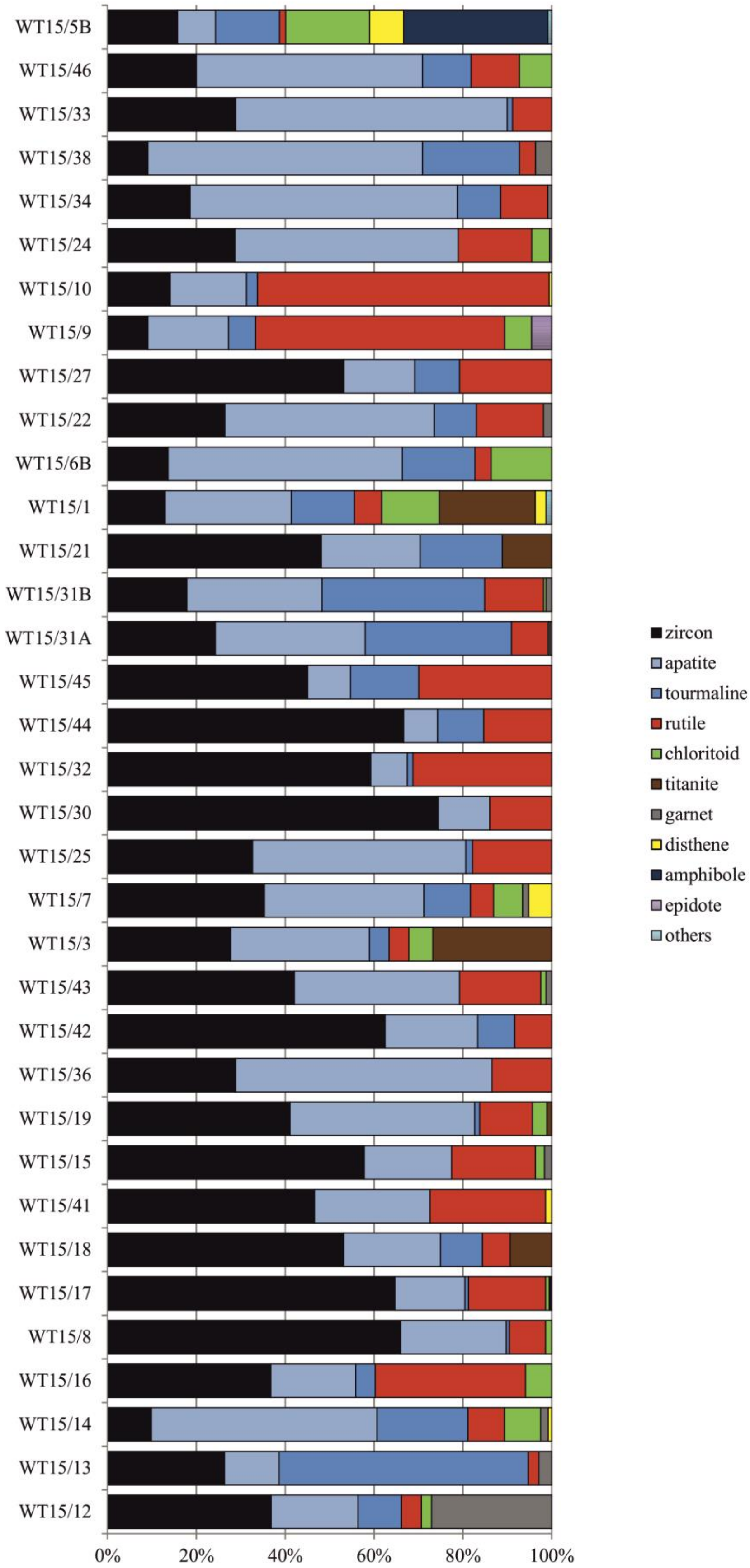

Appendix 4: Full table of all heavy minerals counted in all analysed samples, also including those with less than 100 grains (marked in grey). Samples containing too less heavy mineral grains to count are marked with estimated distribution marks: [++] for a very high proportion, [+] for a high proportion and [~] for low proportion.

L	S	Zir	Apa	Tou	Rut	Chl	Tit	Gar	Dis	Amp	O
2	WT15/12	49	26	13	6	3		36			
	WT15/13	45	21	96	4			5			
	WT15/14	12	62	25	10	10		2	1		
	WT15/39	++	+		+						
3	WT15/16	25	13	3	23	4					
4	WT15/8	97	35	1	12	2					
	WT15/17	235	57	3	63	3	1	1			
	WT15/18	17	7	3	2		3				
	WT15/41	34	19		19				1		
5	WT15/15	141	48		46	5		4			
	WT15/19	76	77	2	22	6	2				
	WT15/36	15	30		7						
	WT15/42	15	5	2	2						
	WT15/43	69	61		30	2		2			
6	WT15/3	31	35	5	5	6	30				
	WT15/7	54	55	16	8	10		2	8		
	WT15/25	108	159	5	59						
	WT15/30	32	5		6						
	WT15/32	144	20	3	76						
	WT15/44	122	14	19	28						
	WT15/45	173	37	59	115						
8	WT15/31A	59	82	80	20	1		1			
	WT15/31B	58	99	119	43	2		4			
9	WT15/20	+	+	~	+						
	WT15/21	13	6	5			3				
10	WT15/1	21	46	23	10	21	35		4		2
	WT15/6B	15	58	18	4	15					
	WT15/22	14	25	5	8			1			

	WT15/26	~	+	+ +	+ +						
	WT15/27	100	30	19	39						
11	WT15/9	6	12	4	37	4					
	WT15/10	23	28	4	107				1		
12	WT15/24	64	112		37	9		1			
13	WT15/34	21	68	11	12			1			
	WT15/38	5	34	12	2			2			
14	WT15/33	49	104	2	15						
	WT15/46	11	28	6	6	4					
15	WT15/5B	35	19	32	3	42			17	72	2

Appendix 5:A selection of heavy minerals: tourmaline, rutile, titanite and zircon (top to bottom).

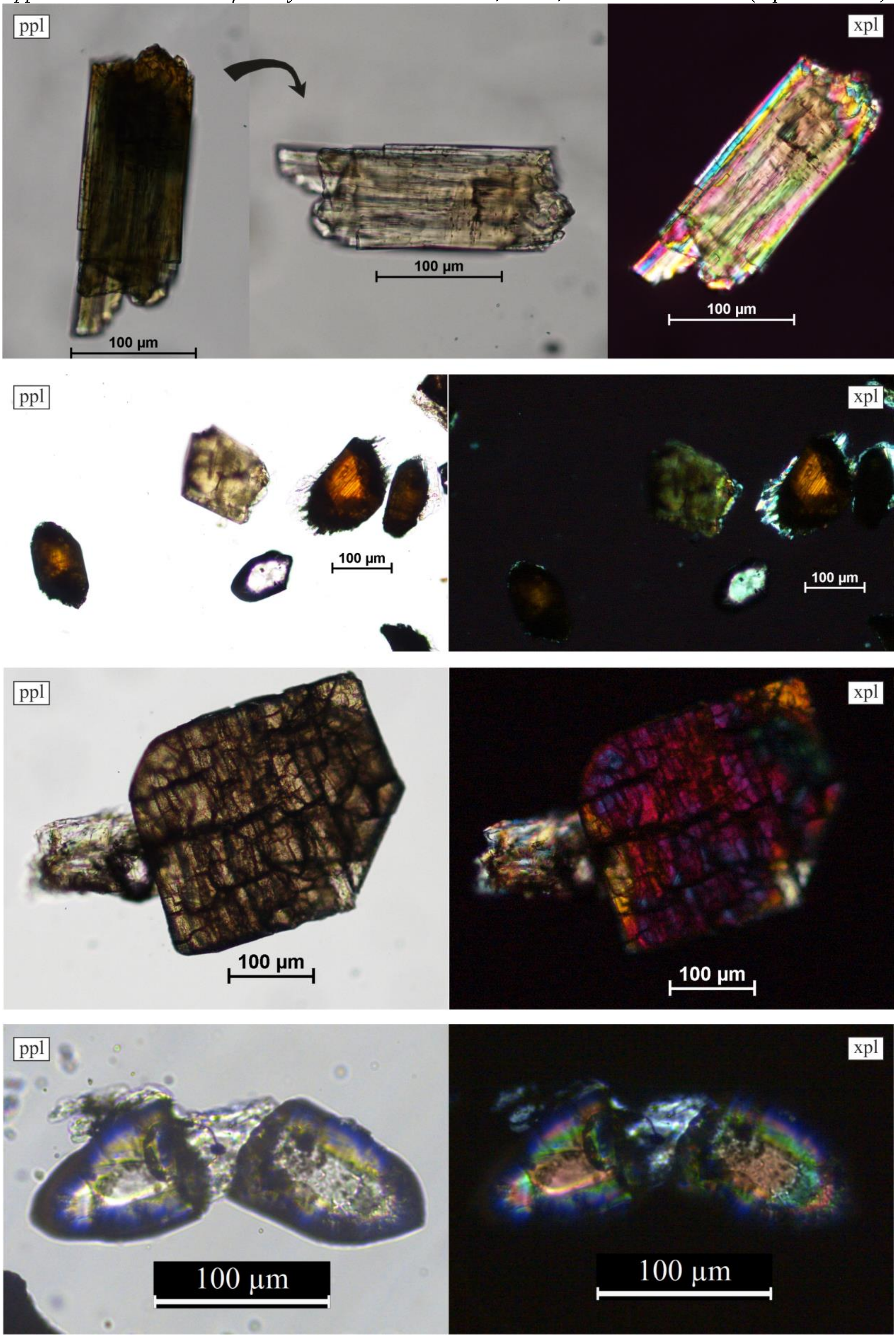

Appendix 6: Table of chemical composition in [%] of non-heavy minerals measured with the microprobe; The acronym M means mineral, S resembles the last number of the sample identifier behind WT15/, dol stands for dolomite, cal for calcite, phe for phengite, mus for muscovite, K-fs for Potassium Feldspar, alb for Albite, qtz for quartz, Ill for illit and chl for chlorite.

M	SiO2	MgO	F	Na2O	Al2O3	K2O	TiO2	MnO	CaO	FeO	Cl	Cr2O3	BaO	NiO	S
dol	0.023	17.245			0.021	0.054		0.018	31.586	0.068					6b
cal	0.082	0.782			0.007	0.035		0.171	55.010	1.636					6b
	0.001	0.991		0.008		0.012		0.198	57.683	1.660		0.010		0.002	6b
	0.020	0.509				0.003		0.262	59.054	1.363		0.003		0.009	6b
	0.014	0.221		0.012		0.001	0.003	0.076	55.813	0.604					35
phe	47.475	2.987	0.060	0.026	26.229	10.281	0.368	0.014	0.089	5.517	0.021	0.032	0.082		41
	48.501	1.728	0.057	0.284	32.151	10.517	0.591	0.023	0.002	2.290	0.007	0.007	0.200		45
	49.281	2.490	0.139	0.044	27.143	11.222	0.581		0.028	4.045		0.014	0.099		45
	45.854	1.168	0.087	0.362	33.381	10.571	1.188	0.020		2.387	0.001	0.012	0.152		45
	50.358	2.633	0.160	0.007	25.478	11.139	0.746	0.008	0.033	4.178	0.005	0.005	0.087		45
	51.643	4.289	0.125	0.040	25.106	10.934	0.218	0.019	0.061	3.186	0.007	0.024	0.263		6b
	51.188	4.052	0.068	0.076	25.016	11.071	0.268			3.036	0.005		0.235		6b
	49.891	3.078	0.072	0.104	28.296	11.007	0.211		0.026	2.159	0.006		0.154		6b
	46.343	1.195	0.043	0.366	32.708	10.730	1.128	0.007	0.024	2.023			0.125		40
	50.764	3.190	0.065	0.050	26.899	10.903	0.877			2.346	0.006		0.117		35
	49.767	3.096	0.143	0.048	27.016	10.948	0.354	0.018	0.009	2.372			0.135		35
	50.884	3.267	0.188	0.038	26.407	10.995	0.916		0.003	2.215		0.016	0.156		35
	50.979	3.236		0.016	26.625	10.968	0.853			1.947			0.135		35
	51.190	3.185	0.148	0.003	25.960	11.084	0.710	0.009	0.019	2.727	0.002	0.009	0.116		35
mus	46.467	1.190	0.024	0.372	31.932	10.567	0.948	0.015	0.048	2.581	0.007	0.003	0.096		35
	46.052	0.568		1.154	37.337	8.807	0.723		0.013	0.978		0.018		0.009	6b
K-fs	64.278	0.009		0.317	18.833	16.193	0.026		0.011	0.053			0.183		45
	63.638	0.013		0.300	18.809	15.733	0.010		0.049	0.105			0.737		45
	62.216	0.001		0.449	18.901	15.849	0.046			0.044			0.188		45
	63.660			0.292	18.884	16.242	0.022		0.031	0.101			0.045		45
alb	68.196	0.008		11.727	19.765	0.027	0.000		0.026	0.046					6b
	68.882		0.027	11.768	19.909	0.056	0.000		0.004	0.013					35
qtz	99.489	0.007	0.045	0.002	0.006	0.000	0.004			0.015	0.001		0.023		35
Ill	53.031	1.104		0.888	35.091	2.387	0.214		0.250	1.308	0.002		0.102		6b
	57.112	0.916	0.001	0.839	30.721	2.686	0.726	0.007	0.094	1.123	0.002	0.029	0.024		6b
	55.412	0.730	0.055	0.560	35.506	3.457	0.398	0.009	0.273	0.683	0.003	0.014	0.068		6b
	51.196	2.838	0.014	1.525	31.641	3.228	2.148	0.341	1.293	2.116	0.005	0.033	0.508		41
chl	27.757	18.792	0.075	0.000	19.885	0.124	0.080	0.023	0.029	19.692	0.000	0.070			6b

Appendix 7: flanking structure (WT15/3) formed in a deformation process younger than the main metamorphosis.

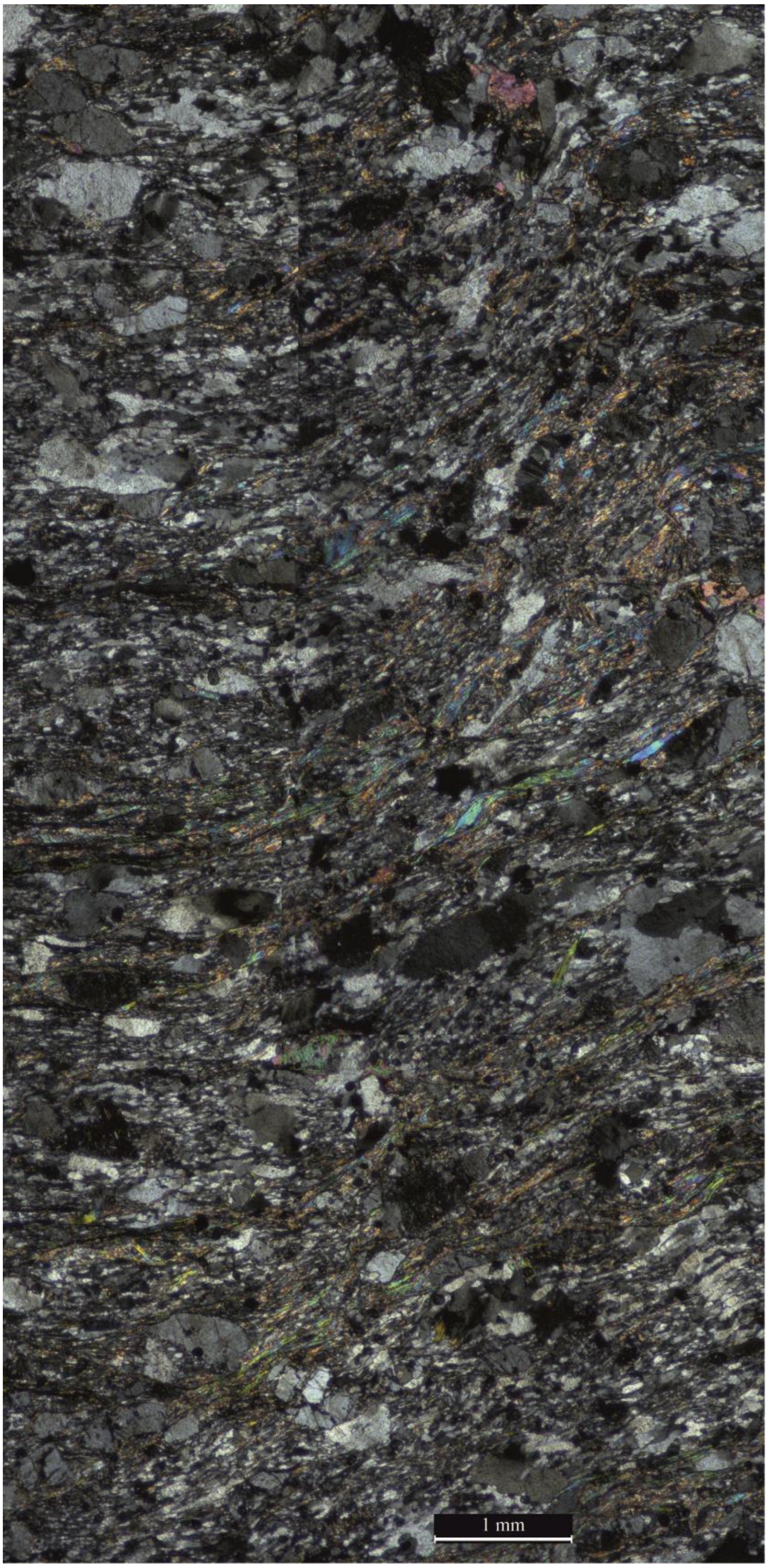

Appendix 8: list of samples

sample	***rock type***	***Lit.***	***GPS***	***sample***	***rock type***	***Lit.***	***GPS***
WT15/1	breccia	10	N47°16'8,36" E12°55'58,99"	**WT15/24**	calcareous sandstone	12	N47°16'3,82" E12°55'57,92"
WT15/2	blackshale	1	N47°15'51.6" E12°56'08.4"	**WT15/25**	sandstone	6	N47°16'3,67" E12°55'58,85"
WT15/3	sandstone	6	N47°16'8,36" E12°55'58,99"	**WT15/26**	breccia	10	N47°16'8,36" E12°55'58,99"
WT15/4	blackshale	1	N47°15'47,73" E12°56'12,67"	**WT15/27**	sandstone	6	N47°16'6,56" E12°55'46,1"
WT15/5a	sandstone	15	N47°15'44,53" E12°56'10,47"	**WT15/28**	sandstone	1	N47°15'49,76" E12°56'11,84"
WT15/5b	sandstone	15	N47°15'44,53" E12°56'10,47"	**WT15/29**	sandstone	8	N47°15'57,59" E12°56'5,23"
WT15/6a	sandstone	10	N47°16'05.9" E12°55'47.0"	**WT15/30**	sandstone	6	N47°15'58,93" E12°56'2,35"
WT15/6b	sandstone	10	N47°16'05.9" E12°55'47.0"	**WT15/31a**	sandstone	8	N47°15'59,59" E12°56'2,03"
WT15/7	limestone/ sandstone	6	N47°16'14,85" E12°55'42,72"	**WT15/31b**	sandstone	8	N47°15'59,59" E12°56'2,03"
WT15/8	sandstone	4	N47°15'56,01" E12°56'4,14"	**WT15/32**	sandstone	6	N47°16'4,87" E12°55'58,64"
WT15/9	chert	11	N47°15'48.4" E12°56'12.8"	**WT15/33**	breccia	10	N47°16'4,94" E12°55'57,46"
WT15/10	chert	11	N47°15'48.4" E12°56'12.8"	**WT15/34**	limestone	13	N47°16'9,09" E12°55'58,37"
WT15/11	sandstone	1	N47°15'50,19" E12°56'10,95"	**WT15/35**	sandstone	5	N47°16'9,51" E12°55'45,57"
WT15/12	calcareous sandstone	2	N47°15'53,69" E12°56'10,3"	**WT15/36**	sandstone	5	N47°16'9,51" E12°55'45,57"
WT15/13	sandstone	2	N47°15'54,46" E12°56'7,08"	**WT15/37**	sandstone	6	N47°16'9,54" E12°55'45,18"
WT15/14	calcareous sandstone	2	N47°15'54,53" E12°56'5,86"	**WT15/38**	breccia	12	N47°16'9,87" E12°55'44,4"
WT15/15	sandstone	5	N47°15'54,53" E12°56'5,86"	**WT15/39**	sandstone	2	N47°15'53,25" E12°56'6,97"
WT15/16	sandstone	3	N47°15'54,53" E12°56'5,00"	**WT15/40**	sandstone	2	N47°15'53,08" E12°56'6,77"
WT15/17	sandstone	4	N47°15'56,43" E12°56'4,14"	**WT15/41**	sandstone	4	N47°15'56,3" E12°56'5,85"
WT15/18	sandstone	4	N47°15'56,43" E12°56'4,14"	**WT15/42**	sandstone	5	N47°15'58,83 E12°56'3,16
WT15/19	sandstone	5	N47°15'58,76" E12°56'3,86"	**WT15/43**	sandstone	3	N47°16'1,48" E12°55'48,4"
WT15/20	limestone	9	N47°16'1,08" E12°56'0,01"	**WT15/44**	sandstone	6	N47°16'5,61" E12°55'46,41"
WT15/21	limestone	9	N47°16'0,84" E12°56'0,44"	**WT15/45**	sandstone	6	N47°16'5,61" E12°55'46,41"
WT15/22	breccia	10	N47°16'2,37" E12°55'59,72"	**WT15/46**	sandstone	10	N47°16'13,19" E12°55'42,85"
WT15/23	sandy breccia	10	N47°16'2,37" E12°55'59,72"				

REFERENCES

BAHLBURG, H., (1998). The geochemistry and provenance of Ordovician turbidites in the Argentine Puna. Geological Society, London, Special Publications 142.1, 127-142.

BAHLBURG, H., & DOBRZINSKI, N.,(2011). A review of the Chemical Index of Alteration (CIA) and its application to the study of Neoproterozoic glacial deposits and climate transitions Geological Society, London, Memoirs 36.1, 81-92.

BERTLE, R., (2004). The sedimentary record of North Penninic Schistes lustrés of the Lower Engadine Window and its correlation to the Tauern Window (Eastern Alps). Jb. Geol .B.A. 144, 165-171.

BHATIA, M. R., & CROOK, K., (1986). Trace element characteristics of graywackes and tectonic setting discrimination of sedimentary basins. Contributions to mineralogy and petrology 92.2, 181-193.

BOUMA, A., et al., (1962). Sedimentology of some flysch deposits: a graphic approach to facies interpretation. Vol. 168. Elsevier, Amsterdam.

BRAUMÜLLER, E., (1939). Der Nordrand des Tauernfensters zwischen dem Fuscher-und Rauristal.

CULLERS, R. L., (2002) Implications of elemental concentrations for provenance, redox conditions, and metamorphic studies of shales and limestones near Pueblo, CO, USA., Chemical Geology 191.4, 305-327.

DAVIS, J. & SAMPSON, R., (1986). Statistics and data analysis in geology., John Wiley & Sons.

DICKINSON, W.R., (1985). Interpreting provenance relation from detrital modes of sandstones, in Zuffa, G.G. (ed.), Provenance of Arenites: NATO ASI Series, C 148, D. Reidel Publishing Company, Dordrecht, p. 333–363.

FAUPL, P., & WAGREICH, M. (1992). Cretaceous flysch and pelagic sequences of the Eastern Alps: correlations, heavy minerals, and palaeogeographic implications. Cretaceous Research, 13(5-6), 387-403.

FAUPL, P. (1996). Tiefwassersedimente und tektonischer Bau der Flyschzone des Wienerwaldes. Exkursionsführer Sediment '96, Wien, 1-32.

FAUPL, P., & WAGREICH, M., (2000). Late Jurassic to Eocene palaeogeography and geodynamic evolution of the Eastern Alps. Mitteilungen der Österreichischen Geologischen Gesellschaft 92.1999, 79-94.

FAUPL, P. (2003). Historische Geologie.–2. Aufl., Stuttgart (UTB).

FEDO, C., NESBITT, H., & YOUNG, G., (1995). Unraveling the effects of potassium metasomatism in sedimentary rocks and paleosols, with implications for paleoweathering conditions and provenance, Geology, 23.10, 921-924.

FLOYD, P. A. & LEVERIDGE, B. E., (1987). Tectonic environment of the Devonian Gramscatho basin, south Cornwall: framework mode and geochemical evidence from turbiditic sandstones., Journal of the Geological Society 144.4, 531-542.

FRISCH, W., 1979. Tectonic progradation and plate tectonic evolution of the Alps. Tectonophysics 60, 121-139.

GAWLICK, H., MISSONI, S., SCHLAGINTWEIT, F., SUZUKI, H., FRISCH, W., KRYSTYN, L., ... & LEIN, R. (2009). Jurassic Tectonostratigraphy of the Austroalpine domain. Journal of Alpine Geology, 50, 1-152.

HÄUSLER, H. (1988). Unterostalpine Jurabreccien in Österreich. Versuch einer sedimentologischen und paläogeographischen Analyse nachtriadischer Breccienserien im unterostalpinen Rahmen des Tauernfensters (Salzburg-Tirol). Jahrbuch der Geologischen Bundesanstalt, 131, 21-125.

HAMMER, Ø., HARPER, D.A.T. & P. D. RYAN, P. D., (2001). PAST-palaeontological statistics, ver. 1.89. Palaeontologia electronica 4.9.

HANDY, M.R., USTASZEWSKI, K. & KISSLING, E., (2015). Reconstructing the Alps–Carpathians–Dinarides as a key to understanding switches in subduction polarity, slab gaps and surface motion. International Journal of Earth Sciences 104, 1–26.

HENRY, D. J., & GUIDOTTI, C. V. (1985). Tourmaline as a petrogenetic indicator mineral- An example from the staurolite-grade metapelites of NW Maine American mineralogist, 70(1-2), 1-15.

HERRON, M. M., (1988). Geochemical classification of terrigenous sands and shales from core or log data. Journal of Sedimentary Research 58.5.

HÖCK, V., SLACZKA, A., UCHMAN, A., (2006). New biostratigraphic and palaeoenvironmental data on metamorphosed limestones from the northern margin of the Tauern Window (Eastern Alps, Austria). Austrian J. Earth Sci. 99, 42–56.

HOMAYOUN, M., & FAUPL, P. (1992). Unter-und Mittelkreideflysch der Ybbsitzer Klippenzone (Niederösterreich). Mitteilungen der Gesellschaft der Geologie und Bergbaustudenten in Österreich, 38, 1-20.

KLEBERGER, J., SÄGMÜLLER, J. J., & TICHY, G. (1981). Neue Fossilfunde aus der mesozoischen Schieferfülle der Hohen Tauern zwischen Fuschertal und Wolfbachtal (Unterpinzgau/Salzburg). Geologisch-Paläontologische Mitteilungen Innsbruck, 10(9), 275-288.

KURZ, W., NEUBAUER, F., GENSER, J., DACHS, E., 1998. Alpine geodynamic evolution of passive and active continental margin sequences in the Tauern Window (Eastern Alps, Austria, Italy): a review. Geol. Rundsch. 87, 225-242.

MANGE, M. A., & MAURER, H. F. (1991). Schwerminerale in Farbe. Ferdinand Enke.

MCLENNAN, S.M. et al., (1991). Sedimentary rocks and crustal evolution: tectonic setting and secular trends., The Journal of Geology, 1-21.

MCLENNAN, S. M., HEMMING, S., MCDANIEL, D. K., & HANSON, G. N. (1993). Geochemical approaches to sedimentation, provenance, and tectonics. Special Papers-Geological Society of America, 21-21.

MORTIMER, C. E., & MÜLLER, U. (2007). Chemie: Das Basiswissen der Chemie; 126 Tabellen. Georg Thieme Verlag.

MORTON, A. C., (1985). Heavy minerals in provenance studies. Provenance of arenites. Springer Netherlands, 249-277.

MORTON, A. C., AND HALLSWORTH. C. R., (1999) Processes controlling the composition of heavy mineral assemblages in sandstones. Sedimentary Geology 124.1, 3-29.

MORTON, A. C., AND CLAIRE HALLSWORTH, C. R., (2007). Stability of detrital heavy minerals during burial diagenesis. Developments in Sedimentology 58, 215-245.

NESBITT, H. W. & YOUNG, G. M., (1982). Early Proterozoic climates and plate motions inferred from major element chemistry of lutites, Nature Vol 299, 1982

NESBITT, H. W., & YOUNG. G. M., (1984). Prediction of some weathering trends of plutonic and volcanic rocks based on thermodynamic and kinetic considerations. Geochimica et Cosmochimica Acta 48.7 (1984): 1523-1534.

PESTAL, G., HEJL, E., BRAUNSTIGL, R., SCHUSTER, R., (2009). Salzburg. Geologie der Österreichischen Bundesländer. *Erläuterungen Geologische Karte von Salzburg 1:200,000*. Geol. B.A., 162 pp.

PETTIJOHN, F. J. (1941). Persistence of heavy minerals and geologic age. The Journal of Geology, 49(6), 610-625.

PETTIJOHN, F. J. J.. POTTER PE. AND SIEVER R.(1973). Sand and Sandstone. Springer, New York, -618 p.

PICKERING, K., STOW, D., WATSON, M., & HISCOTT, R. (1986). Deep-water facies, processes and models: a review and classification scheme for modern and ancient sediments. Earth-Science Reviews, 23(2), 75-174.

PLAŠIENKA, D., HÖCK, V., WAGREICH, M., AUBRECHT, R., 2012. Evolution of the northern Lower Austroalpine – Tatric margin: from Jurassic rifting to Cretaceous stacking. In: JÓZSA, Š., REHÁKOVÁ, D. AND VOJTKO, R. (eds.), Environmental, Structural and Stratigraphical Evolution of the Western Carpathians. 8th Conference 2012, December, 6-7, 2012, Bratislava, Abstract Book, p. 39.

PREY, S., (1975). Vorläufiger Bericht über Untersuchungen an den flyschartigen Serien des östlichen Tauernnordrandes, Verh.Geol.B.-A., p.291-295, Wien.

PREY, S., (1977). Flyscherscheinungen in den „flyschartigen Serien“ des östlichen Tauernnordrandes, Verh. Geol. B.-A., p.313-320, Wien.

READING, H. G. (1996). Sedimentary Environments: Processes, Facies and Stratigraphy. 3rd. Edition. Blackwell Science. Oxford.

REITZ, E., HÖLL, R., HUPAK, W. AND MEHLTRETTER, C., (1990). Palynologischer Nachweis von Unterkreide in der Jüngeren (Oberen) Schieferhülle des Tauernfensters (Ostalpen). Jahrbuch der Geologischen Bundesanstalt 133, 611-618.

ROSENBERG, C. L. et al., (2008). The western termination of the SEMP fault (Eastern Alps) and its bearing on the exhumation of the Tauern Window. Geological Society, London, Special Publications, 298(1), 197-218.

ROSER, B. P., AND KORSCH, R.J., (1986). Determination of tectonic setting of sandstone-mudstone suites using content and ratio" The Journal of Geology 94.5, 635-650.

ROSER, B. P., AND KORSCH, R.J., (1988). Provenance signatures of sandstone-mudstone suites determined using discriminant function analysis of major-element data. Chemical geology 67.1-2, 119-139.

SCHMID, S. M., FÜGENSCHUH, B., KISSLING, E., & SCHUSTER, R., (2004). Tectonic map and overall architecture of the Alpine orogen. Eclogae Geologicae Helvetiae, 97(1), 93-117.

SCHMID, S. M. ET AL, (2013). The Tauern Window (Eastern Alps, Austria): a new tectonic map, with cross-sections and a tectonometamorphic synthesis. Swiss Journal of Geosciences, 106(1), 1-32.

SCHNABEL, W., (1992). New data on the Flysch Zone of the Eastern Alps in the Austrian sector and new aspects concerning the transition to the Flysch Zone of the Carpathians. *Cretaceous Res.* 13, 405-419.

SCHUSTER, R. ET AL, (2004). Introduction to the Geology of the Eastern Alps. Bericht der Geologische Bundesanstalt, 99, 11th workshop on Alpine Geological Studies & 7th IFAA, 121-133.

ŚLĄCZKA, A., HÖCK, V. & IONESCU. C., (2011). "Mesozoic slope-aprons and submarine fans in the NE Tauern Window (Austria)." Austrian Journal of Earth Sciences 104.2.

TAYLOR, S. R. & MCLENNAN, S. M., (1985) “The continental crust: its composition and evolution.”, Blackwell, Oxford.

TERMIER, P., 1904. Les nappes des Alpes Orientales et la synthese des Alpes. Bull. Soc. Géol. France (4) 3, 1903, 711-765.

TOLLMANN, A., 1977. Geologie von Österreich. Band I. Die Zentralalpen. 766 pp., Wien (Deuticke).

TUCKER, M., (1988). Techniques in Sedimentology“, - 394 p., Blackwell Scientific Publications.

WAGREICH, M., (2008). Lithostratigraphic definition and depositional model of the Hütteldorf Formation (Upper Albian - Turonian, Rhenodanubian Flysch Zone, Austria). Austrian J. Earth Sci. 101, 70-80.

WALKER, R. G. (ED.). (1979). Facies models. Geological Association of Canada.

WARD JR., J. H., (1963). Hierarchical grouping to optimize an objective function. Journal of the American statistical association 58.301, 236-244.

WENTWORTH, C. K., (1922). A scale of grade and class terms for clastic sediments. The Journal of Geology 30.5, 377-392.

WINKLER, W. (1988). Mid-to early Late Cretaceous flysch and melange formations in the western part of the Eastern Alps. Paleotectonic implications. Jahrbuch der Geologischen Bundesanstalt (Wien), 131(2), 341-389.

ZHANG, C., LI, X., MATTERN, F., ZENG, Q., & MAO, G. (2017). Composition and sediment dispersal pattern of the Upper Triassic flysch in the eastern Himalayas, China: significance to provenance and basin analysis. International Journal of Earth Sciences, 106(4), 1257-1276.

WEBLINKS

www.salzburg.gv.at

www.schulatlas.com;

www.webmineral.com;